Volume 21, Number 1

July, 1966

SOVIET ATOMIC ENERGY

АТОМНАЯ ЭНЕРГИЯ
(ATOMNAYA ÉNERGIYA)

TRANSLATED FROM RUSSIAN

CONSULTANTS BUREAU

SOVIET ATOMIC ENERGY

Soviet Atomic Energy is a cover-to-cover translation of *Atomnaya Énergiya*, a publication of the Academy of Sciences of the USSR.

An arrangement with Mezhdunarodnaya Kniga, the Soviet book export agency, makes available both advance copies of the Russian journal and original glossy photographs and artwork. This serves to decrease the necessary time lag between publication of the original and publication of the translation and helps to improve the quality of the latter. The translation began with the first issue of the Russian journal.

Subscription
(12 Issues): $95

Single Issue: $30
Single Article: $15

Order from:

CONSULTANTS BUREAU
227 West 17th Street, New York, New York 10011

SOVIET ATOMIC ENERGY

A translation of *Atomnaya Énergiya*

Volume 21, Number 1 July, 1966

CONTENTS

CONTENTS

(continued)

NOTE

The Table of Contents lists all material that appeared in the original Russian journal. Items originally published in English or generally available in the West are not included in the translation and are shown in brackets. Whenever possible, the English-language source containing the omitted items is given.

The Russian press date (podpisano k pechati) of this issue was 7/4/1966. Publication therefore did not occur prior to this date, but must be assumed to have taken place reasonably soon thereafter.

STABILITY OF A NUCLEAR POWER GENERATION PLANT WITH CIRCULATING FUEL

V. D. Goryachenko

UDC 621.039.515

A nuclear power plant with circulating incompressible fuel is discussed. The active zone of the reactor is idealized by a system with lumped parameters and the heat exchanger by a unit with distributed parameters. The stability of such a plant over a small region of the steady state cycle of operation is demonstrated. For the special case when the importance of delayed neutrons is negligibly small, the stability is demonstrated relative to arbitrary deviations from the equilibrium state.

Description of the Mathematical Model

The stability of reactors with circulating fuel has been discussed previously in [1-4], in which the following assumptions were made: 1) The heat exchanger has no effect on the dynamics of the unit and, consequently, the temperature of the fuel on entry into the active zone is constant; 2) delayed neutrons are absent. (The effect of delayed neutrons was studied only for an idealized reactor model with constant heat removal [1, 4].) In practice, these assumptions generally are not fulfilled and therefore in this paper the effect on the dynamics of both delayed neutrons and heat exchanger is taken into account.

The layout of the unit considered is shown in the figure. The fissile material, which is also the coolant, circulates through a closed circuit and passes successively through the active zone of the reactor and the external circulation loop (heat exchanger).

In order to set up the mathematical model of the active zone we shall assume that: 1) The reactor, with a negative temperature coefficient of reactivity ε, operates in the self-compensating regime; 2) the reactivity of the reactor depends only on the fuel temperature T; 3) the fuel in the active zone of the reactor is completely mixed and therefore it can be assumed that all the variables defining the active zone are independent of the space coordinates* (no mixing occurs outside the active zone); 4) the heat release in the active zone is proportional to the neutron density N; 5) the fuel is incompressible and its density and specific heat are constant; 6) the delayed neutron emitters can be defined by a single (equivalent) group with a decay constant λ.

With these assumptions, the equations for the dynamics of the active zone will have the form

$$\frac{dN}{dt} = \frac{k-\beta}{l} N + \lambda C; \tag{1}$$

$$k = k_0 - \varepsilon (T - T_0); \tag{2}$$

$$\frac{dC}{dt} = \frac{\beta}{l} N - \lambda C - \frac{C}{\tau_1} + \frac{C(t-\tau_2)}{\tau_1} e^{-\lambda\tau_2}; \tag{3}$$

$$\tau_1 \frac{dT}{dt} = T_{in} - T + a_1 N. \tag{4}$$

Here, k is the reactivity; τ_1 and τ_2 are the transit times of the fuel through the active zone and the external loop respectively; a_1 is a constant. Equation (1) is the usual neutron balance equation [6]; Eq. (3) is the modified equation for the delayed neutron emitters which contains terms defining the removal and replacement in the active zone of the delayed neutron emitters; Eq. (4) expresses the thermal balance of the fuel within the active zone.

*An example of such a unit is the HRE research reactor [5]. The active zone of the HRE reactor is a sphere with a diameter of about 45 cm, and the fuel enters the active zone tangentially, which causes the formation of vortexes and thus facilitates more rapid mixing of the fuel.

Translated from Atomnaya Énergiya, Vol. 21, No. 1, pp. 3-6, July, 1966. Original article submitted December 8, 1965.

We call the ratio $\xi = \frac{\beta - k_0}{\beta}$ the delayed neutron importance factor. For the model being considered, we obtain from Eqs. (1) to (3), transcribed for steady-state conditions,

$$\xi = \frac{\beta - k_0}{\beta} = \frac{\lambda\tau_1}{\lambda\tau_1 + 1 - e^{-\lambda\tau_2}}. \tag{5}$$

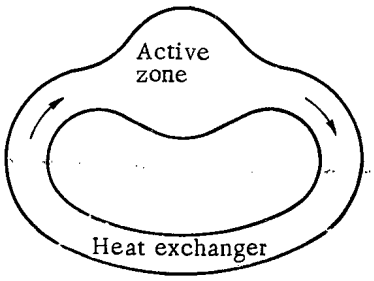

Simplified diagram of a unit with circulating fuel.

In contrast from a reactor with stationary fuel, where $\xi = 1$, there is a reduction of the importance of the delayed neutrons in the given case ($\xi < 1$), due to the fact that part of these neutrons is ejected outside the active zone and does not participate in the fission reaction.

We shall assume that the external circulation loop consists of a heat exchanger with a linear element and distributed parameters. Let $\Phi(p)$ be the heat exchanger heat transfer factor with respect to temperature and $\varphi_{(t)}$ be the inverse Laplace transformation of $\Phi_{(p)}$. Henceforth we shall assume that $\varphi_{(t)}$ satisfies the conditions

$$\varphi(t) \geqslant 0, \tag{6}$$

$$\int_0^\infty \varphi(t)\,dt < 1. \tag{7}$$

Otherwise, the properties of the function $\varphi_{(t)}$ are arbitrary.

The validity of these inequalities becomes obvious if we take into account that $\varphi_{(t)}$ defines the change of temperature at the outlet from the heat exchanger as a result of intermittent change of temperature at the inlet, i. e., for $T(t) - T_0 = \delta(t)$. Actually, as a result of the passage through the primary loop of a fuel particle, carrying a delta-heat pulse, the temperature of the medium of the secondary heat exchanger circuit is increased. The other fuel particles following behind this one give up their heat to the hotter medium of the secondary loop. Consequently, less heat will be removed from these particles than under steady state conditions and their temperature is found to be higher than the steady state temperature. This also implies that $\varphi(t) > 0$. Further, the additional quantity of heat at the heat exchanger inlet, due to the impulsive temperature change at the inlet, is proportional to the integral $\int_0^\infty \delta(t)\,dt = 1$, and, consequently, the quantity of heat at the outlet from the heat exchanger is proportional to the integral $\int_0^\infty \varphi(t)\,dt$ with the same proportionality constant. Since part of the heat is removed in the secondary circuit, then

$$\int_0^\infty \varphi(t)\,dt < \int_0^\infty \delta(t)\,dt = 1.$$

We note that a precise analytical proof of inequalities (6) and (7) is extremely difficult, since in the case of a distributed heat exchanger the actual expression for $\Phi(p)$ proves to be extremely complex [7]. As far as we know, there is no precise proof of these inequalities in the literature, with the exception of the special case when the temperature of the heat exchanger secondary circuit and the heat transfer factor from the primary to the secondary circuit are constant. In this case, it is not difficult to deduce that

$$\Phi(p) = e^{-\alpha\tau_2 - p\tau_2},$$
$$\varphi(t) = e^{-\alpha\tau_2}\delta(t - \tau_2);$$

consequently, inequalities (6) and (7) are fulfilled (the positive constant α is proportional to the heat transfer factor from the primary to the secondary circuit).

The Linearized System and the Characteristic Equation

We shall show that the unit being considered is stable over a small region. In Eqs. (1)-(4), we shall deal with small deviations of the variables from their equilibrium values:

$$y = \frac{N - N_0}{N_0};\quad y_1 = \frac{C - C_0}{C_0};\quad z = T - T_0;\quad z_{\text{in}} = T_{\text{in}} - T_{\text{in}\,0}. \tag{8}$$

We introduce the nomenclature

$$\tau = \frac{t}{\tau_1},$$

$$a = a_1 N_0;\ A = \frac{\varepsilon}{\beta_{\text{eff}}};\ \beta_{\text{eff}} = \xi\beta, \tag{9}$$

$$\sigma = \lambda\tau_1;\ \mu = \frac{\tau_2}{\tau_1},$$

$$\xi = \frac{\lambda\tau_1}{\lambda\tau_1 + 1 - e^{-\lambda\tau_2}} = \frac{\sigma}{1 + \sigma - e^{-\mu\sigma}}.$$

Ultimately, we obtain a linearized system of equations for the active zone:

$$\frac{l}{\tau_1 \xi\beta}\cdot\frac{dy}{d\tau} = y_1 - y - Az, \tag{10}$$

$$\frac{dy_1}{d\tau} = \frac{\sigma}{\xi}(y - y_1) - e^{-\mu\sigma}[y_1 - y_1(\tau - \mu)], \tag{11}$$

$$\frac{dz}{d\tau} = z_{\text{in}} - z + ay, \tag{12}$$

where z_{in} is the change of temperature of the fuel at the inlet to the active zone (at the exit from the heat exchanger):

$$z_{\text{in}}(\tau) = \int_0^{\tau} \varphi(\tau - x)\, z(x)\, dx. \tag{13}$$

Equations (10)-(13) comprise the complete linearized system of equations for the dynamics of the system being considered.

We shall compile the characteristic equation of the system (10)-(13), neglecting the lifetime of the prompt neutrons. This is permissible, because in cases of practical interest the parameter $l/\tau_1\xi\beta$ is small*, and the condition of unimportance of this parameter is fulfilled in the given case [8]. Having applied Laplace's transformation to equations (10)-(13) for zero initial conditions and having compiled the characteristic determinant of the system, we obtain the characteristic equation

$$\frac{\sigma}{\xi} = (p + 1 + \sigma - e^{-\mu\sigma - \mu p})\left[1 + \frac{aA}{p + 1 - \Phi(p)}\right]. \tag{14}$$

Proof of Stability over a Small Region

The parameters σ, μ, a, and A and the heat exchanger parameters contained in $\Phi(p)$ appear in Eq. (14). (The importance factor ξ, according to Eq. (9), depends on μ and σ.) We shall show that with a negative temperature coefficient of reactivity (A > 0) the system being considered is stable over a small region for any physically attainable (positive) values of the parameters μ, σ, and a. First of all, we note that

$$Re\,\Phi(j\omega) < 1; \tag{15}$$

$$Re\,\Phi(u + jV) < 1 \quad \text{and} \quad u > 0. \tag{16}$$

Actually, according to expressions (6) and (7),

$$Re\,\Phi(j\omega) \leqslant |\Phi(j\omega)| = \left|\int_0^{\infty} \varphi(t)\, e^{-j\omega t}\, dt\right| \leqslant \int_0^{\infty} |\varphi(t)|\, dt < 1.$$

Similarly, denoting $e^{-ut}\ \varphi(t)$ by $\psi(t)$, we obtain

$$Re\,\Phi(u + jv) \leqslant |\Phi(u + jv)| = \left|\int_0^{\infty} \psi(t)\, e^{-jvt}\, dt\right| \leqslant \int_0^{\infty} |\psi(t)|\, dt < \int_0^{\infty} \varphi(t)\, dt < 1,$$

since, for u > 0, $0 < \psi(t) < \varphi(t)$ at every instant of time.

We compile the formulas of the D-subdivisions [9] of the plane of the real parameters μ and σ. If we assume in expression (14) that $p = j\omega$ and we separate the imaginary and real parts, we obtain the equations for the D-curve in the form

*As a rule, $l \approx 10^{-5}$-10^{-4} sec, $\tau \geqslant 1$ sec, $0.5 < \xi < 1$ and, consequently, $l/\tau_1\xi\beta < 10^{-2}$.

$$aA\frac{[1-Re\,\Phi(j\omega)](1+\sigma-e^{-\mu\sigma}\cos\mu\omega)+[\omega-Im\,\Phi(j\omega)](\omega+e^{-\mu\sigma}\sin\mu\omega)}{[1-Re\,\Phi(j\omega)]^2+[\omega-Im\,\Phi(j\omega)]^2}+e^{-\mu\sigma}(1-\cos\mu\omega)=0,\qquad(17)$$

$$aA\frac{[1-Re\,\Phi(j\omega)](\omega+e^{-\mu\sigma}\sin\mu\omega)-[\omega-Im\,\Phi(j\omega)](1+\sigma-e^{-\mu\sigma}\cos\mu\omega)}{[1-Re\,\Phi(j\omega)]^2+[\omega-Im\,\Phi(j\omega)]^2}+\omega+e^{-\mu\sigma}\sin\mu\omega=0,$$

where the real parameter ω takes all positive values from 0 to infinity. In addition to the D-curve (17), the D-subdivision itself includes the singular-curve

$$1+\sigma-e^{-\mu\sigma}=0,\qquad(18)$$

corresponding to the value $\omega = 0$.

It is obvious that the singular curve lies outside the region $\sigma > 0$, $\mu \geq 0$, since in this region $1 + \sigma - e^{\mu\sigma} > 0$. We shall show that the D-curve is also located outside this region. Let us consider Eq. (17). Depending on the actual values of μ, σ and ω, four cases are possible:

$$\left.\begin{aligned}\omega-Im\,\Phi(j\omega)&\lesseqgtr 0;\\ \omega+e^{-\mu\sigma}\sin\mu\omega&\gtreqless 0.\end{aligned}\right\}\qquad(19)$$

In view of expression (15), $1 - Re\Phi(j\omega) > 0$ and, consequently, it is not possible to satisfy Eq. (17) simultaneously in any of the four cases. This means that if the inequalities (19) have identical sense, the first equation of (17) will not be satisfied; if the inequalities of (19) have opposite sense, then the second equation of (17) will not be satisfied. Thus, neither the singular straight line (18) nor the D-curve (17) lies in the region of $\mu \geq 0, \sigma > 0$. Consequently, for proof of the stability of the unit, it is sufficient to show that all the roots of the characteristic Eq. (14) have negative real parts at any single point of the region $\mu \geq 0$, $\sigma > 0$. We choose as an example the point with the coordinates $\mu = 0$ (σ is some positive number). In this case, the characteristic Eq. (14) will have the form

$$\sigma=(p+\sigma)\left[1+\frac{aA}{p+1-\Phi(p)}\right].\qquad(20)$$

Let us assume the contrary: suppose that Eq. (20) has roots with a positive real part and that $p = u + jv$ is one of these roots ($Re\ p = u > 0$). We substitute $p = u + jv$ in Eq. (20) and we separate the imaginary and real parts. As a result we obtain the system of identities:

$$\frac{u+\sigma}{1+U}=-\frac{v}{V};\quad u+(u+\sigma)U=vV,\qquad(21)$$

where

$$\left.\begin{aligned}U&=aA\frac{u+1-Re\,\Phi(u+jv)}{[u+1-Re\,\Phi(u+jv)]^2+[v-Im\,\Phi(u+jv)]^2};\\ V&=aA\frac{-v+Im\,\Phi(u+jv)}{[u+1-Re\,\Phi(u+jv)]^2+[v-Im\,\Phi(u+jv)]^2}.\end{aligned}\right\}\qquad(22)$$

According to inequality (16), $U > 0$ and, consequently, the left-hand sides in Eq. (21) are always positive. This latter shows that whatever be the signs of v and V, it is not possible to satisfy simultaneously the identities of (21). Consequently, the characteristic Eq. (20) has no root with a positive real part and the point of the μ, σ plane which we selected belongs to the region of stability. Thus, stability over a small region is proved.

Reactor without Delayed Neutrons

The resulting (nonlinear) system in this limiting case has the form:

$$\left.\begin{aligned}\frac{l}{\tau_1}\cdot\frac{dy}{d\tau}&=-\varepsilon z(1+y);\\ \frac{dz}{d\tau}&=z_{in}-z+ay.\end{aligned}\right\}\qquad(23)$$

It is easy to demonstrate here the stability of the unit being considered in relation to arbitrary deviations of the variables from the equilibrium state, i. e., overall stability. We compile the transfer constant G(p) from power to reactivity, taken with the reverse sign. To an accuracy of up to constant positive coefficients

$$G(p)=\frac{1}{p+1-\Phi(p)}.\qquad(24)$$

According to the Velton-Smets criterion [10], it is sufficient for stability of the reactor that

$$Re\, G(j\omega) > 0 \text{ for all values of } \omega > 0. \tag{25}$$

After substituting $p = j\omega$ in Eq. (24), we obtain

$$Re\, G(j\omega) = \frac{1 - Re\, \Phi(j\omega)}{[1 - Re\, \Phi(j\omega)]^2 + [\omega - Im\, \Phi(j\omega)]^2} > 0$$

by virtue of Eq. (15). Consequently, overall stability is proved.

The author thanks N. A. Zheleztsova and E. F. Sabaeva for critical comments and interest in this work.

LITERATURE CITED

1. W. Ergen, J. Appl. Phys., 25, 6, 702 (1954).
2. W. Ergen and A. Weinberg, Physica, 20, 7, 413 (1954).
3. J. Fleck, BNL-357 (1955).
4. R. Figueuredo, Report No. 1815, presented at the Second International Conference on the Peaceful Uses of Atomic Energy [Russian translation] (Geneva, 1958).
5. Yu. R. Kharper, Basic principles of fission reactors, Chapter 10 [in Russian], Moscow, Gosatomizdat (1963).
6. M. A. Schultz, Control of nuclear reactors and power plants, McGraw-Hill (1961).
7. B. N. Devyatov, Dokl. AN SSSR, 130, 68 (1960).
8. A. B. Vasil'eva and V. F. Butuzov, in the collection "Numerical methods of solving differential and integral equations and quadrature formulas " [in Russian], Moscow, Nauka (1964).
9. Yu. I. Neimark, Stability of linearized systems [in Russian], Leningrad Air Force Engineering Academy, Leningrad (1949).
10. H. Smets, J. Appl. Phys., 30, 1623 (1959).

IN MEMORIAM: HOMI JEHANGIR BHABHA

D. I. Blokhintsev

The aircraft Kanchenjanga crushed on the slopes of Mt. Blanc on January 24 of this year. There were no survivors.

Several days earlier the renowned Indian physicist Homi Jehangir Bhabha, on his way to a meeting of the scientific consultative council of the International Atomic Energy Agency, had changed his ticket from a January 22 flight to a January 24 flight . . . Who is capable of predicting his own fate ? Homi Bhabha was among the victims of the tragedy occurring on the slopes of Mt. Blanc.

News of his death profoundly moved all of us who had the pleasure of becoming acquainted with this outstanding man, talented physicist, prominent organizer of India's atomic science program, consistent fighter for the peaceful uses of atomic energy, and profound and able connoisseur of literature, sculpture, and music.

The mutual acquaintance of Soviet physicists and Homi Bhabha was by written word at the beginning. In 1937 he published, jointly with W. Heitler, work on the cascade theory of electron-photon showers in cosmic rays [1-3]. This theory became the basic theory for understanding the behavior of the soft component of cosmic radiation. Other contributions by Homi Bhabha dealt with a topic of high current interest, the theory of mesons and particles with higher-order spins [4-6]. He was the first to point out the fact that a moving meson has a longer lifetime than a meson at rest. The famous "twin paradox" of Einstein's relativity theory was carried over from the realm of theoretical abstraction to phenomena observed in reality.

Only very recently, physicists of the Joint Institute for Nuclear Research returned to a work of Homi Bhabha [7] in their study of the structure of the meson, to gain insight on the scattering of particles of spin $^1/_2$ by particles of spin 0.

The scientific achievements of Homi Bhabha were given their due when he was elected member of the British Royal Society (1941), and honorary member of the Royal Society of Edinburgh (1957). He was awarded the Adams prize (1942) and the Hopkins prize (1948).

In the post-war period, Homi Bhabha distinguished himself as an outstanding organizer of Indian atomic science and engineering. This was a turning point in the development of physics when the scale of physical experiment underwent a transition from the scale of the laboratory bench to the scale of modern reactors and accelerators, and the staffs of physics institutes expanded from several dozen members to many hundreds and even thousands.

Homi Bhabha correctly evaluated the significance of this turning point and was convinced that his own homeland was capable of playing its part creatively in the contemporary scientific and technical revolution.

When one of the public officials responsible for atomic science attempted to prove the impossibility of the developing countries mastering atomic science and engineering before traditional and older stages of science and engineering had been developed, Homi Bhabha protested vigorously against this variety of shortsighted snobbism.

The Institute of Fundamental Research was founded in Bombay in 1945 on the initiative of Homi Bhabha. Characteristic traits of the initiator of the institute are manifested in the style of the institute. The institute is not only equipped with modern instrumentation, but is embellished with modern literature and sculpture in a delicate and tasteful manner. Art and science, combined here by the deliberate design of Homi Bhabha, serve to create an atmosphere of intellectual culture on a high level.

Not far from Bombay Homi Bhabha founded a second center, the atomic center of Trombay, which he viewed as providing a foundation for the development of India's nuclear power program.

In this "Sturm and Drang" period of post-war atomic science and industry, I had the opportunity to become personally acquainted with Homi Bhabha, who twice visited the World's First Nuclear Power Station at Obninsk following the visits of Jawaharlal Nehru and Indira Gandhi. In 1955, Homi Bhabha chaired the first international

Translated from Atomnaya Énergiya, Vol. 21, No. 1, pp. 7-8, July, 1966

conference on the peaceful uses of atomic energy at Geneva, where the leading nations informed the world of their achievements in the development of atomic power. It was then for the first time that the veil of secrecy surrounding the work of atomic scientists was lifted and that these scientists, already grown accustomed to lack of communication with each other, found to their surprise that scientific truth, like gold, is the same no matter in what part of the earth it is mined.

At that time Homi Bhabha represented a country in which most of the necessary power was furnished by human labor and buffalo.

What was it that placed Homi Bhabha in the chairman's seat at the famous 1955 conference? My feeling is that the basis for the deep respect accorded to Homi Bhabha was his profound faith that the great conquest of human intellect—the mastery of the fission chain reaction in uranium and plutonium—will be used only for the welfare of mankind, and not for war, destruction and annihilation.

Homi Bhabha remarked more than once that India "has the know-how to make an atomic bomb, and has the necessary materials, but will not use them for this purpose."

Even at the first Geneva conference, Homi Bhabha expressed his conviction that in the not too distant future mankind will be in possession of an almost inexhaustible source of energy—the energy of thermonuclear fusion. Now we are less optimistic about that, but work is proceeding ahead, the search is being continued, and it would be incorrect to think that these hopes must be abandoned.

Homi Bhabha's profound faith in the high purpose of science, his conviction in the triumph of reason, clearly flowed from the fortunate combination of high level of scientific culture and the traditional spirit of Indian wisdom, a humanistic and peace loving wisdom which gave birth to the famous "Panch sila" principles.

Homi Bhabha had a deep understanding of the fact that the end does not justify the means. There are bounds beyond which the means will destroy the very essence of the end. The use of atomic weaponry is just such a means, no matter how "important" or how "noble" the ends.

Homi Bhabha took an active part in the work of international organizations. He was a member of the scientific consultative council of the International Atomic Energy Agency (IAEA), where he actively defended the interests of the developing nations.

For several years he headed the Presidium of the International Union of Pure and Applied Physics (IUPAP). As President of this body, Homi Bhabha exercized great tact in combining the interests of persons representing different nations, different political systems, and different races. It was always a pleasure to me to see in him the prototype of the man of the future, with a deep understanding of the interests of mankind and a capability of standing above the temporary but tragic bounds which separate mankind today.

We shall always retain a shining memory of Homi Bhabha.

This article was reprinted from Uspekhi fizicheskikh nauk 89, No. 1, 173 (1966).

LITERATURE CITED

1. H. J. Bhabha and W. Hettler, Proc. Roy. Soc., A 159, 432 (1936).
2. H. J. Bhabha and S. K. Chakrabarty, Proc. Ind. Sci., A15, 464 (1942).
3. H. J. Bhabha and S. K. Chakrabarty, Phys. Rev., 74, 1352 (1948).
4. H. J. Bhabha, Proc. Roy. Soc., A166, 501 (1938).
5. H. J. Bhabha, Rev. Mod. Phys., 17, 200 (1945).
6. H. J. Bhabha, Phil. Mag., 43, 33 (1952).
7. H. J. Bhabha. Proc. Roy. Soc., A164, 257 (1958).

INVERSE SOLUTION OF THE KINETIC EQUATIONS OF A NUCLEAR REACTOR

I. N. Brikker

UDC 621.039.515

A function is derived from the kinetic equations of nuclear reactors that can be used in the determination of the variation of the multiplication coefficient if the variation of the neutron density is known, and also in the derivation of the law of variation of the multiplication coefficient that will yield a given variation of the neutron density.

It is known [1] that the dynamics of the processes taking place in nuclear reactors are governed by the kinetic equations

$$\frac{dn}{dt} = \frac{K_{\text{eff}} - 1 - \beta K_{\text{eff}}}{l} n + \sum_{i=1}^{N} \lambda_i c_i + s, \tag{1}$$

$$\frac{dc_i}{dt} = \frac{\beta_i}{l} K_{\text{eff}}\, n - \lambda_i c_i \quad (i = 1,\ 2,\ 3,\ \ldots,\ N), \tag{2}$$

where n (t) is the neutron density, c_i (t) and λ_i are the concentration and decay constant of the radiators of delayed neutrons of the ith group, i; β_i is the field of the delayed neutrons of the i-th group, i; β and $\sum_i \beta_i$ is the total field of delayed neutrons, l is the mean life of prompt neutrons, K_{eff} is the effective multiplication coefficient of the neutrons, and s(t) is the strength of extraneous neutron sources.

The kinetic equations are usually solved to determine the law of variation of neutron density if the multiplication coefficient varies according to a given law, i. e., a functional $n\{K_{\text{eff}}(t)\}$ is found. It is of interest to find the functional $K_{\text{eff}}\{n(t)\}$ which can be used: 1) for the determination of K_{eff} when the neutron density is known for all preceding times; 2) in the planning of optimum systems of automatic control to find the law of variation of K_{eff} for which n(t) varies according to a given law $n_3(t)$; 3) in the determination of the characteristics of the executive mechanisms and of the absorbing rods ensuring a given law of variation of the neutron density.

The problem of finding the functional $K_{\text{eff}}\{n(t)\}$ is posed and solved in [1] for linearized kinetic equations. In [2] this problem is solved for a special case (considered below), but the method used cannot be employed to find the desired functional for l = const. In the present work we give a complete solution of the problem.

We consider a reactor controlled by influencing the absorption or dissipation of neutrons. In this case, as shown in [3], l is not constant but depends on K_{eff}:

$$l = \Lambda K_{\text{eff}} \tag{3}$$

where the generation time Λ is constant. The values of Λ and l are identical in the critical case.

If this expression for l and the reactivity

$$\varrho = \frac{K_{\text{eff}} - 1}{K_{\text{eff}}}, \tag{4}$$

are used, relations (1) and (2) yield

$$\frac{dn}{dt} = \frac{\varrho - \beta}{\Lambda} n + \sum_{i=1}^{N} \lambda_i c_i + s, \tag{5}$$

$$\frac{dc_i}{dt} = \frac{\beta_i}{\Lambda} n - \lambda_i c_i \qquad (i = 1,2,3,\ \ldots,\ N). \tag{6}$$

We assume that the reactor is in equilibrium for t < 0, i. e.,

Translated from Atomnaya Énergiya, Vol. 21, No. 1, pp. 9-13, July, 1966. Original article submitted November 20, 1965; revised February 2, 1966.

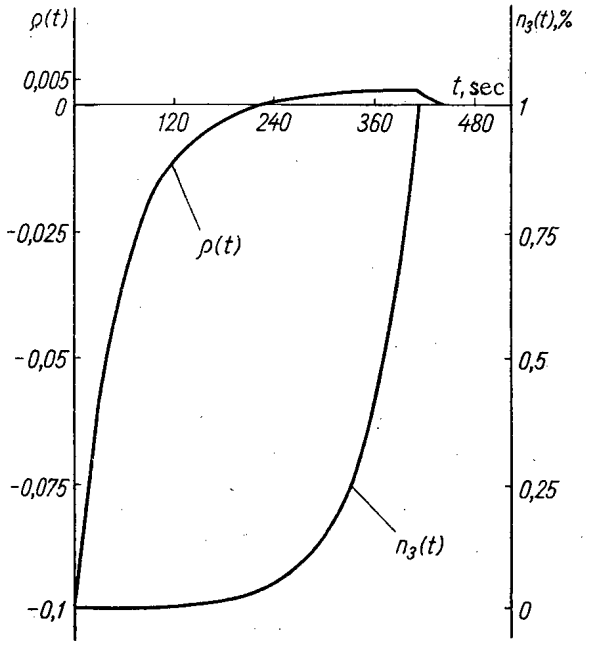

Fig. 1. Variation of reactivity for exponential reactor runaway with a given period.

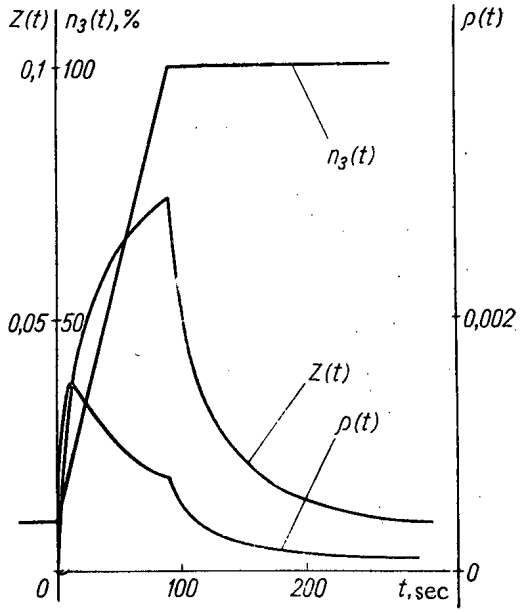

Fig. 2. Variation of reactivity for a linear increase in the neutron current level.

$$n(0) = -\frac{\Lambda s(0)}{\varrho(0)}; \tag{7}$$

$$c_i(0) = \frac{\beta_i}{\Lambda\lambda_i} n(0). \tag{8}$$

In (5) and (6) we introduce the auxiliary variable z(t) = n (t) ρ(t) and then take the Laplace transform of the resulting equations:

$$\Lambda[pN(p) - n(0)] = Z(p) - \beta N(p) + \Lambda \sum_{i=1}^{N} \lambda_i C_i(p) + \Lambda S(p), \tag{9}$$

$$\Lambda[pC_i(p) - c_i(0)] = \beta_i N(p) - \Lambda\lambda_i C_i(p), \tag{10}$$

where

$$N(p) = Ln(t);\ Z(p) = Lz(t),$$
$$C_i(p) = Lc_i(t);\ S(p) = Ls(t)$$

(L denotes the direct Laplace transformation).

Substituting $C_i(p)$ from (10) in (9) and using (8), we have

$$Z(p) = \Lambda[pN(p) - n(0) - S(p)] + [pN(p) - n(0)] \sum_{i=1}^{N} \frac{\beta_i}{p+\lambda_i}. \tag{11}$$

We now apply the convolution theorem and obtain

$$\varrho(t) = \frac{1}{n(t)} \left\{ \Lambda\left(\frac{dn}{dt} - s\right) + \sum_{i=1}^{N} \beta_i \int_0^t \frac{dn}{d\tau} \exp[-\lambda_i(t-\tau)]\, d\tau \right\}. \tag{12}$$

This formula permits the complete solution of the above problem and the determination of the desired functional.

We consider the case in which the reactor is controlled by varying the fission cross section (l = const).

We introduce the excess multiplication factor

$$\Delta K = K_{\text{eff}} - 1 \tag{13}$$

and the auxiliary variable z(t) = n(t)ΔK(t). If we now apply the above reasoning to (1) and (2), we obtain

$$Z(p) = \left\{ l[pN(p) - n(0) - S(p)] + [pN(p) - n(0) - z(0)] \sum_{i=1}^{N} \frac{\beta_i}{p+\lambda_i} \right\} \left[1 - p \sum_{i=1}^{N} \frac{\beta_i}{p+\lambda_i} \right]^{-1}. \tag{14}$$

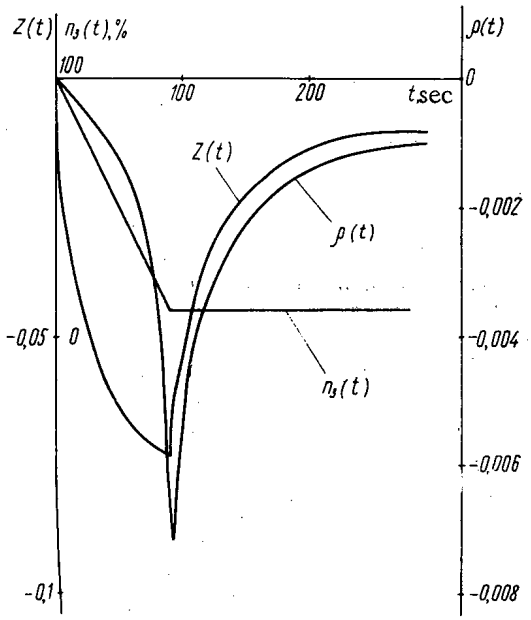

Fig. 3. Variation of reactivity for a linear decrease in the neutron current level.

We denote the inverse Laplace transformation by L^{-1} and write

$$\varphi(t) = L^{-1}\Phi(p), \tag{15}$$

where

$$\Phi(p) = \left[1 - p\sum_{i=1}^{N}\frac{\beta_i}{p+\lambda_i}\right]^{-1} = (1-\beta)^{-1} - \left[1 + \sum_{i=1}^{N}\frac{\beta_i\lambda_i}{(1-\beta)(p+\lambda_i)}\right]^{-1}\sum_{i=1}^{N}\frac{\beta_i\lambda_i}{(1-\beta)(p+\lambda_i)} \tag{16}$$

Applying the operation L^{-1} term by term to (14) and using the convolution theorem, we have

$$\Delta K(t) = \frac{1}{n(t)}\left\{l\int_0^t\left(\frac{dn}{d\tau} - s\right)\varphi(t-\tau)\,d\tau + \int_0^t\frac{dn}{d\tau}\int_0^{t-\tau}\sum_{i=1}^{N}\beta_i\exp[-\lambda_i\vartheta]\,\varphi(t-\tau-\vartheta)\,d\tau\,d\vartheta - z(0)\int_0^t\sum_{i=1}^{N}\beta_i\exp[-\lambda_i\tau]\,\varphi(t-\tau)\,d\tau\right\}. \tag{17}$$

The weighting function $\varphi(t)$ in (17) can be determined exactly from (15) and (16), since λ_i and β_i are known for any given reactor. In the single-group approximation, for example, (15) and (16) easily yield

$$\varphi(t) = \frac{\delta(t)}{1-\beta} - \frac{\lambda\beta}{(1-\beta)^2}\exp\left[-\frac{\lambda t}{1-\beta}\right], \tag{18}$$

which, since $\beta \ll 1$, can be simplified to

$$\varphi(t) = (1+\beta)\,\delta(t) - \lambda\beta\exp[-\lambda t]. \tag{19}$$

In multigroup approximations, the derivation of an exact expression for $\varphi(t)$ is very laborious, and for $N > 4$ there is in general no analytic solution, although we can find a solution with any desired degree of accuracy. Numerical solution is not required in practice, however, since if we use the fact that $\beta \ll 1$ we can determine the functional analytically with sufficient accuracy.

In fact, if we neglect terms of the order of β compared with unity in (16) and (17), we can obtain the relation

$$\Delta K(t) = \frac{1}{n(t)}\left\{l\left(\frac{dn}{dt} - s\right) + \sum_{i=1}^{N}\beta_i\int_0^t\frac{dn}{d\tau}\exp[-\lambda_i(t-\tau)]\,d\tau\right\}. \tag{20}$$

after some transformations.

To find the next term in the expansion in powers of β, we leave out the constant component and introduce a correction function. This operation yields an expression for $\varphi(t)$ with a precision up to terms of the order β:

$$\varphi(t) = (1+\beta)\,\delta(t) - \sum_{i=1}^{N}\lambda_i\beta_i\exp[-\lambda_i t]. \tag{21}$$

Formulas (19) and (21) coincide in the single-group approximation.

Substituting the expression (21) for $\varphi(t)$ in (17), we obtain the following formula with the same accuracy:

$$\Delta K(t) = \frac{1}{n(t)}\left\{l(1+\beta)\left(\frac{dn}{dt} - s\right) + l\sum_{i=1}^{N}\lambda_i\beta_i\int_0^t s(\tau)\exp[-\lambda_i(t-\tau)]\,d\tau + \int_0^t\frac{dn}{d\tau}\left\{\sum_{i=1}^{N}\beta_i\exp[-\lambda_i(t-\tau)]\left[1+\beta-\beta_i\lambda_i(t-\tau) - \sum_{k\neq i}^{N}\beta_k\frac{\lambda_k+\lambda_i}{\lambda_k-\lambda_i} - l\lambda_i\right]\right\}d\tau\right.$$

$$+ls(0)\sum_{i=1}^{N}\beta_i\exp(-\lambda_i t)\left[1+\beta-\beta_i\lambda_i t-\sum_{k\neq i}^{N}\beta_k\frac{\lambda_k+\lambda_i}{\lambda_k-\lambda_i}\right]\Big\rangle. \tag{22}$$

We note that (20) follows from (12) if $\Lambda = l = \text{const}$ and $\Delta K = \rho$, i. e., $K_{eff} \approx 1$. Because of the smallness of β, Eqs. (1) and (2) with ρ replaced by ΔK coincide formally with (5) and (6) independently of K_{eff}, if $\Lambda = l = \text{const}$; this is in agreement with the results of a comparison of the functionals (12) and (20), or it follows from the kinetic equations. In fact, transforming in (14) to the original functions we have

$$z(t)+l\left(s-\frac{dn}{dt}\right)=\sum_{i=1}^{N}\beta_i\int_0^t\left(\frac{dn}{d\tau}+\frac{dz}{d\tau}\right)\exp\left[-\lambda_i(t-\tau)\right]d\tau. \tag{23}$$

It follows similarly from (11) that

$$z(t)+\Lambda\left(s-\frac{dn}{dt}\right)=\sum_{i=1}^{N}\beta_i\int_0^t\frac{dn}{d\tau}\exp\left[-\lambda_i(t-\tau)\right]d\tau. \tag{24}$$

Using the relation between n(t) and z(t) and (23) or (24), we can derive differential equations for n(t) which coincide when terms of the order of n(t) are neglected compared with unity and β is replaced by l Λ and ΔK by ρ. For example in the single-group approximation (23) and (24) become

$$l\frac{dn^2}{dt^2}+[\beta-(1-\beta)\Delta K+\lambda l]\frac{dn}{dt}-\left[\lambda\Delta K+(1-\beta)\frac{d\Delta K}{dt}\right]n=l\frac{ds}{dt}+\lambda ls, \tag{25}$$

$$\Lambda\frac{dn^2}{dt^2}+(\beta-\varrho+\lambda\Lambda)\frac{dn}{dt}-\left(\lambda\varrho+\frac{d\varrho}{dt}\right)n=\Lambda\frac{ds}{dt}+\lambda\Lambda s. \tag{26}$$

In conclusion we consider some examples illustrating the above results.

1. We first find the law of variation of $\rho(t)$ for which the power of the reactor will be converted from power n_0 to power n_1 with conversion exponent τ_0, i. e.,

$$n_3(t)=\begin{cases} n_0, & t\leqslant 0;\\ n_0\exp\left[\frac{t}{\tau_0}\right], & 0\leqslant t\leqslant t_1;\\ n_1=n_0\exp\left[\frac{t_1}{\tau_0}\right], & t\geqslant t\end{cases}$$

(the strength of the sources is taken to be constant). Using (12) for $n_3(t)$, we have

$$\varrho(t)=\begin{cases} -\frac{\Lambda s}{n_0}, & t<0;\\ \frac{\Lambda}{\tau_0}-\frac{\Lambda s}{n_0}\exp\left[-\frac{t}{\tau_0}\right]\\ +\sum_{i=1}^{N}\frac{\beta_i}{(1+\lambda_i\tau_0)}\left\{1-\exp\right.\\ \left.\times\left[-\left(\lambda_i+\frac{1}{\tau_0}\right)t\right]\right\}, & 0\leqslant t<t_1;\\ -\frac{\lambda s}{n_1}+\sum_{i=1}^{N}\frac{\beta_i}{(1+\lambda_i\tau_0)}\\ \times\left\{1-\exp\left[-\left(\lambda_i\right.\right.\right.\\ \left.\left.\left.+\frac{1}{\tau_0}\right)t_1\right]\right\}\\ \times\exp\left[-\lambda_i(t-t_1)\right], & t\geqslant t_1.\end{cases}$$

It follows from the expression for $\rho(t)$ that the reactivity changes discontinuously by a value Λ/τ_0 for $t = 0$. A transitional process follows, leading to the establishment of a constant reactivity

$$\varrho_0 = \frac{\Lambda}{\tau_0} + \sum_{i=1}^{N} \frac{\beta_i}{(1+\lambda_i\tau_0)}.$$

It is easily seen that this is the formula for a reversible process. At time $t = t_1$ the value of $\rho(t)$ alters discontinuously by $-\Lambda s/n_1$ and then a transitional process again commences, which ends with a disruption of the delayed-neutron radiator. Here the reactivity is $-\Lambda s/n_1$. Figure 1 shows graphs of $\rho(t)$ and $n_3(t)$ for $n_1 = 1\%$, $n_0 = 10^{-3}\%$, $\tau_0 = 60$ sec, and $s = 1\%/\text{sec}$. The discontinuities Λ/τ_0 and $\Lambda s/n_1$ are practically imperceptible because of the smallness of Λ.

The graphs in Fig. 1 and 2 are for $\Lambda = 10^{-4}$ sec, $\beta = 0.0065$ and values of λ_i and β_i, taken from [5].

2. We determine the form of $\rho(t)$ for which the power of a reactor will vary linearly from the level n_0 to the level n_1, i. e.,

$$n_3(t) = \begin{cases} n_0, & t \leqslant 0; \\ n_0 + Vt, & 0 \leqslant t \leqslant t_1; \\ n_1 = n_0 + Vt_1, & t \geqslant t_1. \end{cases}$$

Source effects are neglected. From (12) we have

$$\varrho(t) = \begin{cases} 0 & t < 0; \\ \dfrac{V}{n_0+Vt}\left\{\Lambda + \sum\limits_{i=1}^{N}\dfrac{\beta_i}{\lambda_i} \times \left(1-\exp\left[-\lambda_i t\right]\right)\right\} & 0 \leqslant t < t_1; \\ \dfrac{V}{n_1}\left\{\sum\limits_{i=1}^{N}\dfrac{\beta_i}{\lambda_i}\left(1-\exp \times\left[-\lambda_i t_1\right]\right)\right\} \times \exp\left[-\lambda_i(t-t_1)\right] & t \geqslant t_1. \end{cases}$$

In this case the reactivity varies discontinuously for $t = 0$ by an amount $V\Lambda/n_0$ and $z(t) = n_3(t)\,\rho(t)$ varies by an amount $V\Lambda$. A transitional process then sets in, leading to the establishment of a constant value $z_0 = V\left(\Lambda + \sum\limits_{i=1}^{N}\dfrac{\beta_i}{\lambda_i}\right)$; during linear variation of the power, the reactivity must vary according to the law

$$\varrho(t) = \frac{V\left(\Lambda + \sum\limits_{i=1}^{N}\dfrac{\beta_i}{\lambda_i}\right)}{n_0+Vt}.$$

At time $t = t_1$ another transitional process starts, which ends with the disintegration of the delayed-neutron radiator and the reactivity falls to zero. In Fig. 2 we show graphs of $n_3(t)$, $\rho(t)$ and $z(t)$ corresponding to an increase in power from $n_0 = 10\%$ to $n_1 = 100\%$ at a rate of $1\%/\text{sec}$. Figure 3 contains graphs of the same quantities for a fall at the same rate from $n_0 = 100\%$ to $n_1 = 10\%$.

3. We now determine the $\rho(t)$ for which the reactor power varies according to the law

$$n_3(t) = \begin{cases} n_0, & t \leqslant 0; \\ n_0\left\{\dfrac{\beta}{\beta-\delta K_0}\exp\left[\dfrac{\lambda\delta K_0}{\beta-\delta K_0}t\right] - \dfrac{\delta K_0}{\beta-\delta K_0}\exp\left[-\dfrac{\beta-\delta K_0}{\Lambda}t\right]\right\}, & t \geqslant 0. \end{cases}$$

We consider the single-group approximation without sources. Substituting $n_3(t)$ in (12) and using the inequality $\lambda \Lambda \ll \beta - \delta K_0$, we obtain $\rho(t) = \delta K_0$ for $t \geq 0$ and $\rho(t) = 0$ for $t < 0$, which agrees with the results in [6], in which the above law is the solution of the single-group kinetic equations with the above inequality and the discontinuity δK_0 in the reactivity for $t = 0$ taken into account.

The author wishes to thank A. I. Mogil'ner, A. B. Almazov, and A. R. Mirzoyan for their discussions of the work, and also I. V. Nazarova for constructing the graphs and for her help in writing the text.

LITERATURE CITED

1. Nuclear Reactors, T. I. M. [Russian translation], Izd-vo inostr lit. (1956).
2. R. Myrray, C. Bingham, and C. Martin, Nucl. Sci. and Engng, 18, 481 (1964).
3. G. Lewins, Nucl. Sci. and Engng, 7, 122 (1960).
4. S. Glasstone and M. C. Edlund, Elements of Nuclear-Reactor Theory, Van Nostrand (1952).
5. A. G. Sandmaier, Kinetics and Stability of Fast-Neutron Reactors [in Russian], Moscow, Gosatomizdat (1963).
6. M. A. Schultz, Control of Nuclear Power Reactors, McGraw-Hill (1961).

HYDRAULIC RESISTANCE OF NARROW ANNULAR CHANNELS WITH HELICAL FINS

V. I. Subbotin, P. A. Ushakov, and A. V. Sheinina

UDC 621.039.546.3

Hydraulic losses in narrow (d/D = 0.895) annular channels with three fins wound helically on a central column were measured. For relative fin pitches of $3.5 < T/d < \infty$, the hydraulic losses under turbulent flow conditions are mainly determined by frictional losses at the channel walls. These losses may be calculated from the ordinary formulas for an annular channel without fins. An increase in the hydraulic resistance of the channel for a fixed liquid flow rate only becomes appreciable for small relative fin pitches ($T/d < 10$). The data obtained for annular channels approximately coincide with measurements of hydraulic losses in staggered bundles of finned rods with S/d = 1.05 in a longitudinal flow of heat carrier.

In some reactors the cylindrical fuel elements are cooled by a heat carrier flowing in annular channels. Longitudinal fins are used for centering the fuel elements. Technological tolerances for the dimensions of the fuel elements and channels, however, fail to guarantee precise centering, even in the presence of fins; this is particularly apparent for narrow channels.

The existence of eccentricity leads to nonuniform temperatures around the perimeter of the fuel elements. For molten-metal heat carriers this nonuniformity is due mainly to nonuniformity of the preheating of the heat carrier at various points on the perimeter of the channel.

Helical finning tends to even out the temperature around the perimeter of the fuel elements. With diminishing fin pitch (T/d) the efficiency of this increases, but the hydraulic losses also become greater.

In the present investigation we studied the effect of fin pitch on the hydraulic resistance of narrow annular channels.

The experimental arrangement constituted a closed circuit with a centrifugal pump. The various components of the circuit were made of stainless steel. Experiments were made with distilled water under isothermal conditions at a temperature of 6 to 50° C.

The arrangement of the experimental channel is shown in Fig. 1. An outer tube of stainless steel was machined on its inner surface to a diameter of D = 95 ± 0.05 mm. The inner Dural rod, with d = 85 ± 0.05 mm, had three helical brass fins fixed to the rod with screws. The diameter of the rod over the fins was 95 ± 0.1 mm; the width of the fins was b = 5.4 ± 0.1 mm. The surface was given a Class-7 finish. The length of the annular slit with d/D = = 0.895 was 1900 mm.

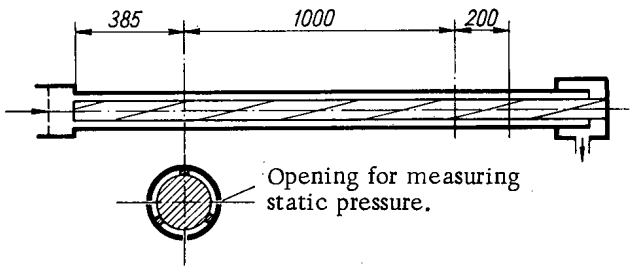

Fig. 1. Arrangement of experimental channel.

Openings for measuring static pressure, 0.8 mm in diameter, were made in sections at distances of 385, 1385, and 1585 mm from the entrance. Three such openings were provided at each section.

The pressure drops were measured with glass differential manometers filled with mercury, tetrabromoethane, carbon tetrachloride, chlorobenzene, or aniline, depending on the extent of the pressure drop. Three pressure drops were measured at the same time, since there were three pressure-measuring openings at each section. The pressure drops were then averaged.

Translated from Atomnaya Énergiya, Vol. 21, No.1, pp. 13-16, July, 1966. Original article submitted December 8, 1965.

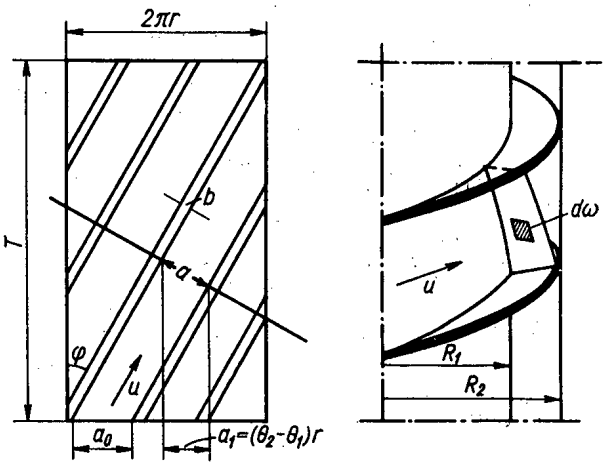

Fig. 2. Schematic representation of the geometric characteristics of the channel.

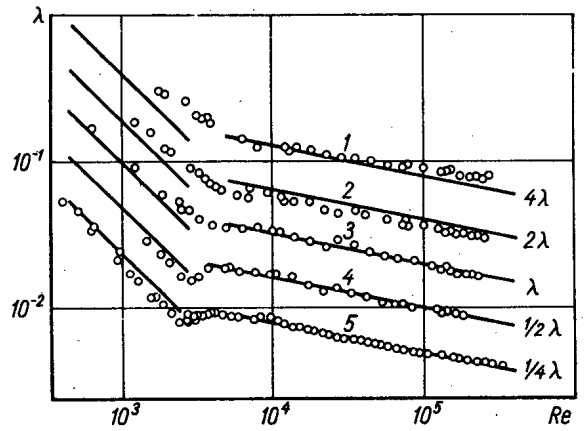

Fig. 3. Coefficient of friction λ as a function of Re in annular channels with finning: 1, 2, 3, 4) Experimental data for relative fin pitch T/d = 3.5, 6, 10, and 25 resepctively; 5) experimental data for an annular channel with longitudinal fins. Lines are constructed from formulas (11) to (13).

The water flow was measured with calibrated Venturi tubes or measuring tanks. The water temperature was monitored with copper resistance thermometers, and the room temperature (needed in order to determine the specific gravity of the liquids in the differential manometers) with mercury thermometers.

The coefficient of friction λ was determined from the formula:

$$\lambda = \frac{8\Delta p}{\rho V^2} \cdot \frac{\omega^3}{P\Delta L}, \tag{1}$$

where ω is the through cross section of the channel, P the wetted perimeter, ΔL the distance between the openings for measuring the pressure, V the volume flow of water, Δp the pressure drop, and ρ the density of the water.

The Reynolds numbers were calculated from the mean velocity and the equivalent hydraulic diameter of the channels: $Re = \bar{u}d_r/\nu = 4V/P\nu$.

The through cross section perpendicular to the current lines (Fig. 2) was determined from the expression

$$\omega = 3\int_{R_1}^{R_2}\int_{\theta_1}^{\theta_2} d\omega = 3\int_{R_1}^{R_2}\frac{r\,dr}{\cos\varphi}\int_{\theta_1}^{\theta_2} d\theta = 3\int_{R_1}^{R_2}\frac{r\,dr}{\cos\varphi}(\theta_2-\theta_1), \tag{2}$$

where R_1 and R_2 are the radii of the shell and central rod respectively, φ is the slope of the fin relative to the longitudinal axis, and θ is an angle reckoned in a plane perpendicular to the central-rod axis.

Remembering that

$$\theta_2-\theta_1 = \frac{a_0\cos^2\varphi}{r} = \frac{2\pi}{3}\cos^2\varphi - \frac{b}{r}\cos\varphi,$$

$$\cos\varphi = \frac{T}{\sqrt{T^2+(2\pi r)^2}}$$

(see Fig. 2) and carrying out the integration of formula (2), we obtain

$$\omega = \frac{\pi D^2}{4}(1-\Phi)\left[\frac{2\Phi\xi}{1-\Phi}(A-B)-\beta\right]. \tag{3}$$

Here we have used the following notation:

$$\Phi = \frac{d}{D}, \quad \xi = \frac{T}{\pi d}, \quad \beta = \frac{6b}{\pi D}, \quad A = \sqrt{1+(\Phi\xi)^2}, \quad B = \Phi\sqrt{1+\xi^2}.$$

The expression for the wetted perimeter is

$$P = 2\pi R_2\left[\Phi\cos\varphi_1 + \cos\varphi_2 + \frac{3}{\pi}(1-\Phi)-\beta\right],$$

where

$$\cos\varphi_1 = \frac{T}{\sqrt{T^2+(2\pi R_1)^2}} = \frac{\xi\Phi}{B}, \quad \cos\varphi_2 = \frac{T}{T^2+(2\pi R_2)^2} = \frac{\xi\Phi}{A}.$$

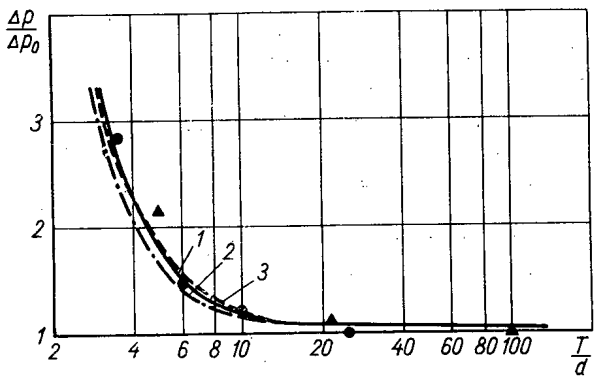

Fig. 4. Relative pressure drop as a function of the fin pitch for the turbulent condition with V = idem: ● – experimental data for an annular channel; ▲ – experimental data for longitudinally-washed staggered bundles, the rods of which each have four helical distance pieces (fins) (S/d = 1.05); 1), 2), 3) calculations from formulas (9), (10), and (14) respectively.

After some transformations we obtain

$$P = \pi D \left[\Phi\xi \left(\frac{1}{A} + \frac{\Phi}{B} \right) + \frac{3}{\pi} (1 - \Phi) - \beta \right]. \quad (4)$$

The effective length ΔL of the channel was found as the arithmetic-mean value of ΔL^{max} (for $r = R_1$) and ΔL^{min} (for $r = R_2$):

$$\frac{\Delta L}{\Delta L_0} = \frac{1}{\cos \varphi_2} + \frac{1}{\cos \varphi_1} = \frac{A+B}{2\Phi\xi}, \quad (5)$$

where ΔL_0 is the distance between the pressure-measuring openings along the axis of the central rod ($\Delta L_0 = \Delta L_{\varphi = 0}$).

For a channel with longitudinal fins ($\varphi = 0$),

$$\omega_0 = \frac{\pi D^2}{4} (1 - \Phi) [(1 + \Phi) - \beta], \quad (6)$$

$$p_0 = \pi D^2 \left[(1 + \Phi) + \frac{3}{\pi} (1 - \Phi) - \beta \right]. \quad (7)$$

The pressure losses in the channel may be expressed in the following way:

$$\Delta p = \lambda \frac{\varrho V^2}{8} \cdot \frac{P \Delta L}{\omega^3}. \quad (8)$$

For a particular liquid with a fixed flow rate V,

$$\frac{\Delta p}{\Delta p_0} = \frac{\lambda}{\lambda_0} \cdot \frac{P}{P_0} \cdot \frac{\Delta L}{\Delta L_0} \left(\frac{\omega_0}{\omega} \right)^3.$$

If we suppose that the coefficient of friction in channels with longitudinal and helical fins (λ_0 and λ) is described by the same formula, then, allowing for formulas (3) to (8), the relation for the hydraulic losses may be transformed into

$$\frac{\Delta p}{\Delta p_0} = \left(\frac{\omega_0}{\omega} \right)^3 \left(\frac{P}{P_0} \right)^{1+n} \frac{\Delta L}{\Delta L_0} = \frac{A+B}{2\Phi\xi} \left[\frac{(1+\Phi)+\beta}{\frac{2\Phi\xi}{A+B}(1+\Phi)-\beta} \right]^3 \left[\frac{\Phi\xi \left(\frac{1}{A} + \frac{\Phi}{B} \right) + \frac{3}{\pi}(1-\Phi)-\beta}{(1+\Phi)+\frac{3}{\pi}(1-\Phi)-\beta} \right]^{1+n}. \quad (9)$$

Assuming that for narrow annular gaps $\Phi \approx 1$, we obtain the approximate formula

$$\frac{\Delta p}{\Delta p_0} \approx \sqrt{\frac{1+\xi^2}{\xi}} \left(\frac{1-0.5\beta}{\frac{\xi}{\sqrt{1+\xi^2}} - 0.5\beta} \right)^{2-n}. \quad (10)$$

For turbulent conditions the value of n was taken as equal to 0.22 on the basis of experimental data obtained earlier by the authors for an annular channel without fins. The results of these experiments may be approximated by the following formulas:

$$\lambda = \frac{96}{Re} \quad \text{for} \quad Re < 3 \cdot 10^3, \quad (11)$$

$$\lambda = 0.24\, Re^{-0.22} \quad \text{for} \quad 6 \cdot 10^3 < Re < 10^5, \quad (12)$$

$$\lambda = 1.07\,(0.032 + 0.221 Re^{-0.237}) \quad \text{for} \quad Re > 10^5. \quad (13)$$

The measured values of hydraulic resistance for channels with longitudinal fins and fins wound into helices (T/d = 25, 10, 6, and 3.5) are shown in Fig. 3 in the form of λ: Re curves. The calculated limiting errors in the coefficient of friction λ were generally no greater than ± 8 to 9%. Exceptions were certain experiments with low Reynolds numbers, for which aniline was used as working liquid in the differential manometers. In this case the limiting calculated errors reached about 20% (T/d = 3.5, Re < 4000).

For a channel with longitudinal fins, under laminar flow, the experimental points lie 10 to 15% below the calculated line λ = 96/Re. A channel formed by two cylindrical surfaces and fins is approximately equivalent to a rectangle with side ratio 0.06. The coefficient of friction in such a rectangle under laminar flow is approximately 10% lower than in an infinite plane slit, for which formula (11) holds.

As the fin pitch diminishes, the transition from the turbulent-flow condition of the liquid to the laminar condition draws out and becomes smoother. In every case of channels with T/d values of 3.5 and 6, pure laminar conditions have still not set in at Re = 1600 to 2000.

Under turbulent conditions there is satisfactory agreement between the experimental data and the results calculated from formulas (12) and (13) for the whole range of fin pitches studied. A certain difference between experimental and calculated data for T/d = 3.5 is probably due to errors in determining the geometric characteristics of the channel with helical fins. As the fin pitch diminishes, the error associated with the assumptions made in deriving formula (5) increases.

In the range of Re numbers studied (corresponding to the turbulent condition of liquid flow), the effect of the fin pitch on the pressure drop (Δp) had practically no effect on the Re number. Hence we may present the value of $\Delta P/\Delta P_0$ as a function of fin pitch T/d. This is done in Fig. 4, where the pressure losses in a channel with helical fins (Δp) are compared with those associated with longitudinal fins (Δp_0). The results agree with calculations from formula (9). This confirms that the energy losses in rotating the stream and forming eddies are small.

For approximate calculations it is more convenient to use the following simple formula (see Fig. 4):

$$\frac{\Delta p}{\Delta p_0} \approx 1 + \frac{20}{(T/d)^2} . \qquad (14)$$

The results of calculations from approximate formulas (10) and (14) were compared with those derived from formula (9). For T/d < 6, calculation from the approximate formula (10) with n = 0.22 gives slightly too low values of $\Delta p/\Delta p_0$. On the other hand, calculation with formula (14) gives slightly too high pressure drops. These deviations, however, are no more than 10 to 12%. For larger relative fin pitches the difference in the results calculated from formulas (10) and (14) diminishes.

Earlier, the authors studied the hydraulic resistance of staggered bundles of rods with S/d = 1.05 in an axial flow of liquid. The rods had distance pieces (fins) wound into helices. It is interesting to note that the effect of the fin pitch in the clusters of rods and in the annular channel was almost the same (see Fig. 4).

We see from Fig. 4 that, as the fin pitch diminishes, the liquid flow rate remaining constant, the pressure losses first rise slowly and then, for T/d < 10, rise very sharply. Hence we have the possibility of varying the fin pitch over a fairly wide range of T/d values with little change in the hydraulic losses of the channel.

A. M. Barabanov played a direct part in the measurements.

DIFFUSION-CHEMICAL AND PHASE RESISTANCE DURING CONDENSATION AND EVAPORATION OF ALKALI METALS

V. I. Subbotin, M. N. Ivanovskii, and Yu. V. Milovanov

UDC 621.039.517.5

It is shown that, for s.v.p. in the range 1-100 mm Hg, evaporation (condensation) of alkali metals goes via liberation (absorption) of both monatomic and diatomic molecules by the liquid surface. In this pressure range, dimerization (dissociation) occurs as the result of a chemical reaction at the liquid surface, and the coefficients of condensation of monatomic and diatomic molecules are close to unity.

According to the mechanism presently accepted for the evaporation of alkali metals, dimerization takes place after evaporation [1, 2], and therefore the coefficient of condensation of diatomic molecules is $\alpha_2 = 0$.

When calculated from the value $\alpha_2 = 0$, the coefficient of heat transfer increases with rise in temperature (pressure) of the saturated vapor. For the case of sodium, the coefficient of heat transfer is calculated to be 97 $kw/m^2 \cdot deg$ at 973° K and 465 $kw/m^2 \cdot deg$ at 1130° K. Experimental proof of the proposed mechanism of evaporation, based on measurements of the coefficients of heat transfer at high saturated vapor temperatures, would require very great experimental accuracy.

However, at lower saturated vapor temperatures and pressures ($p \simeq 1$-100 mm Hg), α_2 must be close to unity, since the present authors failed to find any diffusion resistance in measurements of the temperature fields in the vapor.

The Kinetics of the Dimerization Reaction in the Vapor Phase

The effect of the evaporation mechanism on heat transfer was discussed in [3, 4]. As a result of experiments on free evaporation, it was shown that the difference between the molecular forms of the solid and vapor leads to a sharp reduction in the rate of the phase transition.

The vapors of the alkali metals are known to consist of a mixture of monatomic and diatomic molecules. However, according to the presently accepted mechanism [1, 2], evaporation of these metals goes via liberation from the liquid of monatomic molecules only; these molecules then enter the vapor and on colliding begin to dimerize. According to [5], the probability of dimerization is of order unity for triple collisions of the type

$$A + A + M \rightleftarrows A_2 + M. \tag{1}$$

The M particle can be either an atom of A, or a molecule A_2. This particle takes up the excitation from the A_2 molecule formed. The resultant rate of formation of A_2 molecules is equal to the difference between the rate of the forward and reverse reactions:

$$\frac{dn_2}{d\tau} = -\frac{1}{2} \cdot \frac{dn_1}{d\tau} = k_r n_1^3 + k_r' n_1^2 n_2 - k_d n_2 n_1 - k_d' n_2^2. \tag{2}$$

Here n_1 and n_2 are the numbers of monatomic and diatomic molecules in 1 cm^3, τ is the time in sec, k_r and k_r' are the velocity constants of the dimerization reaction, and k_d and k_d' are the velocity constants of the dissociation reaction. The latter are linked by the relation

$$\frac{k_d'}{k_r'} = \frac{k_d}{k_r} = \frac{n_{1\infty}^2}{n_{2\infty}}. \tag{3}$$

(The subscript ∞ refers to the equilibrium condition.) On the assumption that every collision between atoms in the presence of a third particle leads to the formation of an A_2 molecule [5], the rate of the forward reaction (dimerization) is

$$n_1^2 \bar{v} \sigma \frac{4\pi r^3}{3} (n_1 + n_2) \text{ molecules } A_2/cm^3 \cdot sec, \tag{4}$$

Translated from Atomnaya Énergiya, Vol. 21, No. 1, pp. 17-22, July, 1966. Original article submitted November 20, 1965.

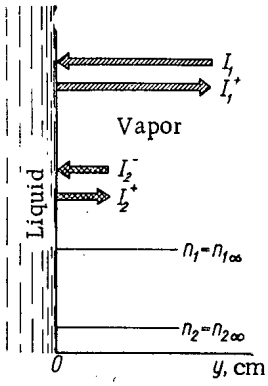

Fig. 1. Concentrations and fluxes in thermodynamic equilibrium.

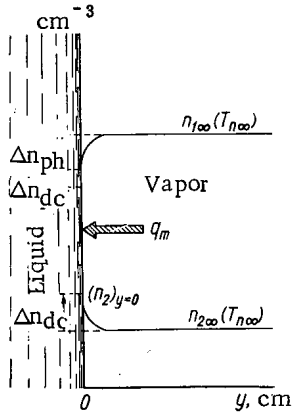

Fig. 2. Distribution of concentrations of monatomic and diatomic molecules in the vapor, for the case of condensation.

where $\bar{v}$ is the mean velocity of thermal motion in cm/sec, σ is the gas-kinetic cross section in cm^2, r is the radius of the molecule in cm, and

$$k_r = \bar{v}\sigma \frac{4\pi r^3}{3}. \tag{5}$$

The dimerization rate depends on the nature of the third particle. Thus, according to [5], nitrogen atoms are 13 times more efficient than nitrogen molecules as third particles in the dimerization of atomic nitrogen. Remembering also that, for alkali metals, usually $n_{2\infty} \ll n_{1\infty}$, we can without appreciable error neglect the terms $k_r' n_1^2 n_2$ and $-k_d' n_2^2$ in (2). Then, by (2) and (3),

$$\frac{dn_2}{d\tau} = -\frac{1}{2}\cdot\frac{dn_1}{d\tau} = k_r\left(n_1^3 - \frac{n_{1\infty}^2}{n_{2\infty}} n_2 n_1\right), \tag{6}$$

where k_r is found from (5).

By Taylor's theorem, we can write (6) in the form

$$\frac{dn_2}{d\tau} \approx \left(\frac{dn_2}{d\tau}\right)_{n_2=n_{2\infty}} + \left[\frac{d_2}{dn}\left(\frac{dn_2}{d\tau}\right)\right]_{n_2=n_{2\infty}} (n_2 - n_{2\infty}). \tag{7}$$

However, $\left(\frac{dn_2}{d\tau}\right)_{n_2=n_{2\infty}} = 0$. Introducing the notation

$$B \equiv \left[\frac{d}{dn_2}\left(\frac{dn_2}{d\tau}\right)\right]_{n_2=n_{2\infty}}, \tag{8}$$

we thus get

$$\frac{dn_2}{d\tau} \approx B\,(n_2 - n_{2\infty}). \tag{9}$$

The error introduced by this approximation is only a few per cent.

Thermodynamic Equilibrium

Let us examine the accepted evaporation mechanism [1, 2] in more detail, and find out in what conditions thermodynamic equilibrium can occur in the liquid-vapor system. We shall take the case when the liquid is in equilibrium with its saturated vapor (Fig. 1).

Let I_1^- and I_2^- be the numbers of monatomic and diatomic vapor molecules colliding during 1 sec per 1 cm^2 liquid surface, and let I_1^+ and I_2^+ be the numbers of monatomic and diatomic molecules entering the vapor from the liquid during 1 sec per 1 cm^2 liquid surface. We shall take the coefficient of condensation of monatomic molecules, α_1, as equal to unity (α_1 is the ratio between the number of monatomic molecules which condense, i.e., go across into the liquid, and the total number of monatomic vapor molecules colliding with the liquid surface). Assuming that evaporation occurs only by liberation of monatomic molecules from the liquid surface, we get

$$\left.\begin{aligned} I_1^+ &= I_1^- + 2\alpha_2 I_2^-, \\ I_2^+ &= I_2^- - \alpha_2 I_2^-. \end{aligned}\right\} \tag{10}$$

From (10) it follows that when $\alpha_2 \neq 0$ a mixture of molecules must leave the liquid for the vapor, this mixture containing much more monatomic molecules than the vapor present at the interface with the liquid. In this case, concentration gradients of monatomic and diatomic molecules would arise in the vapor layer at the interface with the liquid:

$$\frac{dn_1}{dy} < 0, \quad \frac{dn_2}{dy} > 0.$$

A consequence of this would be violation of chemical and thermal equilibrium in the vapor.

Calculation of Diffusion-Chemical Resistance for Condensation and Evaporation of Sodium ($q = 233$ kw/m^2)

Parameter	Temperature of saturated vapor, °K		
	973	1056	1130
$n_{1\infty}$, molecules/cm^3	$0{,}875 \cdot 10^{18}$	$2{,}09 \cdot 10^{18}$	$4{,}17 \cdot 10^{18}$
$n_{2\infty}$, molecules/cm^3	$0{,}125 \cdot 10^{18}$	$0{,}36 \cdot 10^{18}$	$0{,}82 \cdot 10^{18}$
$\bar{v}\sqrt{8kT/\pi m}$, cm/sec	94 500	98 500	102 000
$k_r = \bar{v}\sigma 4\pi r^3/3$, cm^6/sec ($\sigma = 10^{-15}$ cm^2, $r = 2 \cdot 10^{-8}$ cm)	$0{,}316 \cdot 10^{-32}$	$0{,}33 \cdot 10^{-32}$	$0{,}346 \cdot 10^{-32}$
B, sec^{-1}	—25 900	—132 000	—510 000
D_2, cm^2/sec	8,83	3,75	1,91
$w_2 = q_m/2n_0$, cm/sec	75	30,6	15
$w_2/2D_2$, cm^{-1}	4,25	4,08	3,93
$(w_2/2D_2)^2$, cm^{-2}	18	16,7	15,4
B/D_2, cm^{-2}	—2 930	—35 200	—267 000
l_2, cm	—0,0187 (—0,020)	—0,00535 (—0,00544)	—0,00194 (—0,00195)
$w_2 l_2/D_2$	—0,145 (—0,17)	—0,0437 (—0,0444)	—0,0152 (—0,0153)
$(n_2)_{y=0}$, molecules/cm^3	$0{,}146 \cdot 10^{18}$ $(0{,}1068 \cdot 10^{18})$	$0{,}377 \cdot 10^{18}$ $(0{,}345 \cdot 10^{18})$	$0{,}833 \cdot 10^{18}$ $(0{,}807 \cdot 10^{18})$
Δn_{dc}, molecules/cm^3	$2{,}1 \cdot 10^{16}$ $(-1{,}82 \cdot 10^{16})$	$1{,}7 \cdot 10^{16}$ $(-1{,}5 \cdot 10^{16})$	$1{,}3 \cdot 10^{16}$ $(-1{,}3 \cdot 10^{16})$
ΔT_{dc}	2,1° (—1,82°)	0,85° (—0,75°)	0,4° (—0,4°)
ΔT_{ph}	±0,3°	±0,15°	±0,1°
$\Delta T = \Delta T_{dc} + \Delta T_{ph}$	2,4 (—2,12)	1 (—0,9)	0,5 (—0,5)
Coefficient of heat transfer $q/\Delta T$, kw/m^2 · deg	97 (110)	233 (260)	465 (465)

Note. Figures in parentheses refer to the case of evaporation.

Thus, by taking $\alpha_2 \neq 0$ for the adopted evaporation mechanism, we have arrived at a contradiction. So in this scheme the liquid can be in equilibrium with its saturated vapor only if $\alpha_2 = 0$. We shall assume that for this mechanism α_2 also vanishes for slight deviations from equilibrium, i. e., when the resultant mass transfer rate is much smaller than the maximum rate of evaporation or condensation. On this hypothesis we shall consider the processes of evaporation of liquid and condensation of "stagnant" vapor.

Condensation (evaporation)

We shall find the maximum rate of evaporation of the liquid (rate of evaporation into a vacuum), $q_{m\,max}$. This rate is equal to the hypothetical rate of evaporation of liquid in equilibrium with its saturated vapor. Since in equilibrium the rate of evaporation is equal to the rate of condensation, the rate of evaporation into a vacuum is given by the formula

$$q_{m\,max} = \alpha_1 I_1^- + 2\alpha_2 I_2^- \text{ atoms/cm}^2 \cdot \text{sec}. \tag{11}$$

According to the kinetic theory of gases,

$$I_1^- = \frac{n_{1\infty}(T)}{\sqrt{\frac{2\pi m}{kT}}} \text{ molecules } A_1 \text{ per cm}^2 \cdot \text{sec}, \tag{11'}$$

$$I_2^- = \frac{n_{2\infty}(T)}{\sqrt{\frac{4\pi m}{kT}}} \text{ molecules } A_2 \text{ per cm}^2 \cdot \text{sec},$$

where m is the mass of an atom in grams, $k = 1.38 \cdot 10^{-16}$ is Boltzmann's constant in degrees, and T is the temperature in °K.

Thus, when the temperature of the liquid surface (condensate) is T_K, its maximum evaporation rate is

$$q_{m\,\max} = \frac{\alpha_1 n_{1\infty}(T_K) + \alpha_2 \sqrt{2}\, n_{2\infty}(T_K)}{\sqrt{\frac{2\pi m}{kT_K}}}. \tag{12}$$

In the particular case when $\alpha_1 = 1$ and $\alpha_2 = 0$,

$$q_{m}\max = I_1^- = \frac{n_{1\infty}(T_K)}{\sqrt{\frac{2\pi m}{kT_K}}}. \tag{13}$$

If the vapor at the interface with the liquid (condensate) has concentrations $(n_1)_{y=0}$ molecules A_1 per cm^3, $(n_2)_{y=0}$ molecules A_2 per cm^3, and temperature $(T_n)_{y=0} > T_K$, then the resultant rate of condensation is given by formula

$$g_m = f_1\left[\frac{(n_1)_{y=0} - n_{1\infty}(T_K)}{\sqrt{\frac{2\pi m}{kT_K}}}\right] + 2f_2\left[\frac{(n_2)_{y=0} - n_{2\infty}(T_K)}{\sqrt{\frac{4\pi m}{kT_K}}}\right], \tag{14}$$

where

$$f_1 = \frac{2\alpha_1}{2-\alpha_1}, \quad f_2 = \frac{2\alpha_2}{2-\alpha_2} \quad \text{(see [6, 7])} \tag{14'}$$

In the particular case when $\alpha_1 = 1$ and $\alpha_2 = 0$, we have $f_1 = 2$, $f_2 = 0$, and

$$q_m = 2\frac{(n_1)_{y=0} - n_{1\infty}(T_K)}{\sqrt{\frac{2\pi m}{kT_K}}}. \tag{14''}$$

In the derivation of (14), (14") and (32) (vide infra) we assume for simplicity that $\sqrt{(T_n)_{y=0}} \approx \sqrt{T_K}$. If $q_m \ll q_{m\,\max}$, the error due to this approximation is small. Diatomic vapor molecules, brought to the condensate surface by convection currents in the vapor, are reflected from the condensate surface and diffuse in the opposite direction to the convection current. The concentration of diatomic molecules in the vapor therefore decreases with increasing distance y from the condensate surface, and when $y \to \infty$ it tends to the equilibrium concentration $n_{2\infty}(T_{n\infty})$, which depends on the temperature of the saturated vapor at an infinite distance from the condensate surface (Fig. 2). The concentration of diatomic molecules near the condensate surface is higher than the equilibrium concentration $n_{2\infty}(T_{n\infty})$, and therefore endothermic dissociation of diatomic molecules will take place in the vapor phase, causing supercooling of the vapor.

During evaporation, the concentration of diatomic molecules in the vapor increases with increasing distance from the liquid surface, tending towards the equilibrium concentration $n_{2\infty}$. Since the concentration of diatomic molecules near the liquid surface is lower than the equilibrium value, dimerization must occur in the vapor near the evaporating liquid. The heat liberated by this reaction superheats the vapor. Thus, in the scheme adopted, there must be a positive temperature gradient in the vapor during evaporation. As shown by the solution to the diffusion problem which we shall give below, the dimensions of the region in which the main concentration and temperature changes occur depend on the temperature of the saturated vapor and the direction and magnitude of the resultant mass transfer flux q_m. For example, for sodium with saturated vapor at 773° K and evaporation rate $q_m = 1.5 \cdot 10^{20}$ atoms/cm^2 · sec (thermal flux q = 233 kw/m^2), the size of this region is of order 10 cm. Note that the boundary conditions are not used in the derivation of this size. It is therefore independent of the absolute value of α_2.

The distribution of the diatomic-molecule concentration can be found by solving one of the differential equations

$$D_1 \frac{d^2 n_1}{dy^2} \pm w_1 \frac{dn_1}{dy} + \frac{dn_1}{d\tau} = 0, \tag{15}$$

$$D_2 \frac{d^2 n_2}{dy^2} \pm w_2 \frac{dn_2}{dy} + \frac{dn_2}{d\tau} = 0 \tag{16}$$

using the condition that the total pressure is constant at all points in the vapor phase:

$$p_0 = p_1 + p_2 = n_1 kT + n_2 kT = n_0 kT = \text{const},$$

i. e.

$$n_1 + n_2 = n_0 = \text{const}. \tag{17}$$

The lower (minus) sign attached to the convective term in (15) and (16) refers to the case of evaporation. Hence we find

$$\frac{dn_1}{dy} = -\frac{dn_2}{dy}. \tag{18}$$

Substituting from (18) into (15) and remembering that $\frac{dn_1}{d\tau} = -2\frac{dn_2}{d\tau}$, we find that

$$D_1 \frac{d^2 n_2}{dy^2} \pm w_1 \frac{dn_2}{dy} + 2\frac{dn_2}{d\tau} = 0. \tag{19}$$

Let us now write down the boundary conditions for (16). When y = 0 there is no resultant flux of diatomic molecules through the phase interface, because the coefficient of condensation of diatomic molecules $\alpha_2 = 0$. It follows that the convective flux of diatomic molecules must, when y = 0, be equal to the diffusion flux of diatomic molecules flowing in the opposite direction, i. e.,

$$\mp w_2 (n_2)_{y=0} = D_2 \left(\frac{dn_2}{dy}\right)_{y=0}. \tag{20}$$

The convection velocity w_2 is found from the condition that the resultant mass flux q_m (atoms/cm^2 · sec) is constant for all points in the vapor space,

$$\pm D_1 \frac{dn_1}{dy} \pm 2D_2 \frac{dn_2}{dy} + w_1 n_1 + 2w_2 n_2 = q_m = \text{const}. \tag{21}$$

Using (17) and (18), and remembering that $D_1 = 2D_2$ and that $w_1 = 2w_2$, we can simplify (21):

$$2w_2 n_0 = q_m = \text{const}, \tag{22}$$

whence

$$w_2 = \frac{q_m}{2n_0} = \text{const}. \tag{23}$$

The second boundary condition is

$$n_2 \longrightarrow n_{2\infty}\,(T_{n\infty}) \text{ when } y \longrightarrow \infty. \tag{24}$$

Thus we have to solve the equation

$$D_2 \frac{d^2 n_2}{dy^2} \pm w_2 \frac{dn_2}{dy} + \frac{dn_2}{d\tau} = 0 \tag{25}$$

with boundary conditions (20) and (24). We linearize (25), using (9). We get

$$\frac{d^2 n}{dy^2} \pm \frac{w_2}{D_2} \cdot \frac{dn}{dy} + \frac{B}{D_2} n = 0. \tag{26}$$

Here $n = n_2 - n_{2\infty}\,(T_{n\infty})$ and

$$B = \left\{\frac{d}{dn_2}\left[k_r\left(n_1^3 - \frac{n_{1\infty}^2}{n_{2\infty}} n_2 n_1\right)\right]\right\}_{n_2 = n_{2\infty}} = k_r\left[3n_{1\infty}^2 + \frac{n_{1\infty}^2}{n_{2\infty}}(n_{1\infty} - n_{2\infty})\right]. \tag{26'}$$

Expression (26) corresponds to the characteristic equation

$$\left(\frac{1}{l}\right)^2 \pm \frac{w_2}{D_2} \cdot \frac{1}{l} + \frac{B}{D_2} = 0. \tag{27}$$

The roots of this equation are

$$\frac{1}{l_1} = \mp \frac{w_2}{2D_2} + \sqrt{\left(\frac{w_2}{2D_2}\right)^2 - \frac{B}{D_2}} > 0, \quad \frac{1}{l_2} = \mp \frac{w_2}{2D_2} - \sqrt{\left(\frac{w_2}{2D_2}\right)^2 - \frac{B}{D_2}} < 0. \tag{28}$$

The general solution of (26) is of the form

$$n = C_1 e^{y/l_1} + C_2 e^{y/l_2}.$$

When $y \to \infty$, $n_2 \to n_{2\infty}$ and $n \to 0$, so that $C_1 = 0$ and $n = C_2 e^{y/l_2}$, or, returning to our previous notation, $n_2 - n_{2\infty} = C_2 e^{y/l_2}$. When $y = 0$, $(n_2)_{y=0} - n_{2\infty} = C_2$ and

$$n_2 - n_{2\infty} = [(n_2)_{y=0} - n_{2\infty}]\, e^{y/l_2}. \tag{29}$$

Differentiating (29),

$$\frac{dn_2}{dy} = [(n_2)_{y=0} - n_{2\infty}]\, \frac{1}{l_2}\, e^{y/l_2},$$

and, when $y = 0$,

$$\left(\frac{dn_2}{dy}\right)_{y=0} = [(n_2)_{y=0} - n_{2\infty}]\, \frac{1}{l_2}. \tag{30}$$

But, according to (20),

$$\left(\frac{dn_2}{dy}\right)_{y=0} = \mp \frac{w_2 (n_2)_{y=0}}{D_2}. \tag{31}$$

From (30) and (31) it follows that

$$(n_2)_{y=0} = \frac{n_{2\infty}}{1 \pm \frac{w_2 l_2}{D_2}} \qquad (l_2 < 0).$$

From the constant-pressure condition (17) it follows that

$$n_{1\infty}(T_{n\infty}) - (n_1)_{y=0} = (n_2)_{y=0} - n_{2\infty}(T_{n\infty}).$$

Now let us introduce the notation

$$\Delta n_{ph} \equiv n_{1\infty}(T_{n\infty}) - (n_1)_{y=0},$$
$$\Delta T_{dc} \equiv T_{n\infty} - (T_n)_{y=0},$$
$$\Delta n_{\Phi} \equiv (n_1)_{y=0} - n_{1\infty}(T_{\kappa}); \quad \Delta T_{ph} \equiv (T_n)_{y=0} - T_{\kappa},$$
$$\Delta n = \Delta n_{dc} + \Delta n_{ph} = n_{1\infty}(T_{n\infty}) - n_{1\infty}(T_{\kappa}),$$
$$\Delta T = \Delta T_{dc} + \Delta T_{ph}.$$

The subscript dc denotes quantities associated with the diffusion-chemical resistance. The relative concentration difference arising from the phase transition can be found from (14"):

$$\Delta n = \pm \frac{q_m}{2} \sqrt{\frac{2\pi m}{kT_{\kappa}}} \approx \pm \frac{q_m}{2} \sqrt{\frac{2\pi m}{kT_{n\infty}}}. \tag{32}$$

Knowing $n_{1\infty}$ as a function of T_{∞} (see the table) we easily go from the concentration differences to the corresponding temperature differences.

For the case of condensation and evaporation of sodium with condensation (evaporation) rate $q_m = 1.5 \cdot 10^{20}$ atoms/cm^2 · sec (thermal flux $q = 233$ kw/m^2) we calculated the concentration differences Δn_{dc}, Δn_{ph}, and Δn, and the corresponding temperature differences ΔT_{dc}, ΔT_{ph}, and ΔT. The table gives the initial data and the course and results of this calculation.

The diffusion-chemical resistance depends markedly on the kinetics of the dimerization reaction. Unfortunately, we have no data on the kinetics of this reaction or on the possible variation of α_2 with the degree of deviation from equilibrium, $q_m/q_{m\,max}$, the changes of liquid structure with temperature, and other factors unknown to us, and so were unable to analyse this process in more detail.

Nevertheless, we can assert that at pressures near to atmospheric the coefficient of heat transfer is very large (more than 150 kw/m^2 · deg), even allowing for diffusion-chemical resistance (of course, in the absence of impurities,

non-condensing gases and other extraneous factors hindering heat transfer). From the table it will be seen that for the chosen scheme of evaporation ($\alpha_2 = 0$) the diffusion-chemical resistance must increase with decreasing saturated vapor pressure. This is explained by the sharp retardation of the chemical reaction which occurs when the pressure is reduced. However, measurements [9] of the temperature field in the vapor near the condensate surfaces of condensing potassium and sodium have shown that at low pressures (1-100 mm Hg) there is no diffusion-chemical resistance, despite the fact that there are quite a lot of diatomic molecules (1-12%) at these pressures.

In this pressure range, much smaller amounts of non-condensing gas (argon) give a diffusion resistance which exceeds the phase-transition resistance by a factor of ten, and leads to the appearance of a temperature gradient in the layer of vapor near the liquid surface. Such gradients were measured by the present authors in experiments on the condensation of mercury and the alkali metals. The absence of diffusion-chemical resistance for pure vapor at low pressures shows that at these pressures the coefficient of condensation of the diatomic molecules is close to unity.

At low pressures evaporation proceeds via liberation from the liquid surface of monatomic as well as diatomic molecules. If the accepted scheme of evaporation, which entails dimerization in the vapor, is correct for high pressures, there must be a transitional region in which α_2 changes from zero to unity.

LITERATURE CITED

1. Symposium: "Liquid Metal Heat-Transfer Agents," translated under the editorship of A. E. Sheindlin, Moscow, Izd. inostr. lit. (1958).
2. É. É. Shpil'rain and É. I. Asinovskii, Inzh.-fiz. zh., V, No. 4 (1962).
3. F. Metzger and E. Miescher, Helv. phys. acta, 16, 205, 323 (1943).
4. O. Knacke and I. Stranski, Progr. Metal. Phys., 6, 181 (1956).
5. Ya. B. Zel'dovich and Yu. P. Raizer, Physics of Shock Waves and High-Temperature Hydrodynamic Phenomena, Moscow, Fizmatgiz (1963), p. 285.
6. R. Ya. Kucherov, and L. É. Rikenglaz, ZhÉTF, 37, No. 1 (1959).
7. R. Ya. Kucherov and L. É. Rikenglaz, Dokl. AN SSSR, 133, No. 5 (1960).
8. V. I. Subbotin et al., Teplofizika vysokikh temperatur, 2, No. 4 (1964).

All abbreviations of periodicals in the above bibliography are letter-by-letter transliterations of the abbreviations as given in the original Russian journal. *Some or all of this periodical literature may well be available in English translation.* A complete list of the cover-to-cover English translations appears at the back of the first issue of this year.

THERMAL DEFORMATION OF FUEL ELEMENTS

E. Ya. Safronov, B. A. Briskman,
V. D. Bondarev, and V. S. Shishov

UDC 621.039.548

The authors calculate the temperature drops in the walls of cassette-type fuel elements under neutron fluxes with radial gradients. The thermal deformations of the walls are measured in the working range of temperature drops.

In the fuel elements of nuclear reactors, together with their reflectors and control or compensating rods, there arises a radial neutron-flux gradient due to splashing in the reflector or neutron absorption in the rods. Simultaneously there is created a radial gradient of heat emission in the fuel element; for constant heat removal at the circumference of the fuel element, this leads to the appearance of a radial temperature drop which causes thermal deformation of the casing [1]. For complex fuel-element geometry, it is very difficult to calculate the deformation, and therefore practically the only method of determining the deformation in such cases is the use of experiment.*

To widen the scope of our ideas on the operation of fuel elements we have studied the thermal deformation of a model cassette-type fuel element of hexagonal cross section.

Analytical Determination of Temperature Drops

The calculation is performed for an external hexagonal casing in the form of a thin plate. Let us write down the equation of thermal conductivity for a thin plate (one-dimensional problem) with an internal heat source:

$$\frac{\partial^2 T}{\partial x^2} + \frac{q_v}{\lambda} = 0. \tag{1}$$

Here

$$q_v = q_{v_1} + q_{v_2}, \tag{2}$$

$$q_{v_1} = q_{v\min}\left[1 + \frac{x}{L}(n-1)\right] \tag{3}$$

(we are taking a linear heat-emission gradient); and

$$q_{v_2} = -\alpha \frac{S}{V}(T - t_0), \tag{4}$$

where n is the degree of non-uniformity of heat emission, L is the semiperimeter of the model fuel-element casing, λ is the coefficient of thermal conductivity, α is the coefficient of heat transfer from the wall to the water, $q_{v\min}$ is the minimum rate of heat emission, t_0 is the mean temperature of the cooling water, S/V is the surface-to-volume ratio, and T is the temperature of the casing.

If the boundary conditions are

$$\left(\frac{\partial T}{\partial x}\right)_{x=0} = 0, \tag{5}$$

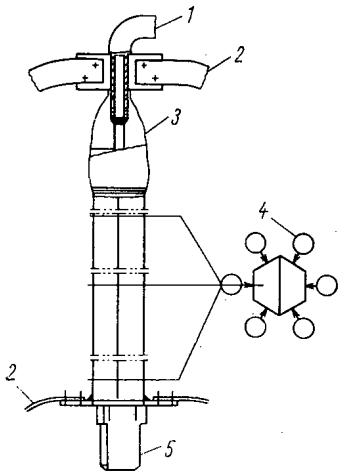

Fig. 1. Diagram of working section. 1) Water; 2) current busbars; 3) rubber sheath; 4) indicators; 5) ebonite manifold.

*Some experimental results on deformation of model fuel elements, obtained at the affiliated branch of the A. I. Ioffe Physicotechnical Institute, Leningrad, were available to the authors of the present article.

Translated from Atomnaya Énergiya, Vol. 21, No. 1, pp. 22-26, July, 1966. Original article submitted November 17, 1965.

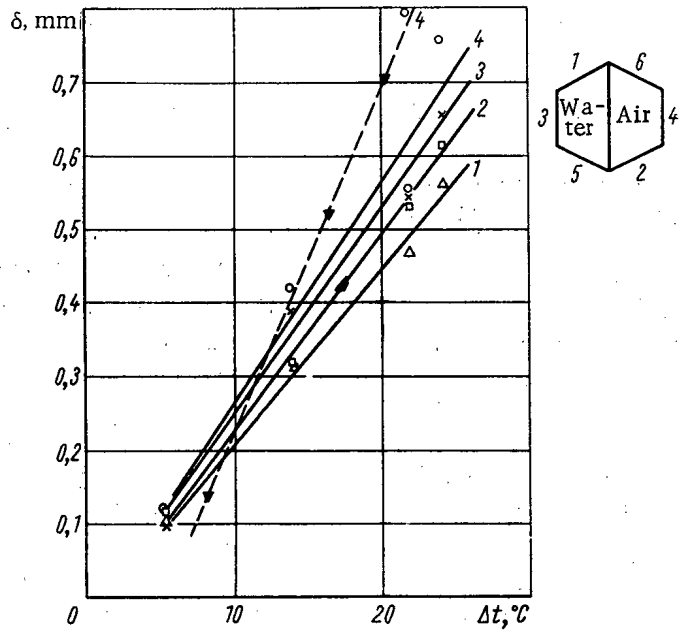

Fig. 2. Deflection versus temperature drop between faces 4 and 3 half-way up the fuel element. (1)-(6): Numbers of faces. ————) Outer casing of fuel element; – – – – – –) inner casing of fuel element, face 4. Experimental results: ○, ▼) Face 4 for outer and inner casing, respectively; △) face 1; ×) face 3; □) face 2.

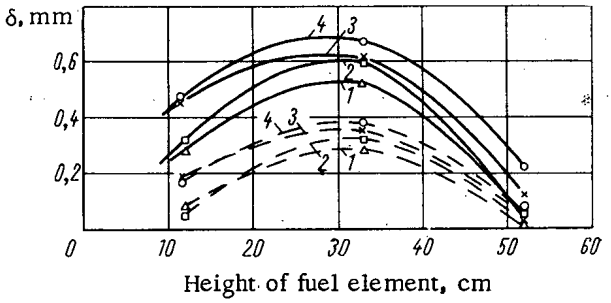

Fig. 3. Distribution of deformation over height of fuel element. (1)-(4) Numbers of faces. ————) Δt = 24.2 °C; – – – – –) Δt = 14 °C. Notation of experimental points: same as for Fig. 2.

$$\left(\frac{\partial T}{\partial x}\right)_{x=L}=0, \tag{6}$$

then (1) has the solution

$$\Delta T=\frac{q(n-1)\delta}{2\alpha}-\frac{q(n-1)\delta}{LaB}\cdot\frac{e^{BL}-1}{e^{BL}+1}, \tag{7}$$

where δ is the wall thickness.

Here,

$$B^2=2\frac{\alpha}{\lambda\delta}.$$

For the range of heat emissions studied, ΔT_0 varies from 12.5 to 20.2 °C when n = 1.5, and from 25 to 40.4 °C when n = 2.

Formulation of the Problem and Description of Apparatus

From what has been said, it follows that the thermal deformation of the model fuel element must be studied for temperature drops up to 40° C. With constant coefficient of heat transfer α across the gap, the maximum temperature drop must occur in the outer casing. However, since the inner casing has lower rigidity, the point of maximum drop does not necessarily coincide with that of maximum deformation. Thus the deformation must be measured both for the external jacket and for a possibly greater number of internal jackets. Since the model is an exact copy, we can quite correctly transfer our results to the prototype fuel element.

Figure 1 is a diagram of the experimental equipment. The model was heated by direct current from an AND-5000/2500 set (nominal power 30 kw). The model was cooled by means of circulating water. To create the required temperature drop, the model was divided into two halves in cross section, one cooled and one not cooled.

The head and foot of the model were of ebonite. The water pipes were so arranged as to cool the current leads as well as the model. The current busbars were made of packets of 0.5 mm thick copper foil, sufficiently flexible to eliminate any influence on the rigidity of the model.

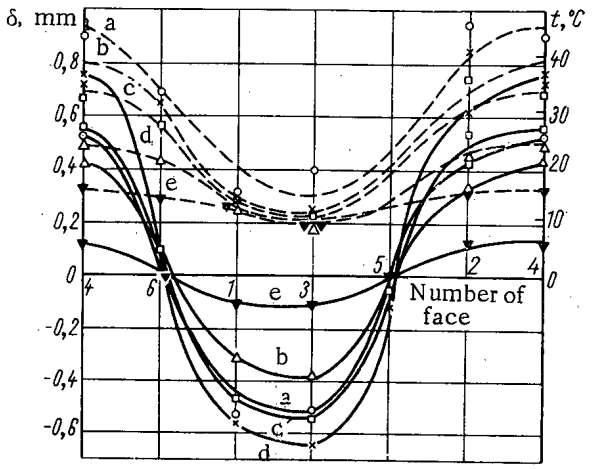

Fig. 4. Distributions of temperature and deflection in central cross section of fuel element, round the perimeter. ———) Deflection of fuel element; – – – – ·) temperature distribution. Curves with the same letter were measured in the same experiment. Designation of experimental points: same as Fig. 2.

The casings were welded together alternately in the upper and lower parts of the assembly, so that by connecting them in series the total electric resistance should be as large as possible. The resistance of the model was $3.7 \cdot 10^{-4}$ ohm at t = 0 °C.

The fastening of the lower end of the model was exactly the same as the attachment of the fuel element in the support grid of the separator. The upper part was fixed down with special bolts allowing for free movement in a vertical direction. In a slot in the base was a slide bar to which were attached the gauges (type ICh, scale division 0.01 mm) for the deformation measurements.

The depth of camber was measured for each face of the model. The wall temperature was measured by means of 15 chromel-copel thermocouples of diameter 0.4 mm arranged in three cross sections at different heights.

Experimental Method

When conditions (as read on a recording device) were steady, we measured the temperatures, deformations and voltage drops ΔU in the model. (The ΔU measurements were made so as to record the generator currents in order to calculate the relation between the temperature drop and current strength.)

Owing to the comparatively high temperature coefficient of the resistance, the current in the model's periphery changed quite appreciably (with the temperature drop). In these conditions, the current strength J through the model was given by

$$J = \frac{\Delta U}{2LR_0} \int_0^L \frac{dx}{1+\beta t(x)}, \tag{8}$$

where β is the temperature coefficient of the resistance in $°C^{-1}$, R_0 the resistance of the casing at 0 °C, and t(x) the measured temperature distribution on the periphery.

In the actual conditions we took as an approximate value of the integral the expression

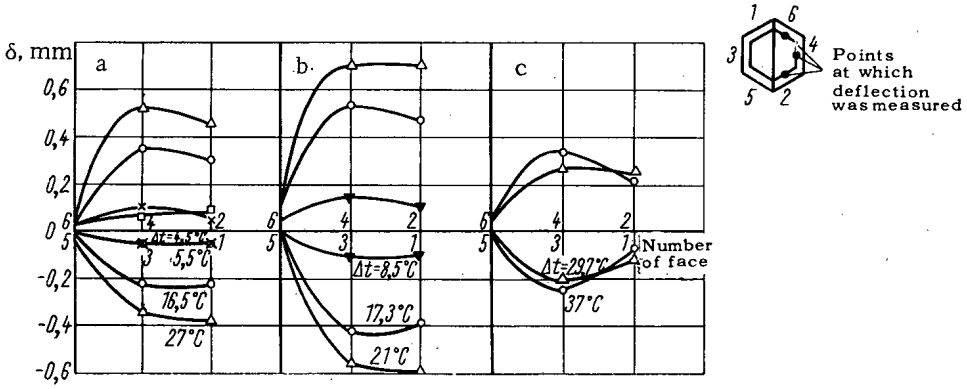

Fig. 5. Distribution of deformation round perimeter of fuel element. (a) Lower cross section; (b) central cross section; (c) upper cross section. Positive deformations refer to the inner casing, negative deformations to the outer casing. Deformation of inner casing refers to Δt for outer casing.

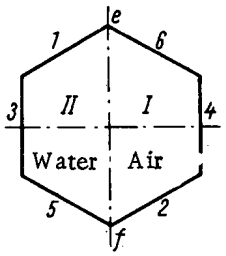

Fig. 6. Cross section of fuel element. 1-6: numbers of faces.

$$J \approx \frac{\Delta U}{12R_0} \sum_{i=1}^{6} \frac{1}{1+\beta t_i}. \qquad (9)$$

We made a spot check on the use of (9) to evaluate the integral in (8), by planimetry of the curve $1/[1 + \beta t(x)]$: the error made by using (9) was less than 2%.

The apparatus was constructed so as to allow measurement of the deformation of the first internal casing on the uncooled side. For this purpose, after a series of tests on the deformation of the external casing on the uncooled side, sets of three holes were drilled on the axes of the faces at the three heights at which the measurements had been made. Repeat measurements in the same conditions, made in order to test for changes of rigidity of the outer casing due to the drilling, showed that there were no appreciable changes in the deformations. We made simultaneous measurements of the deformation of the outer casing (on the cooled side) and the inner casing (on the uncooled side) under various conditions. As no temperature measurements were made on the inner casing, the temperature drops were determined by calculation in this case (see Appendix). The appropriate curves were constructed from the calculated relation between the temperature drop and the current strength. The results of the calculations were found to be in good agreement with the experimental data for the external casing ($\Delta t = 12°C$ for $J = 3500$ A, $\Delta t = 21°C$ for $J = 4500$ A). The calculated results could thus be regarded as trustworthy and could be used for determining the temperature drop in the inner casing. In practice, the curves of Δt versus J were almost the same for both casings; this is explained by the fact that the greater heat emission for the internal case was compensated for by the smaller distance between opposite faces of the casing, i. e., the corresponding reduction in thermal resistance to heat flux from the uncooled to the cooled section.

Discussion of Results

The results of the deformation measurements are plotted in Figs. 2-5. Figure 2 plots the deflection of the wall, δ, in mm, versus Δt, in °C, for the cross section halfway up the model. Figure 3 shows the variation of the deflection with height for the various faces of the model. Figure 4 shows the deflection around the perimeter of the casing half-way up the model, for various values of Δt. It also gives the corresponding temperature curves. Figure 5 gives the results of the simultaneous measurements on the internal and external casings for various cross sections around the perimeter for various values of Δt.

The straight lines in Fig. 2 were obtained by processing the experimental results by the method of least squares [2]. This figure also gives the relation between δ and Δt for the internal casing at the middle cross section, face 4. As seen from this graph, in the range of Δt under examination, the deformation of the inner casing was about 20% greater than that of the corresponding face of the outer casing, i. e., the inner casing was less rigid than the outer one.

It should be noted that in the prototype the specific heat emission in the inner casings is practically equal to that in the outer ones, while the temperature drop is less. In the experimental apparatus the current strength was the same in both casings (which were connected in series), and therefore the specific heat emission in the inner casing was the higher, although the temperature drops obtained were practically the same.

It must be pointed out that the two opposing factors—reduction in rigidity and decrease in temperature drop for the internal casing—compensated each other to some extent, and therefore the deformations of the external and internal casings should be approximately equal. In actual fact, the values of ΔT calculated from (7) confirm the present authors' assumptions.

As will be seen from Fig. 2, in the region plotted there is no tendency for the curve of δ versus Δt to deviate from linearity, i. e., it is possible to extrapolate to the neighboring regions.

From Fig. 3 it is seen that there is a certain asymmetry in the distribution of deformation with height of the model. This is due to the different possible ways of fastening the model (two degrees of freedom at the upper attachment and one at the lower), which are also characteristic of the fastening of a fuel element in the reactor.

The deformation and temperature distributions round the central perimeter of the outer casing, shown in Fig. 4, show that the corresponding temperature and deformation profiles are symmetrical; as Δt decreases the corresponding profiles become smoothed out. The rigidity nodes (points of zero deformation) approximately coincide with the

boundaries of the cooled and uncooled halves. The scatter for varying Δt of the points corresponding to the rigidity nodes is due to inaccurate setting of the gauges on the central axes of the faces. This error is characteristic of the temperature curves. In this case a specially large error can occur for faces 6, 1, 5, and 2, because the derivative dt/dx is a maximum on the joints between the cooled and uncooled parts.

In conclusion, we must note that all the deformations were elastic.

The results of this research were thus as follows:

1. We have devised a method of simultaneous measurement of the thermal deformation of the different casings of a model cassette-type fuel element.

2. We have obtained calculated data on the temperature drops in fuel elements as functions of the magnitude and degree of non-uniformity of the heat emission.

3. We found that with temperature drops of ~ 25° C the maximum deflection in the central cross section is 0.6-0.7 mm.

4. We derived theoretical formulae for the temperature drop in terms of the current strength for an electrically-heated assembly (allowing for the temperature dependence of the ohmic resistance).

5. Since the gaps between the casings are small, the deformations obtained are very substantial, and show that the deformation behavior of a fuel element in a reactor must be studied (in theoretical and experimental research on heat transfer in the distorted cell). It is quite probable that temperature deformation of the fuel elements will be the factor limiting the power of a reactor.

Appendix (calculation of relation between temperature drop and current strength)

A solid hexagonal section of thickness δ, height H, and perimeter 4L (where L is $^3/_2$ of the length of a side) is electrically heated by a current of strength J.

The section is divided by an impermeable diaphragm (Fig. 6). Section I is cooled by air with heat-transfer coefficient α_1; section II is cooled by water with heat-transfer coefficient α_2. We are to determine the stationary temperature profile round the perimeter, given that H is infinitely large; the air temperature (mean) is t', the water temperature (mean) is t".

We write down the equation of thermal conduction for regions I and II:

$$\text{I.}\quad \frac{\partial^2 t}{\partial x^2}+\frac{q_v-\alpha_1\frac{S}{V}(t-t')}{\lambda}=0, \tag{10}$$

$$\text{II.}\quad \frac{\partial^2 t}{\partial x^2}+\frac{q_v-\alpha_2\frac{S}{V}(t-t'')}{\lambda}=0. \tag{11}$$

Here $\frac{S}{V}=\frac{2}{\delta}$.

Let us write down the boundary conditions. We take the origins of coordinates for the two regions on faces 4 and 3 (cf. Fig. 6). Then $(\partial t/\partial x)_{x=0}=0$.

At points e and f we must have

$$t_{\text{I}}=t_{\text{II}}, \qquad x=\pm L;$$
$$\left(\frac{\partial t}{\partial x}\right)_{\text{I}}=-\left(\frac{\partial t}{\partial x}\right)_{\text{II}}, \qquad x=\pm L.$$

We introduce the notations

$A=(0.86\,R_0/\lambda)J^2$, R_0 = resistance of jacket at t = 0° C;

$$a_1^2=\frac{2\frac{\alpha_1}{\delta}-A\beta}{\lambda}, \quad a_2=\frac{A+2\alpha_1\frac{t'}{\delta}}{\lambda}; \quad b_1^2=\frac{2\frac{\alpha_2}{\delta}-A\beta}{\lambda}, \quad b_2=\frac{A+2\alpha_2\frac{t''}{\delta}}{\lambda}.$$

If $a_1^2 = \frac{2\frac{a_1}{\delta} - A\beta}{\lambda} > 0$: , the solution of (10) and (11) is

$$\Delta t = t_0 - t_3 = \left(\frac{a_2}{a_1^2} - \frac{b_2}{b_1^2}\right)\left(1 - \frac{1 + \frac{b_1}{a_1}\cdot\frac{\operatorname{sh} b_1 L}{\operatorname{sh} a_1 L}}{\operatorname{ch} b_1 L + \frac{b_1}{a_1}\cdot\frac{\operatorname{sh} b_1 L}{\operatorname{sh} a_1 L}\operatorname{ch} a_1 L}\right), \tag{12}$$

while if $a_1^2 = \frac{2\frac{a_1}{\delta} - A\beta}{\lambda} < 0$:

$$\Delta t = t_0 - t_3 = \left(\frac{a_2}{a_1^2} - \frac{b_2}{b_1^2}\right)\left(\frac{\frac{b_1}{a_1}\cdot\frac{\operatorname{sh} b_1 L}{\operatorname{sh} a_1 L} - 1}{\frac{b_1}{a_1}\operatorname{sh} b_1 L \operatorname{ctg} a_1 L - \operatorname{ch} b_1 L} - 1\right). \tag{13}$$

The relations between Δt and J found from (12) and (13) have been confirmed by experiment.

LITERATURE CITED

1. A. Rapier and T. Jones, J. Nucl. Energy, 19, A/B, 145 (1965).
2. R. S. Guter and B. V. Ovchinskii, Elements of Numerical Analysis and Mathematical Processing of Experimental Data, Moscow, Fizmatgiz (1962).

STUDY OF THE SPECTRA AND DOSES CREATED IN THE IRON – WATER SHIELDING OF A MONOENERGETIC NEUTRON SOURCE

O. A. Barsukov, V. S. Avzyanov, and V. N. Ivanov

UDC 621.039.58:539.125.5

Many-group calculations were made for the penetration of neutrons, emitted from monoenergetic sources, through water, iron, and water–iron systems of finite dimensions; the results of these calculations are presented. The neutron spectra resulting from the passage of such neutrons through water and iron shielding layers were calculated on the twenty-group diffusion-transport approximation. Detailed attention was paid to the high-energy part of the spectrum; certain peculiarities in neutron migration and moderation processes in shielding of the type in question were elucidated. Dose curves D(r) were plotted for neutrons of various energies.

By using the superposition principle, the results enable the neutron spectrum to be determined for sources having any arbitrary spectrum.

Presentation of the Problem and Method of Calculation

In developing optimum neutron shielding it is important to know the structure of the internal neutron field. In order to solve this kind of problem, the real source, with its complex spectrum, may be replaced by a set of monoenergetic sources. This approach makes it possible to observe some important effects which are difficult to observe when studying integral fluxes created by sources with complex spectra. Moreover the results obtained by studying the neutron distributions of monoenergetic sources are easy to interpret physically.

The problem reduces to the consideration of a monoenergetic neutron source screened by a layer of finite thickness. The space–energy distribution of neutrons inside the shielding is found. The following shielding compositions are considered: 1) water shielding 62 cm thick; b) iron shielding 62 cm thick; c) iron–water shielding, the iron forming an inner layer 10 cm thick and the water forming an outer 52-cm layer.

The basis of the calculations is a multi-group diffusion-transport approximation to the kinetic Boltzmann equation

$$D_i\nabla^2\varphi_i - \Sigma_i\varphi_i = -f_i \quad (i=1,\ 2,\ \ldots,\ m), \tag{1}$$

where φ_i is the integral neutron flux of the i-th group, D_i is the diffusion coefficient, Σ_i is the neutron transfer cross section (i. e., that characterizing capture and transition to lower groups), f_i is a neutron source including (in general) both source neutrons and neutrons brought into the range of the group as a result of slowing-down processes.

Energy Groups

Group	Energy range, MeV	Group	Energy range
I	10,8—9,8	XI	1,5—1,1 MeV
II	9,8—9,4	XII	1,1—55 keV
III	9,4—7,75	XIII	55—28 keV
IV	7,75—7	XIV	28—15 keV
V	7—6	XV	15—6 kev
VI	6—5,45	XVI	6—1,5 kev
VII	5,45—4,8	XVII	1,5—450 eV
VIII	4,8—4	XVIII	450—220 eV
IX	4—3,1	XIX	220—6 eV
X	3,1—1,5	XX	6—0,025 eV

Translated from Atomnaya Énergiya, Vol. 21, No. 1, pp. 27-35, July, 1966. Original article submitted September 16, 1965; revised March 2, 1966.

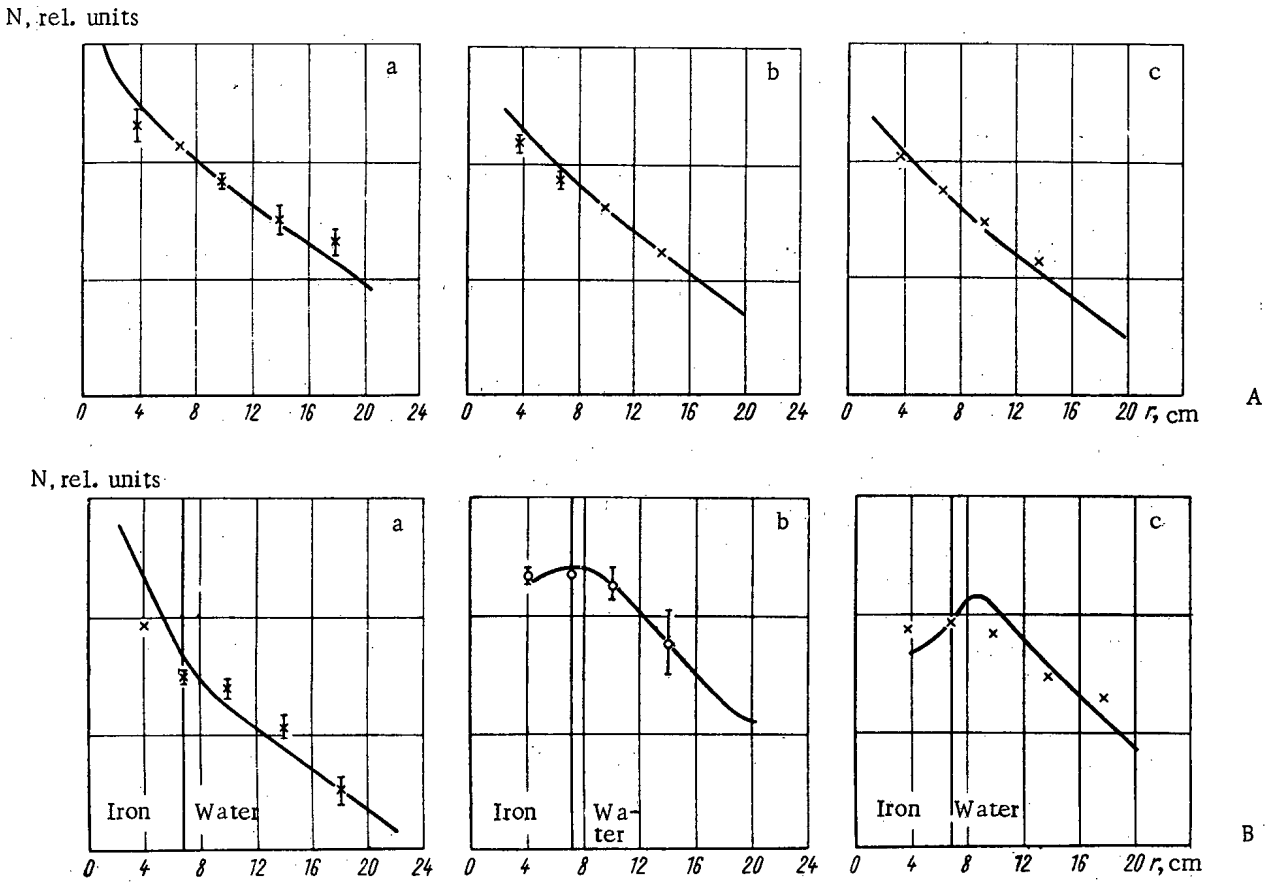

Fig. 1. Radial distribution of neutrons of various energies: A) In water; B) in iron–water shielding. a) First neutrons; b) neutrons with energies between 5 and 220 eV; c) neutrons with energies between 0.025 and 5 eV; ×, O) experiment; ———) calculation.

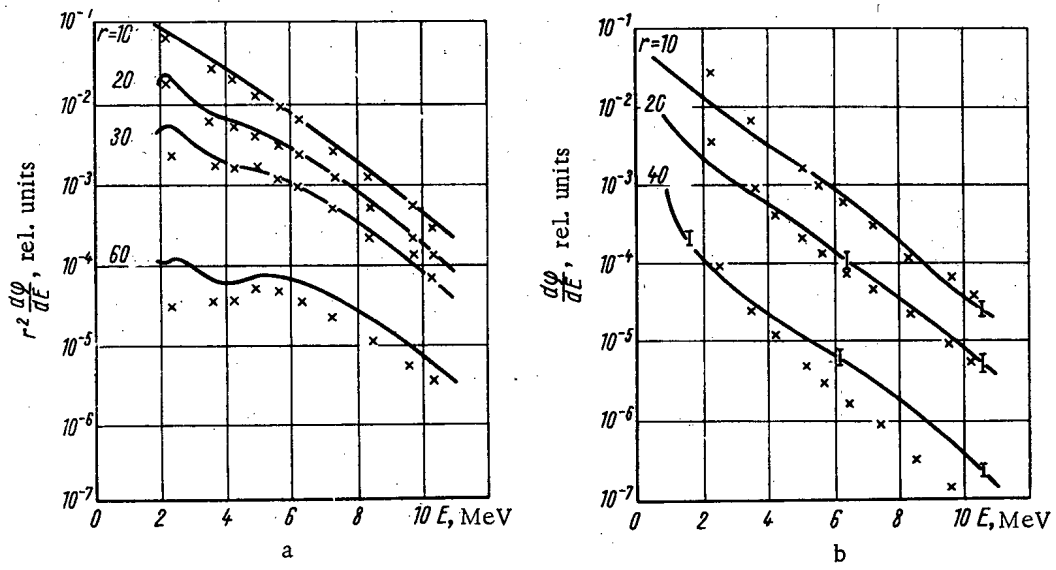

Fig. 2. Neutron spectrum in water for a point source (a) and in iron for a plane source (b). (r is measured in cm.)

The system of Eq. (1) was solved numerically by the method of differential factorization [1]. In order to allow for the transformation of the neutron spectrum arising from migration in nonmultiplying media, we used the method of successive approximations (iteration over the spectrum). The latter reduces to a refinement (with respect to a variable spectrum) of the group cross sections and group diffusion coefficients defining the constants of the

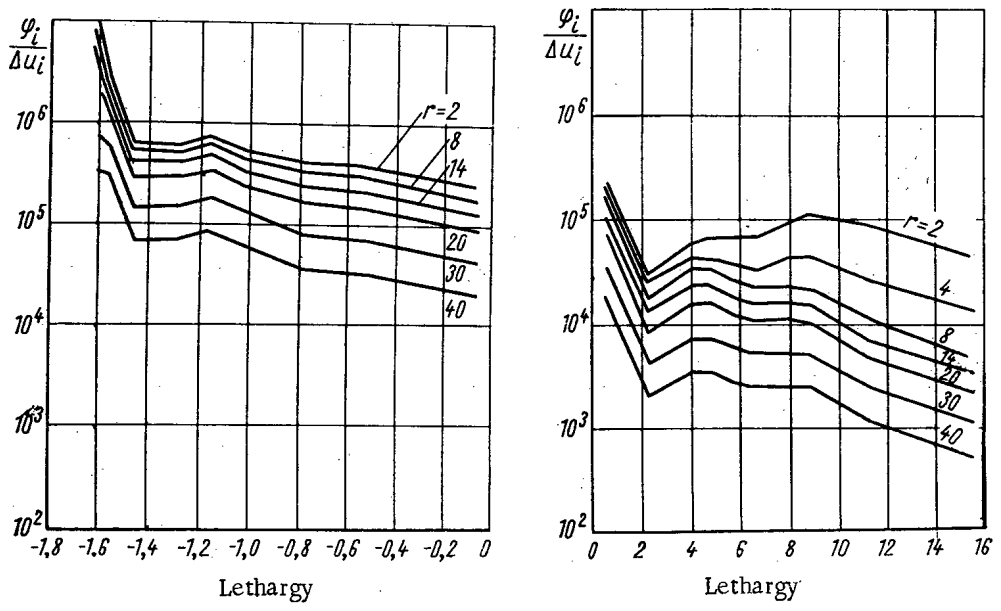

a

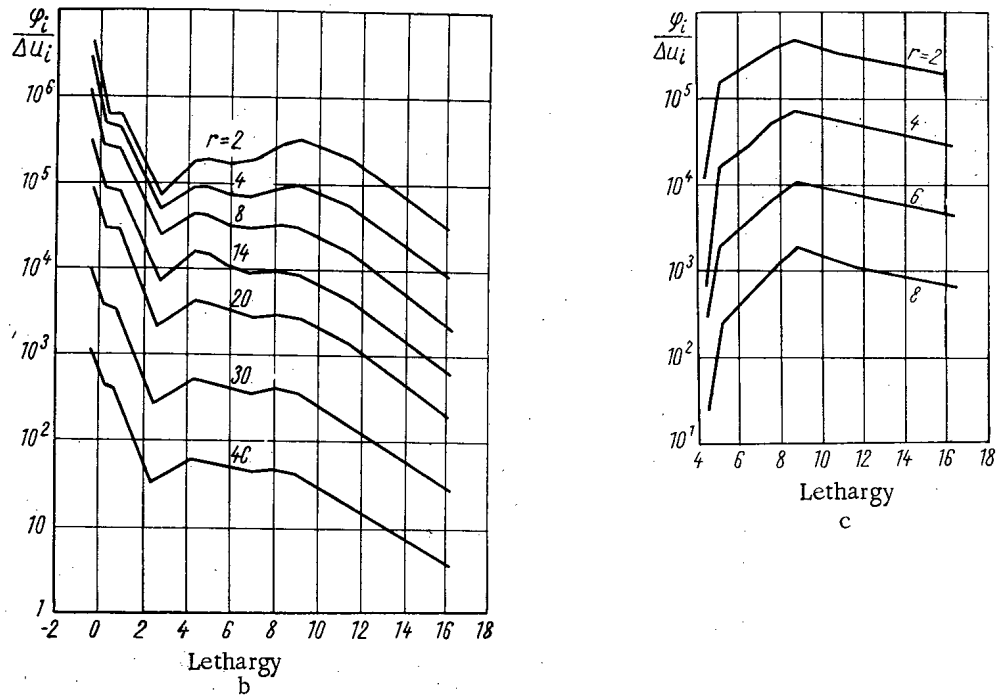

b c

Fig. 3. Neutron spectrum in water. Source: a) In group I; b) in group IX; c) in group XIV. (r is measured in cm.)

difference equations [2]. The Fermi spectrum was taken as the original. The variation of the microscopic cross sections with energy and other neutron parameters were taken from [3-6]. Data from these papers were used in setting up the matrix of elastic transitions in hydrogen and inelastic transitions in iron.

The distribution of monoenergetic electrons from the source was determined by analytic solution of Eq. (1). This was due to the fact that there was a deviation from the exact solution of the diffusion equation when the method of differential factorization was used at large distances from a concentrated source.

The analytic solution for a plane source in a homogeneous finite medium has the form

$$\varphi_i(r) = \frac{Q_i L_i}{2D_i} \cdot \frac{e^{-\frac{r}{L_i}} - e^{-\frac{1}{L_i}(2a_i - r)}}{1 + e^{-\frac{2a_i}{r}}},$$

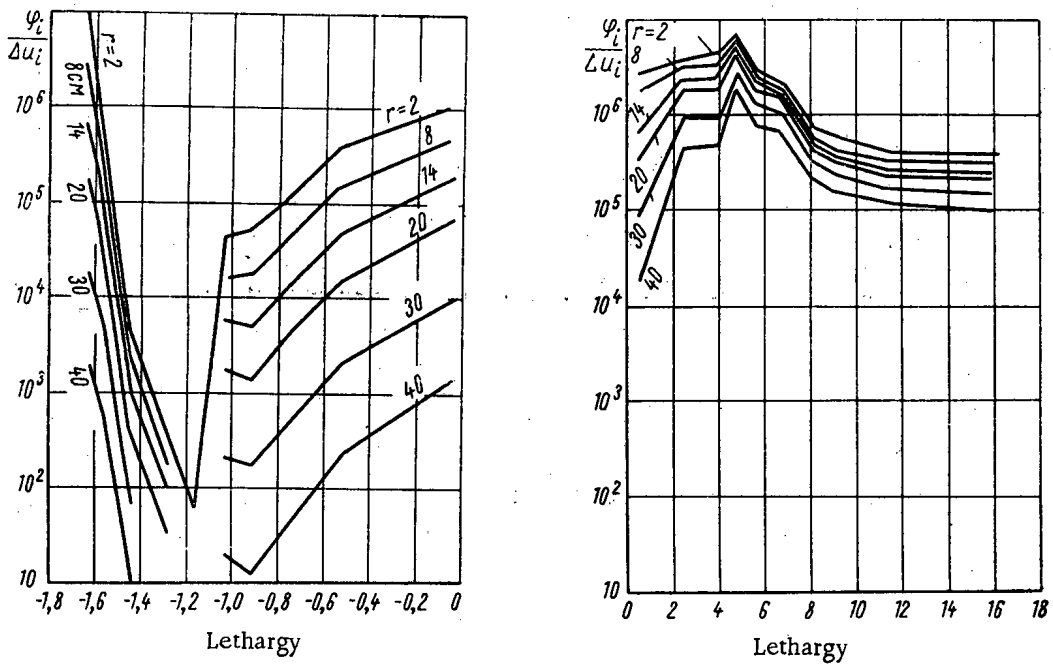

a

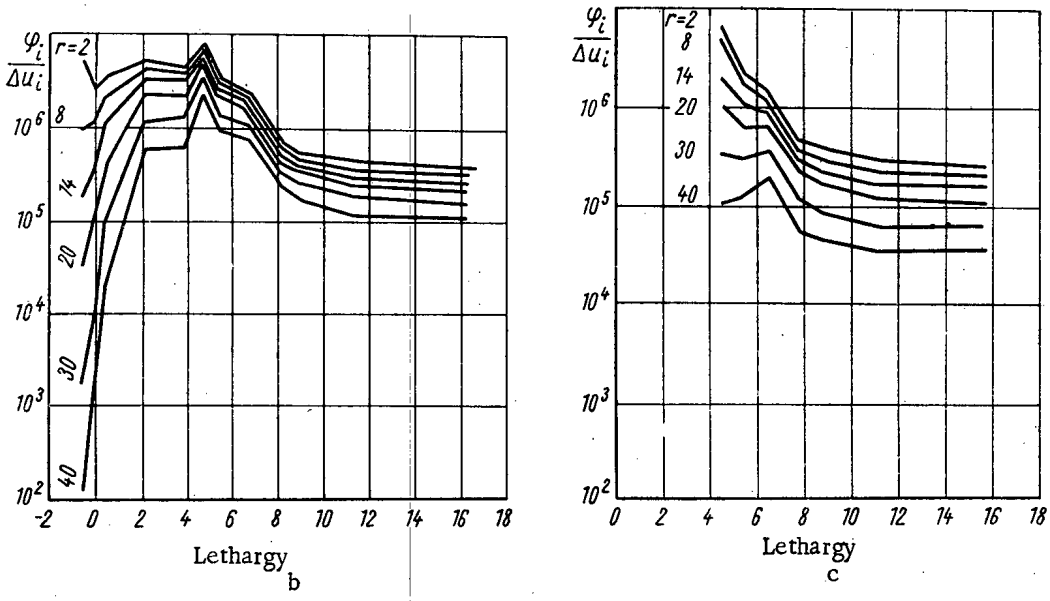

b c

Fig. 4. Neutron spectrum in iron. Source: a) In group I; b) in group IX; c) in group XIV. (r is measured in cm.)

where Q_i is the strength of the course in neutrons /cm^2 · sec, L_i is the fictitious diffusion length of monoenergetic neutrons in cm, a_i is the thickness of the shield, including the extrapolation length, and r is the distance from the source in cm.

If, however, the source neutrons diffuse in two adjacent layers of iron and water of finite thickness, the solution may be put in the form

$$\varphi_{i\mathrm{Fe}}(r) = \frac{Q_{i\mathrm{Fe}} L_{i\mathrm{Fe}}}{2D_{i\mathrm{Fe}}} \left\{ \frac{B_i}{B_i - 1} e^{-\frac{r}{L_{i\mathrm{Fe}}}} + \frac{1}{B_i - 1} e^{\frac{r}{L_{i\mathrm{Fe}}}} \right\},$$

$$\varphi_{i\mathrm{H_2O}}(r) = \frac{Q_{i\mathrm{Fe}} L_{i\mathrm{Fe}}}{2D_{i\mathrm{Fe}}} \cdot \frac{\frac{B_i}{B_i - 1} e^{-\frac{r_0}{L_{i\mathrm{Fe}}}} + \frac{1}{B_i - 1} e^{\frac{r_0}{L_{i\mathrm{Fe}}}}}{e^{-\frac{r_0}{L_{i\mathrm{H_2O}}}} - e^{-\frac{1}{L_{i\mathrm{H_2O}}}(2a_i - r_0)}} \left\{ e^{-\frac{r}{L_{i\mathrm{H_2O}}}} - e^{-\frac{1}{L_{i\mathrm{H_2O}}}(2a_i - r)} \right\}.$$

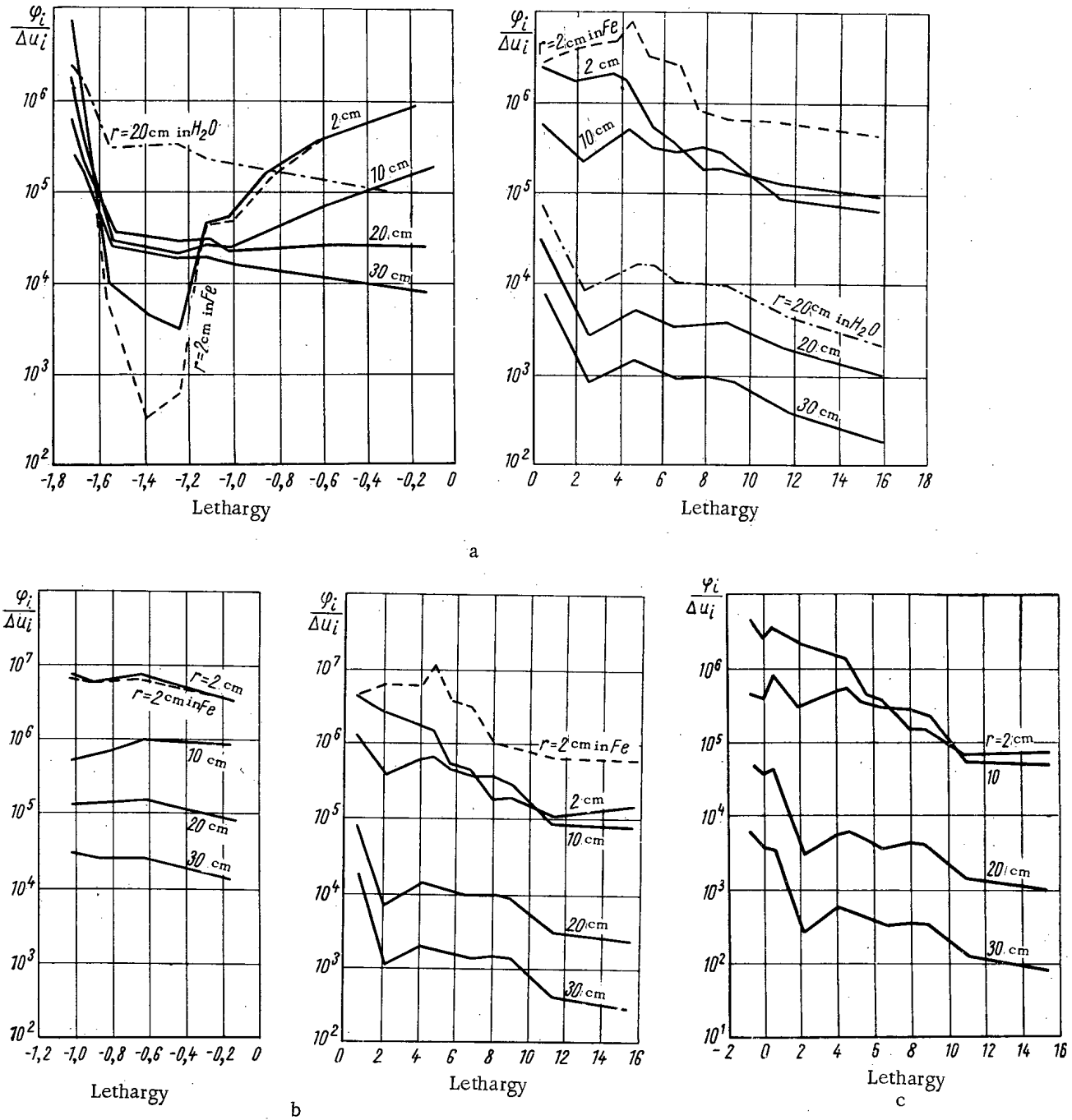

Fig. 5. Neutron spectrum in the iron–water system. Source: a) In group I; b) in group VII; c) in group IX.

Here we have introduced the following notation:

$$B_i = e^{\frac{2a_i}{L_{i\mathrm{Fe}}}} \frac{\left(\frac{D_{i\mathrm{Fe}}}{L_{i\mathrm{Fe}}} + \frac{D_{i\mathrm{H_2O}}}{L_{i\mathrm{H_2O}}}\right) - \left(\frac{D_{i\mathrm{Fe}}}{L_{i\mathrm{Fe}}} - \frac{D_{i\mathrm{H_2O}}}{L_{i\mathrm{H_2O}}}\right) e^{-\frac{2(a_i - r_0)}{L_{i\mathrm{H_2O}}}}}{\left(\frac{D_{i\mathrm{Fe}}}{L_{i\mathrm{Fe}}} - \frac{D_{i\mathrm{H_2O}}}{L_{i\mathrm{H_2O}}}\right) - \left(\frac{D_{i\mathrm{Fe}}}{L_{i\mathrm{Fe}}} + \frac{D_{i\mathrm{H_2O}}}{L_{i\mathrm{H_2O}}}\right) e^{-\frac{2(a_i - r_0)}{L_{i\mathrm{H_2O}}}}};$$

r_0 is the thickness of the first layer (Fe); $\varphi_{i\mathrm{Fe}}$ and $\varphi_{i\mathrm{H_2O}}$ are the fluxes of monoenergetic neutrons in the layers of iron and water respectively.

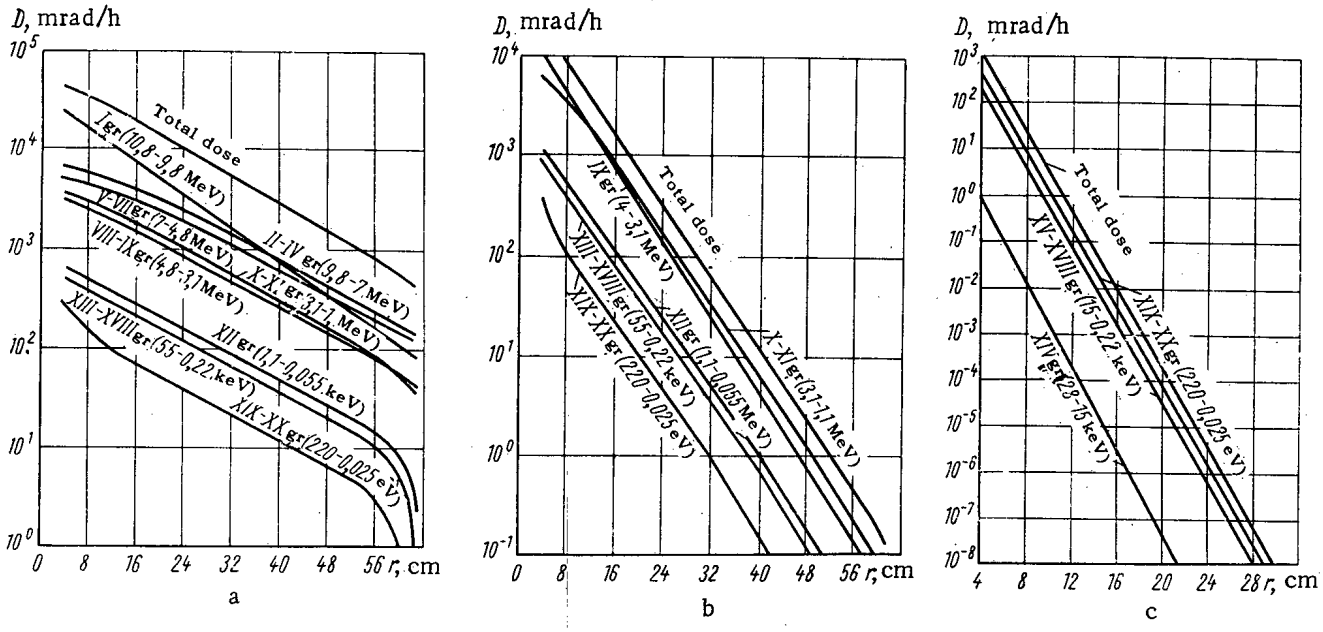

Fig. 6. Doses of neutrons of various energies in water. Source: a) In group I; b) in group IX; c) in group XIV.

The calculation was made in plane geometry for twenty monoenergetic sources with strengths of $2 \cdot 10^6$ neutrons/cm^2 · sec, embracing the energy range between 11 MeV and thermal energies (see Table).

The results of these calculations enable us to find the neutron distribution in other shield geometries also. The transformation from plane to spherical geometry (assuming a point-source center) may be effected by means of the formula

$$\varphi_{sph}(\bar{r}) = \frac{1}{2\pi L} \cdot \frac{1}{r} \varphi_{pl}(\bar{\eta}).$$

The transformation from plane to cylindrical geometry with a filament source at r = 0 is effected by means of the approximate relation

$$\varphi_{cyl}(\bar{r}) \approx \frac{1}{\sqrt{2\pi L}} \cdot \frac{1}{\sqrt{r}} \varphi_{pl}(\bar{r}),$$

where L is the diffusion length of the neutrons, and $\varphi(\bar{r})$ is the neutron flux in the corresponding geometry. For deriving the latter relationship, an asymptotic expansion of the function k_0 is used [7].

We compared the calculated results with our own experimental data and the data of other authors.

Figure 1 shows the radial distribution of neutrons with various energies emitted by a point Po-Be source in a sphere of water and in aniron—water system. The theoretical curve agrees closely with the experimental data.

Figure 2a shows neutron spectra in water at distances of 10, 20, 30, and 60 cm from the fission source. The continuous curves correspond to the neutron distributions obtained by the method of moments [8]. The crosses indicate the values calculated from the superposition principle on the basis of the results in the present paper. The spectra agree closely in the range E > 6 MeV. The discrepancies at low energies are due to leakage of the moderated neutrons, since in the second case the medium is finite.

Figure 2b gives an analogous comparison between calculation and experimental data for iron [9]. The calculated spectrum is normalized to the experimental results for E = 4.8 to 5.45 MeV at a distance of 20 cm from the source. There is good agreement for r values of 10 and 20 cm. For r = 40 cm the calculated curve lies below the experimental. In all cases the calculated values exceed the experimental in the range E_n < 2 to 3 MeV; this is apparently due to the different geometries used in experiment and theory. The experimental and theoretical curves have the same general character.

The comparison shows that the diffusion-transport approximation gives calculated values of practically acceptable accuracy, at least in a range up to 50 or 60 cm.

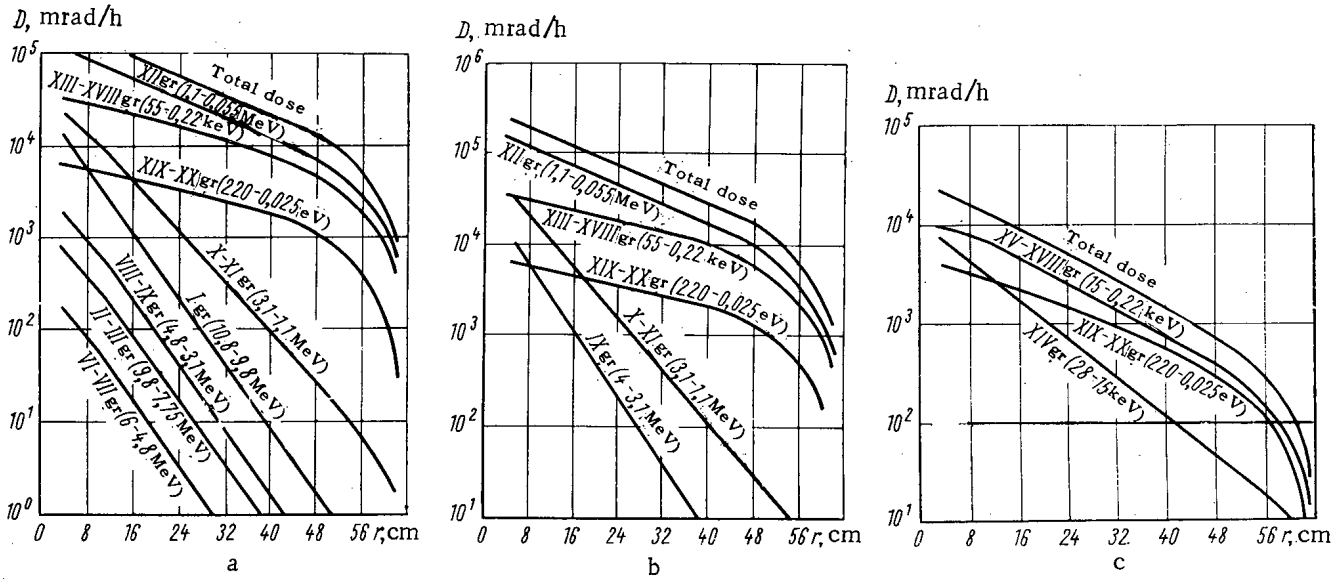

Fig. 7. Doses of neutrons of various energies in iron. Source: a) in group I; b) in group IX; c) in group XIV.

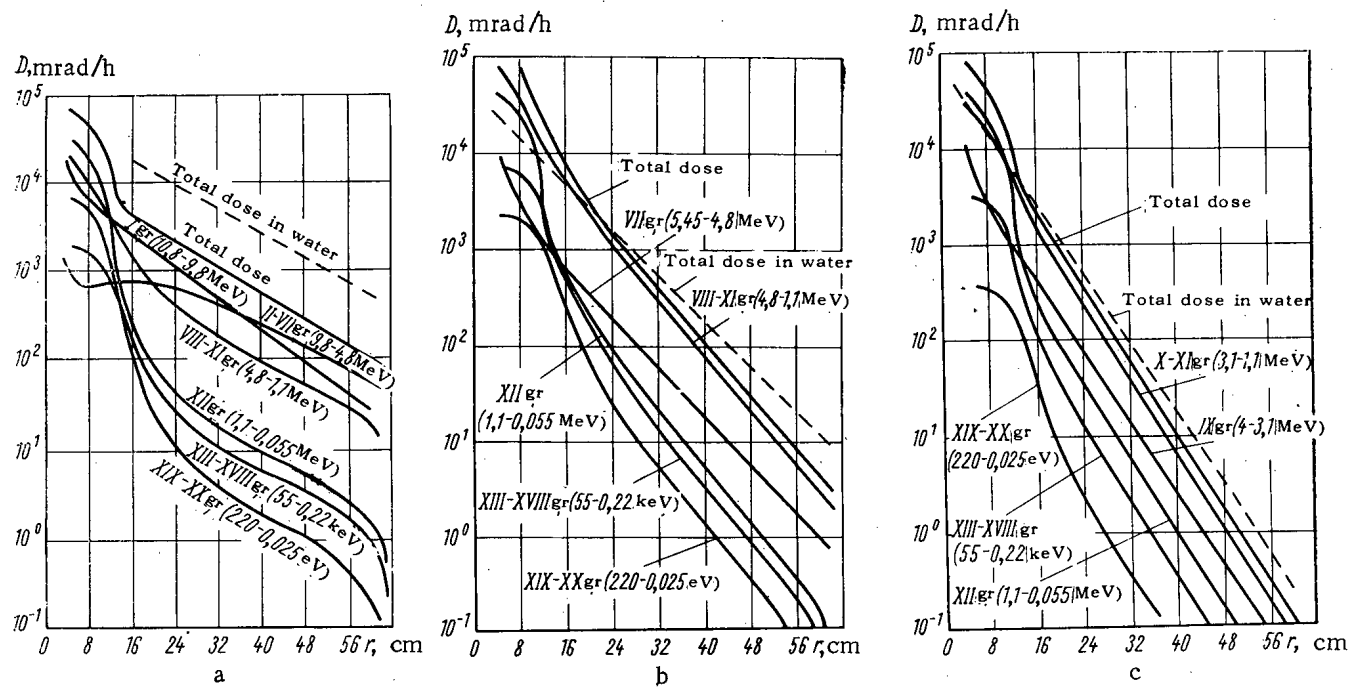

Fig. 8. Doses of neutrons of various energies in the iron–water system. Source: a) in group I; b) in group VII; c) in group IX.

Energy Spectra of Neutrons Emitted by Monoenergetic Sources

The results of the calculations enable us to trace the transformation of the neutron spectra during migration in the compositions considered.

Figures 3 to 5 show the energy spectra of neutrons for several monoenergetic sources situated in water, iron, and an iron–water system.*

Analysis of the histograms shows that the neutron spectrum has certain characteristic features in water (see Fig. 3, a, b, c; initial neutron energy 10 MeV, 4 MeV, and 20 keV respectively). In the high-energy range, even

*In the histograms the middles of the energy ranges are connected together for clarity. In calculating lethargy, the standard energy is taken as E = 2 MeV.

near the source, the spectrum passes from the monoenergetic to the continuous (and hence softer) type. The inversion of the spectrum is maintained on further increasing r. For an initial energy below 1 MeV, the monoenergetic source neutrons are absent even in the neighborhood of the source, which is explained by the effective slowing down of the neutrons at hydrogen nuclei.

Analysis of histograms 4, a,b, c, shows that in iron there is a considerable softening of the spectrum with increasing distance from the source. The characteristic feature in the high-energy region (see Fig. 4,a) is the dip in the curves over the range 6 to 7 MeV, later transforming into a high maximum at E < 1 MeV. This is due to the fact that, during the inelastic slowing-down processes, the neutrons pass into the intermediate-energy range, missing out the values E > 1 MeV. However, further slowing down of the neutrons at the iron nuclei takes place extremely slowly, in general as a result of elastic scattering. As a result of this, there is an accumulation of neutrons with energy E < 1 MeV.

The neutron spectrum in the iron-water system is a peculiar superposition of those corresponding to homogeneous iron and water shields and contains the characteristic features of both (see Fig. 5,a, b, c).

For example, for a source in the first group (see Fig. 5,a) and r = 2 cm (i. e., at a point within the iron layer), there is a dip in the spectral curve at 6 to 7 MeV. In this case, however, the minimum is less severe than in the case of homogeneous iron.

This circumstance implies the development of a counterflow of neutrons with energies between 6 and 7 MeV in the two-layer system, moving from the water to the iron. Hence the effect of the water on the spectrum is even felt at this great depth in the iron. The leveling effect of the water rises still more with increasing r. Thus the curve for r = 10 cm (boundary point) is characterized by quite a small minimum in the range in question, while a long way from the iron, in the water (r = 20 cm), the character of the histogram resembles the analogous distribution in water.

In the case of a source in groups VII and IX (see Fig. 5, b, c) the histograms have smooth curves in the high-energy range, while in the low-energy part of the spectrum the curves are much the same as in the preceding case (see Fig. 5a).

Effectiveness of Various Shielding Compositions

The effectiveness of the shielding was estimated from the distribution curves of the doses created by neutrons of various energies.

Figure 6 shows some D(r) curves for water. In the case of a source lying in the first group (see Fig. 6a), at a distance of 40 cm from the source, the total dose of the I-to-XI energy groups (fast-neutron dose) is more than 30 times that of the XII-to-XVIII energy groups, which correspond to neutrons of medium energy. If, however, the source lies in group IX, the contribution of fast neutrons exceeds that of the intermediate neutrons by an order of magnitude (see Fig. 6, b). In all cases considered, the contribution of the slow neutrons is small.

If the source lies in the low-energy part of the spectrum (E < 1 MeV) then the dose falls to zero even in the source zone (see Fig. 6, c). Hence for such sources a single layer of water shielding is so effective that additional layers of iron are superfluous.

The spectral composition of the dose in iron differs considerably from that described above (Fig. 7, a, b, c). Thus the dose distribution for a source in the first group (see Fig. 7, a) shows that the total dose is mainly affected by neutrons of intermediate energies (groups XII to XVIII, corresponding to energies between 1 MeV and 0.22 keV). At r = 40 to 50 cm, the contribution of these to the total dose is almost two orders greater than that of the fast neutrons. As regards the latter (groups I to XI, E > 1 MeV), the dose curves of these groups rapidly fall to zero with increasing r.

The energy distribution of the doses has a similar character for all the remaining groups of sources (see Fig. 7, b, c). It should be noted that, as the initial energy of the neutrons falls, the curves for the total dose approach the component curves. Hence the spectral composition of neutron radiation must be taken into account for sources with a spectrum situated above 1 MeV.

A point worth noting is the slow fall in the total-dose curve, which indicates the undesirability of using a homogeneous iron shield.

The dose distributions for the iron-water system are shown in Fig. 8, a,b, c. We see from the D(r) curves that a characteristic trait of these is the existence of a break at the boundary between the media, due to the redistribution

of the neutron fluxes. By way of example, let us consider the dose distribution for a source of the first group (see Fig. 8, a). The curves have a considerably greater slope in the iron layer than in the water. This is because the water slows the neutrons of this group (9.8 to 10.8 MeV) down very poorly.

The dose curve of groups II to VII (4.8 to 9.8 MeV) falls out of the general picture, being very shallow. The point is that there is a peculiar vacuum for neutrons of these energies in iron. This creates conditions for the migration of neutrons from the water into the iron, and it is this which causes the peculiar form of the curve.

The neutrons from energy groups XII to XVIII, which in the case of an iron shield constitutes one of the main components, contribute less than 10% of the total dose in the iron-water system.

It is interesting to make a quantitative comparison of the doses in water and in the iron-water system (see broken curves in Fig. 8, a, b, c). Thus, for fast neutrons with energies between 9.8 and 10.8 MeV, the total-dose curves in the iron-water system lie half an order lower than in the case of pure water. This difference gradually diminishes and vanishes entirely at about E = 1 MeV. Hence the iron-water shielding is effective for an initial source-neutron energy of over 1 MeV.

The detailed study of fast-neutron migration in iron, water, and iron-water shielding enables us to make a quantitative estimate of the effectiveness of these forms of shielding for neutrons of various energies. The dose curves presented may be used for calculating the neutron shielding associated with a source of any energy spectrum.

LITERATURE CITED

1. G. I. Marchuk, Numerical Methods of Calculating Nuclear Reactors [in Russian], Moscow, Atomizdat (1958).
2. O. A. Barsukov and V. S. Avzyanov, Atomnaya Énergiya, 10, 478 (1961).
3. D. Hughes, Neutron Cross Sections, BNL (1958); Supplement, No. 1 (1960).
4. I. V. Gordeev et al., Handbook on Nuclear-Physical Constants for Reactor Calculations [in Russian], Moscow, Gosatomizdat (1960).
5. I. V. Gordeev et al., Nuclear-Physical Constants [in Russian], Moscow, Gosatomizdat (1963).
6. L. P. Abagyan et al., Group Constants for Calculations of Nuclear Reactors [in Russian], Moscow, Atomizdat (1964).
7. I. N. Bronshtein and K. A. Semendyaev, Handbook on Mathematics [in Russian], Moscow, "Nauka" (1964).
8. Shielding of Transport Equipment with Nuclear Motors [Russian translation], Moscow, IL (1961), p. 40.
9. A. P. Veselkin et al., Atomnaya Énergiya, 17, 32 (1964).

METHOD OF DEMARCATING OIL-BEARING AND WATER-BEARING STRATA BASED ON THE RECORDING OF DELAYED NEUTRONS

M. M. Dorosh, Ya. É. Kostyu,
V. A. Shkoda-Ul'yanov, A. M. Parlag,
and A. K. Berzin

UDC 543.53

A method of differentiating between oil- and water-bearing rock strata based on the difference between the nuclear compositions of oil and water (as regards O^{18} content) is described. A property of N^{17} nuclei based on the emission of delayed neutrons is used.

The separation of the oil- and water-bearing components of a stratum in uncased wells is in the majority of cases quite easily effected by electrometric methods. In cased wells, this problem can only be solved by non-electrical (e. g., radiometrical) methods.

Oxygen and carbon, by the percentage content of which water and oil are distinguished, have small cross sections with respect to the processes usually used for the solution of such problems, and main attention in nuclear geophysics is concentrated on the properties of other elements present in water (Na, Cl, etc.). The establishment of indirect methods by no means fully solves the problem, as is very apparent when working with weakly-mineralized waters, or waters freshened by the injection of fresh water used for extracting oil during the intensive exploitation of oil fields.

One possibility not so far studied is the use of the (γ, n)-reaction of the C_6^{13} nucleus which occurs on bombarding this with monochromatic γ quanta; another possibility is the use of the nuclear properties of the O_8^{18} isotope. This is less abundant than other isotopes (around 0.2%), but on bombarding this nucleus with γ of fairly high energy the specific reaction $O^{18}(\gamma, p)N^{17} \xrightarrow{\beta^-} O^{17} \rightarrow O^{16} + n$ takes place*. The unstable N^{17} nucleus is a well-known source of delayed neutrons with a half-life of 4.15 sec. Since determination of the boundaries of water-containing media by existing methods presents no difficulty, we have here a new principle for separating water- and oil bearing strata in these media by recording the delayed neutrons formed in the $O^{18}(\gamma, p)N^{17}$ reaction.

*Preliminary experiments show that the "next zone" does not eliminate the effect, but only necessitates an increase in the intensity of the γ quanta, since the delayed-neutron yield falls by 20 to 30% because of the "next-zone" effect.

Delayed-Neutron Yields from Water- and Oil-Bearing Strata

E, MeV	Q, × 10^{-8} delayed neutrons		Q, × 10^{-6} delayed neutrons		Q, × 10^{3} delayed neutrons	
	Water-bearing stratum	Oil-bearing stratum	Water-bearing stratum	Oil-bearing stratum	Water-bearing stratum	Oil-bearing stratum
17	0,10	0,05	12,90	7,43	3,87	2,23
18	1,57	0,86	19,83	11,81	5,95	3,56
19	5,19	2,93	21,01	12,50	6,33	3,75
20	11,03	6,17	23,74	14,36	7,12	4,32
21	18,88	10,72	—	19,69	—	5,92

Translated from Atomnaya Énergiya, Vol. 21, No. 1, pp. 35-38, July, 1966. Original article submitted January 20, 1966.

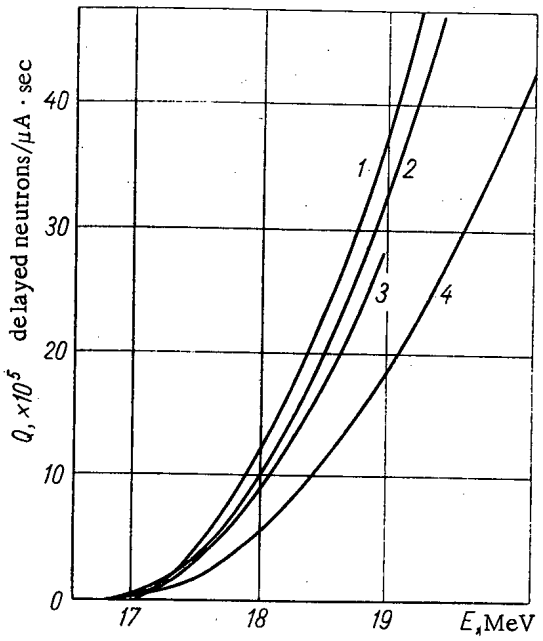

Fig. 1. Calculated curves for the delayed-neutron yield from: 1) water; 2) water-bearing stratum (70% SiO_2 + 30% H_2O); 3) sand; 4) oil-bearing stratum (70% SiO_2 + 30% petroleum).

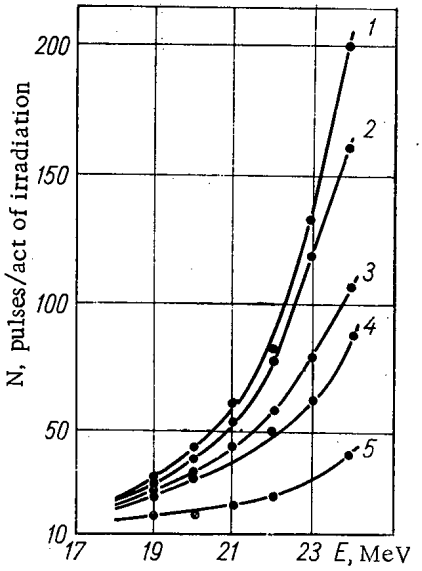

Fig. 2. Measured delayed-neutron yields per act of γ quantum irradiation for: 1) water, 2) water-bearing stratum, 3) sand, 4) oil-bearing stratum, 5) petroleum.

The point is that petroleum contains a negligibly-small quantity of oxygen, so that on passing from the oil-bearing to the water-bearing stratum there will be a sharp change in the neutron yield. As regards the deleterious effects of the "next zone" in actual strata, these will be small in the method proposed owing to its great depth.

In the present investigation, we calculated the delayed-neutron yields for a target of almost infinite thickness by means of the Belen'kii-Tamm avalanche theory, using the excitation function of the $O^{18}(\gamma, p)N^{17}$ reaction, experimentally measured in [1]. Figure 1 shows the results of these calculations for water, sand, and also for oil- and water-bearing strata when these are bombarded by 17-to-20MeV electrons.

The small variation in the delayed-neutron yields for water, sand, and a water-bearing stratum is due to the fact that there is a special kind of compensation between the oxygen in the SiO_2 and the water. This gives rise to the sharp jump on passing to an oil-bearing stratum. The greater the petroleum content, the lower will the curve giving the delayed-neutron yield from the oil-bearing stratum lie in relation to curve 2 (Fig. 1), which serves as a boundary criterion.

For the petroleum concentration in question (order of 30% petroleum in the stratum), the jump in the delayed-neutron yield on passing from the oil- to the water-bearing stratum, corresponding to irradiation in the 17-to-20-MeV energy range, is characterized by a factor of 2.

The Table shows the delayed-neutron yields for the case of primary bombardment by γ radiation. As might be expected, the yields are considerable.

In order to elucidate the practical possibilities of the proposed method of warding off water-petroleum contact, we made some experiments on the 25-MeV betatron of Uzhgorod State University. At maximum energy, the intensity of the radiation is 30 R/min · m for a γ quantum pulse length of 10 to 12 μsec and a repetition frequency of 50 cps. The mean beam electron-current falling on the target is of the order of 10^{-8} A.

The thick target constituted a metal tank 72 cm long and 13 cm in diameter, filled successively with petroleum, stratal water, and mixtures of sand with water or petroleum, these imitating water-bearing and oil-bearing strata, respectively.

The apparatus for recording the delayed neutrons consisted of a paraffin cube 50 × 60 × 70 cm in size with a central channel 13 cm in diameter for accommodating the samples and two counters of the SNM-8 type. The neutron-recording efficiency of this system, using a Po-Be source, was 0.33%.

Relative monitoring of the beam was effected by means of a straight-through integral chamber with an RC circuit having a time constant of 6 sec, equal to $1/\lambda$ for the N^{17} isotope; this enabled errors in the experimental data due to changes in the intensity of the γ radiation to be avoided.

After 15 to 20 sec of irradiation, the activity of the N^{17} nuclei practically reached saturation. Assuming that the interval between two successive pulses of γ quanta in the betatron equals 20 msec and the maximum operating time of the relay is of the same order, we may consider that the recording of neutrons took place within not more than 40 msec after removing the γ beam. The corresponding loss in neutron count is of the order of 0.7% for N^{17} with a half-life of 4.15 sec.

The leading edge of the sample was placed at a distance of 44 cm from the tungsten target of the betatron, the beam intensity of which did not exceed 10 to 15 R/min (at a distance of 1 m from the target) and a maximum energy of 25 MeV during the experiments. In the basic measurements, the intensity of the γ beam was measured by an absolute aluminum ionization chamber.

The experimental results for the delayed-neutron yields are shown in Fig. 2. The x axis represents the maximum energy of γ quanta and the y axis represents the number of pulses per act of irradiation (each point corresponds to the results of five to seven measurements).

We see from the results presented that even for relatively small γ beam intensities (current of the order of 10^{-9} A in the absolute ionization chamber at the position of the sample) at an energy of 21 MeV and higher there is quite a marked jump in the delayed-neutron yield on passing from the oil-bearing to the water-bearing stratum and vice versa, i. e., we obtain information on the position of the contact zone. The method proposed may also possibly provide quantitative information on the petroleum content of the strata, although there are certain difficulties in this owing to specific characteristics of each particular well. We note that it is not absolutely necessary that the recording of the delayed neutrons should only be carried out after the accelerator has been switched off.

In the present experiments, delayed neutrons were also recorded in the intervals between γ quantum pulses within 7 msec of the electron throw on to the inner target of the betatron. The neutron-count rate for water-bearing strata (recorded with a neutron apparatus of about 1% efficiency) was 100 to 130 pulses/min.

Thus the theoretical and experimental results presented show that there is a real possibility of warding off water-oil contact if an accelerator giving γ quanta with an energy higher than the 16.4-MeV threshold of the $O^{18}(\gamma, p)N^{17}$ reaction (say 17 to 20 MeV) is available.

Experiment showed that a delayed-neutron intensity adequate for recording is obtained if there is a γ quantum flux at the stratum sufficient to give a current of the order of 10^{-9} A in the absolute ionization chamber described in [2]. This order of intensity can be obtained even with low-powered equipment.

The creation of a small-scale cyclic accelerator giving γ quanta of 17 to 20 MeV at an adequate intensity is a complex and as yet unsolved problem; considerable work has however already been done in this direction and a certain amount of success has been achieved. The following possibilities, in the opinion of the authors, deserve attention in this respect.

It is well known that, on bombarding lithium or tritium targets with protons, the following reactions take place:

$$_3Li^7 + {}_1H^1 \rightarrow {}_4Be^8 + \gamma \text{ with } E = 17.6 \text{ MeV},$$
$$_1H^3 + {}_1H^1 \rightarrow {}_2He^4 + \gamma \text{ with } E = 20 \text{ MeV}.$$

In the first reaction γ quanta with an energy of around 17.6 MeV are formed; this is sufficient for excitation of the $O^{18}(\gamma, p)N^{17}$ reaction.

Approximate calculations showed that, in order to ward off water-oil contact, the proton-accelerator current should be not less than 100 μA.

Work being done on the design of small-scale (oil-well) betatrons in the Tomsk Polytechnic Institute under the direction of A. A. Vorob'ev [3], heavy-current small-scale iron-free betatrons with equilibrium-orbit radii of 3 to 20 cm (A. I. Pavlovskii et al. [4]), plasma accelerators, and iron-free synchrotrons (under the direction of G. I. Budker) [5], all suggest that the method described here [6] will prove promising as regards further technical development.

LITERATURE CITED

1. W. Stephens, J. Halpern, and R. Sher, Phys. Rev., 82, 511 (1951).
2. B. Flowers, J. Lawson, and F. Fossey, Proc. Phys. Soc., 65B, 286 (1952).

3. Summaries of Papers Presented to the Fifth Inter-University Scientific Conference on Electron Accelerators (Tomsk, March 17 to 21, 1964) [in Russian], Tomsk, izd. Tomsk. gosudarstvennogo univ.: V. A. Gorbunov, G. A. Kunitsyn, and Yu. A. Otrubyannikov, Starting an Iron-Free Pulse Betatron; L. M. Anan'ev and V. L. Chakhlov, Economic System for Throwing Electrons in Heavy-Current and Small-Scale Betatrons; V. L. Chakhlov and M. M. Shtein, Small-Scale Source of Gamma Radiation with an Energy of 17.4 MeV; L. M. Anan'ev and Ya. S. Pekker, Single-Pulse Iron-Free Betatron; L. M. Anan'ev et al., Portable Small-Scale Betatron for the Defectoscopy of Large-Scale Features in Field and Assembly Conditions; V. A. Vorob'ev, G. V. Titov, and V. L. Chakhlov, Use of Small-Scale Betatrons for the Radioscopic Control of Materials under Erection-Platform Conditions.
4. A. I. Pavlovskii et al., DAN SSR, 160, 68 (1965).
5. G. I. Budker et al., Iron-Free Single-Turn Synchrotron (BSV) [in Russian] Preprint, Novosibirsk (1965).
6. A. K. Berzin et al., Authors' Certificate No. 174, 284, December 12, 1963.

DOSIMETERS BASED ON GLASSES WITH OPTICAL DENSITIES VARYING ON IRRADIATION

G. V. Byurganovskaya, E. G. Gvozdev, and A. I. Khovanovich

UDC 621.387.46:621.386.82

Information on the composition and sensitivity of glass dosimeters, the operation of which is based on the change in optical density caused by irradiation, is reviewed. The principal dosimetric characteristics of the Soviet γ dosimeter SGD-8 and the γ neutron dosimeter L-15 (based on sodium- and lithium-silicate glasses with nickel additives) are described; these enable doses from a few tens of roentgens to a million roentgens to be determined.

In view of the growing use of nuclear radiations in various departments of science and technology, it has become necessary to devise a simple, versatile dosimeter capable of repeated use. Glass dosimeters have proved promising in this respect. By suitable choice of compositions it is possible to produce glasses by means of which the γ component in mixed γ and neutron radiation can be determined.

The first glass dosimeter which found practical application was made of a home-produced optical glass (with a large content of alkali-metal oxides); this darkened substantially under the influence of γ- and x radiation. The dose was measured from the increment in the optical density of the irradiated glasses. However, since this glass is sensitive to slow neutrons and also undergoes severe spontaneous decolorization (regression), it is very limited in application.

Outside the Soviet Union, a phosphate glass composed of 50 wt. % $Al(PO_3)_3$, 25 wt. % $Ba(PO_3)_2$, and 25 wt. % KPO_3 has been proposed for dosimetric purposes [1]. The transparency of this glass falls linearly with increasing dose up to 10^5 R (for larger doses saturation effects set in).

Of special interest are silicate glasses containing traces of cobalt oxide, which raises the sensitivity of the glasses to radiation in the short-wave part of the spectrum [2-4]. Glasses containing 60 to 70 wt. % SiO_2, 10 to 20 wt. % Na_2O, 1 to 20 wt. % B_2O_3, CaO, MgO, Al_2O_3, with the addition of 0.1 to 16 wt. % Co_3O_4 have been studied. With increasing cobalt-oxide content, the sensitivity of the glasses to radiation increases and the regression diminishes. The glasses may be used for doses from several hundred to 10^7 R. The presence of boric anhydride makes the glasses sensitive to neutrons and hence suitable for the dosimetry of mixed radiations. The marked spontaneous decolorization of the boron-silicate glasses, however, limits their field of use.

Dosimeters for doses of 10^4 to 10^7 R may be made from silicate glasses containing manganese and cerium oxides [5, 6]. For stabilization of the induced absorption of manganese glasses, compounds of iron and tin are introduced into them. The addition of vanadium or chromium to manganese glasses raises their sensitivity to small doses. Examination of the possibilities of determining large doses of radiation (10^6 to 10^9 R) showed [7] that the most promising in this respect were glasses with a high content of Sb_2O_3 (60 to 70 wt. %), and also glasses [8] containing 50 wt. % Bi_2O_3; in these glasses there was no saturation even at a dose of 10^9 R; the optical density after irradiation with 10^8 R was of the order of 10 in 1 cm. Great sensitivity to radiation is shown by iodide-metaphosphate glass [9], which changes its tint on irradiation by a dose of 70 R. Sodium-borate glass tinted to a blue color with elementary sulfur may be used as an indicator. Under the influence of γ and x radiation this becomes colorless [10].

The authors of the present paper made a special study of glasses not containing B_2O_3, BaO, and PbO. As additives, cobalt and nickel oxides were introduced.

The sensitivity of the glasses to radiation was expressed in terms of the increment in the optical density (for $\lambda = 350\ m\mu$) per unit thickness (in the present case 1 cm) after irradiation with a dose of 10^4 R, i. e.,

Translated from Atomnaya Énergiya, Vol. 21, No. 1, pp. 38-41, July, 1966. Original article submitted May 21, 1965; revised December 22, 1965.

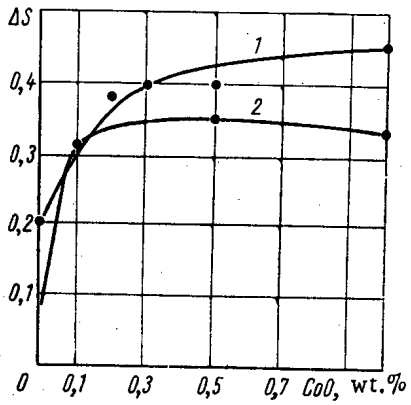

Fig. 1. Sensitivity of silicate and phosphate glasses irradiated with γ radiation (up to a dose of 10^4 R) as a function of the cobalt-oxide concent (λ = 350 mμ): 1) Silicate glasses; 2) phosphate glasses

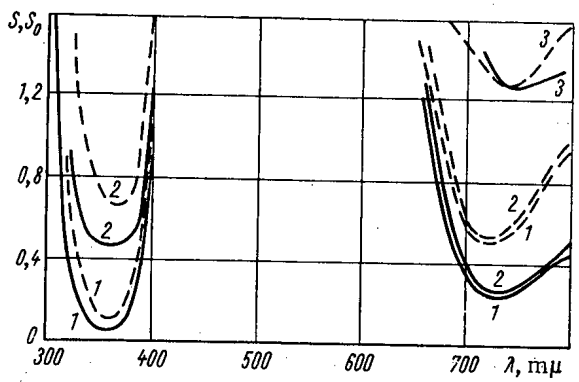

Fig. 2. Spectral curves of optical density: ———) silicate glass; – – – –) barium-silicate glass; 1) before irradiation; 2) 10^4 R; 3) $2 \cdot 10^6$ R.

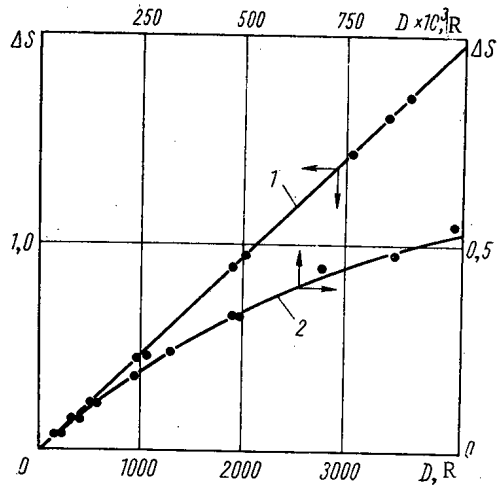

Fig. 3. Sensitivity of silicate glass containing nickel as a function of γ radiation dose: 1) λ = 350 mμ; l = 100 mm; 2) λ = 740 mμ; l = 5 mm.

$$\Delta S = \frac{S - S_0}{l},$$

where S is the optical density of the irradiated sample (S = –log T, T = transmission coefficient), S_0 = optical density of the nonirradiated sample, and l = sample thickness.

Study of silicate and phosphate glasses containing various quantities of CoO (0.1 to 1 wt. %) showed that the sensitivity systematically increased with increasing cobalt-oxide content (Fig. 1), being considerably smaller for the phosphate glasses. Increasing the cobalt-oxide content to 10 wt. % reduces the sensitivity of the glasses to radiation. Glasses containing cobalt and nickel are two or three times more sensitive to radiation than those containing other additives (CeO_2, Nd_2O_3, Fe_2O_3, SnO_2 and etc.).

The most suitable types for dosimetric purposes were silicate glasses of complex composition containing NiO. These had a rather larger sensitivity to radiation than cobalt glasses, a smaller regression factor, and a rapid fall in induced radioactivity after irradiation with a mixed radiation flux. The regression factors K = $\log(S_1/S_2)/\log(t_2/t_1)$ (where S_1 and S_2 are the optical densities at times t_1 and t_2 respectively) of cobalt glasses for λ values of 350 and 740 mμ are 0.02 and 0.05 respectively, while for nickel glasses they are 0.005 and 0.02. The spectral curves for the optical density of the glasses (SGD-8) before and after irradiation are shown in Fig. 2. The sensitivity of the glass with the nickel additive equals 0.45. The relationship between the sensitivity (for λ = 350 mμ) and the radiation dose is linear over the range studied (Fig. 3). By measuring* the optical density (for λ = 350 mμ) of samples 100 and 5 mm thick, we can determined doses in two ranges: 50 to 4000 and 2000 to 80,000 R respectively.

In order to determine doses of $2 \cdot 10^4$ to 10^6 R, the long-wave part of the spectrum (λ = 740 mμ) is used with sample thicknesses of 5 mm. A study of the sensitivity of glasses 100 mm thick to radiation in the energy range 50 to 1500 keV showed that, on using lead filters of appropriate thickness (0.3 to 0.5 mm), the readings of the dosimeters would be practically independent of the energy of radiation above 60 keV. When using the dosimeters in the temperature range –100 to + 100° C, the error in determining the optical density due to decolorization does not exceed ± 10%. By heating the irradiated glasses to 400 or 450° C for 6 h, the original optical density can be completely restored; since the sensitivity of the glass dosimeters does not depend on the number of restorations, they can be used repeatedly.

*On the SF-4 spectrophotometer or the photoelectric colorimeter FÉK-60.

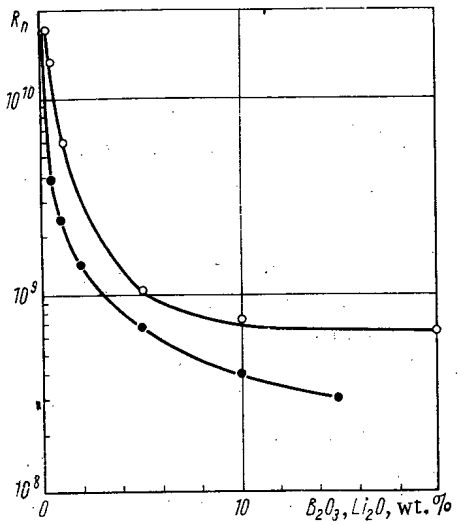

Fig. 4. Sensitivity of silicate glass to slow neutrons as a function of B_2O_3 and Li_2O content (λ = 350 mμ): ○) B_2O_3; ●) Li_2O.

For measuring doses of γ radiation with a narrow spectral energy range, for example, from a Co^{60} source, we may use glasses of any composition having negligible regression.

A study of the effect of P_2O_5, B_2O_3, Bi_2O_3, BaO, CdO and PbO on the sensitivity of silicate glasses containing nickel to radiation showed that the lowest sensitivity for λ = 350 mμ belonged to the borate glasses and the highest to the barium-silicate glasses. On increasing the proportion of boric anhydride in the glasses to 20 wt.%, the sensitivity of the silicate glasses falls to less than half. On introducing up to 40 wt. % barium oxide and up to 10 wt. % cadmium oxide, the sensitivity of the glasses systematically increases, reaching values of 0.65 (see Fig. 2). Further increasing the quantities of these oxides has little effect. The optical density of the barium-silicate glass falls by 5% within 100 h after irradiation has ceased.

In order to examine the possibility of setting up a γ–neutron dosimeter the sensitivity of certain experimental glasses with various proportions of boric anhydride and lithium oxide to slow neutrons was determined. The presence of B_2O_3 or Li_2O produces an additional increase in sensitivity as a result of the $B^{10}(n, \alpha)Li^7$ and $Li^7(n, \alpha)T$ reactions. The sensitivity of the glasses to neutrons is characterized by the quantity

$$R_n = \frac{\Pi_n}{D_n},$$

where Π_n is the neutron flux in 1 cm^2, $D_n = D_{n+\gamma} - D_\gamma$ is the dose of neutrons in rem.cm^2/neutron ($D_{n+\gamma}$ is the total dose of γ and neutron radiation, determined by measuring the optical density of the irradiated glasses with a correction for regression, D_γ is the dose of γ radiation). As the content of B_2O_3 or Li_2O in the glasses increases, the neutron flux producing the same darkening as γ radiation (dose of 1 R) systematically falls, tending to a certain definite value in the case of boron-silicate glasses (Fig. 4). Hence there is no point in raising the boric-anhydride content of the glasses above 20 wt. %. The Li_2O content is limited by the chemical stability of the glasses. For dosimetry of a mixed flux of radiation, we can recommend lithium-silicate glass containing a nickel additive (L-15). In sensitivity to γ radiation, type of absorption spectrum, relationship between optical density and the dose and energy of the radiation, and kinetics of spontaneous and thermal decolorization, L-15 glass hardly differs from SGD-8 and is suitable for repeated use.

LITERATURE CITED

1. J. Schulman, C. Keick, and H. Rabin, Nucleonics, No. 2, 30 (1955).
2. N. Kreidl and J. Hensler, J. Amer. Ceram. Soc., 38, 423 (1955).
3. N. Kreidl and H. Blair, Nucleonics, No. 1, 56 (1956).
4. N. Kreidl and H. Blair, Nucleonics, No. 3, 82 (1956).
5. J. Paymal, M. Bonnaud, and P. Clerk, J. Amer. Ceram. Soc., 43, 430 (1960).
6. J. Kügler, Atomkernenergie, 4, 67 (1959).
7. W. Hedden, J. Kireher, and B. King, J. Amer. Ceram. Soc., 43, 413 (1960).
8. A. Bishey, Phys. Chem. Glasses, 2, 33 (1961).
9. A. Hiesenrod and B. Gehauf, Chem. Phys., 24, 914 (1956).
10. K. Otley and W. Weyl, J. Appl. Phys., 23, 499 (1952).

REFLECTION OF 250-1200 keV ELECTRONS

L. M. Boyarshinov

UDC 539.124:539.121.72

For primary radiation with energies of 250-1200 keV, the electron reflection coefficient (back scattering) was measured for targets of bismuth, tin, molybdenum, copper, and iron. The reflected electrons were collected in an aluminum Faraday cup and recorded with a microammeter.

The values of the reflection coefficients for primary monoenergetic electrons with energies of 1200 and 250 keV are shown in Figs. 1 and 2, respectively. In addition, a determination was made of the secondary electron emission coefficient, which was 10-15% of the value of the reflection coefficient for primary electrons.

As is clear from Figs. 1 and 2, the values for the reflection coefficient at 1200 keV are approximately 15% less than the reflection coefficients for the same targets at 250 keV. Such a reduction in reflection coefficient with increasing primary electron energy was first established in this work for the 250-600 keV energy range and was verified for the 600-1200 keV region.

Also shown in Fig. 1 is a comparison of the results of this work with published data [1-3] obtained from measurements using a similar technique. As can be seen from Fig. 1, the results of the present work are in good agreement with published data. The curve in Fig. 1 was constructed from data for 22 independent measurements of reflection coefficients for 18 elements in the periodic table with atomic numbers 4-92, and can be used to determine the nature of the dependence of reflection coefficient η on atomic number Z. From this most representative curve, and also from similar curves for other primary electron energies, one of which is shown in Fig. 2 for 250 keV (where the reflection coefficient for aluminum was taken from [4]), it is possible to establish that this dependence is determined by the expression

$$\eta = AZ^n,$$

where A is a constant.

In determining the thickness of coatings [5], and in doing chemical analysis by reflected β radiation, it has been shown that sensitivity is greater for larger exponents n. For monoenergetic electrons, it was established that the exponent n increases with increasing energy, and therefore it is most advisable to use harder radiation sources for the abovementioned practical purposes.

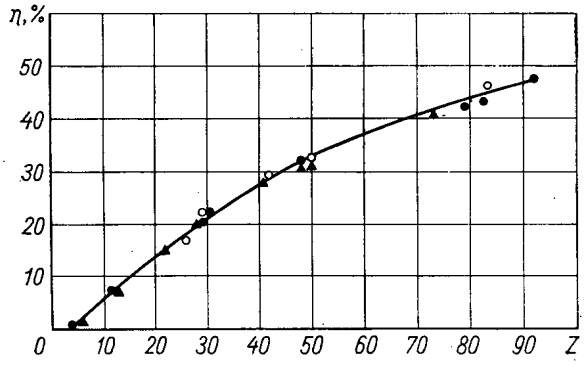

Fig. 1. Reflection coefficient as a function of atomic number for 1200 keV electrons: ○) This work; ▲) [1, 2]; ●) [3].

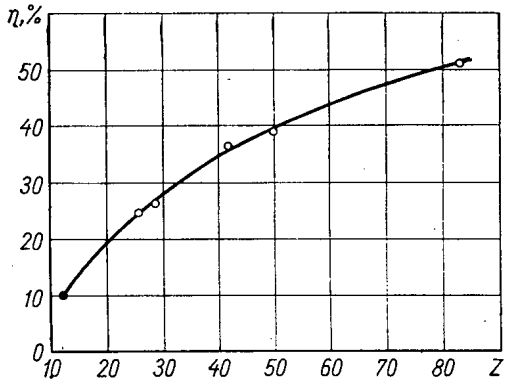

Fig. 2. Reflection coefficient as a function of atomic number for 250 keV electrons: ○) This work; ●) [4].

Translated from Atomnaya Énergiya, Vol. 21, No. 1, pp. 42-43, July, 1966. Original article submitted February 18, 1966; abstract submitted March 17, 1966.

Note that the reflection coefficients for copper are higher than those for nickel with 600-1200 keV primary beam energies, which is not in agreement with the data of Danguy [6] obtained by using β sources. According to [6], nickel has an anomalous reflection coefficient which is 0.5% higher than the reflection coefficient for its neighboring element in the periodic table with higher atomic number, copper.

LITERATURE CITED

1. P. Ya. Glazunov and V. G Guglya, Dokl. AN SSSR, 159, 632 (1964).
2. V. G. Guglya, Candidate's Dissertation, Moscow (1964).
3. K. Wright and I. Trump, J. Appl. Phys., 33, 687 (1962).
4. I. Trump and R. Van de Graaf, J. Appl. Phys., 19, 599 (1948).
5. N. N. Shumilovskii and L. V. Mel'ttser, Fundamentals of the Theory of Automatic Control Equipment [in Russian], Moscow, Izd-vo AN SSSR (1959).
6. L. Danguy, Inst. Interuniv. Sci. Nucl. Monographic, No. 10, 3 (1962).

PULSED ELECTRON INJECTOR

S. B. Goryachev and I. N. Meshkov

UDC 621.384.611.3

To increase the intensity of a high-current betatron with spiral storage [1], an external 500 keV injector with a current of several amperes was developed. The operating length of the current pulses is ~ 20 μsec. An overall view of the apparatus is shown in the figure. The injector is a high-voltage dc accelerator which uses as a voltage source a controlled pulsed voltage generator (PVG) with short-circuiting spark-gap cascade permitting smooth regulation of the length of the voltage pulse in the range 1-1000 μsec. The accelerating unit consists of an electron gun at 200 keV and a 300 keV accelerating tube with an intensity of 10 kV/cm. The insulators are porcelain and are in sections. To increase electrical stability, the external surface of the tube is located in a tank filled with transformer oil. Supply for the cathode heater of the gun is obtained from a GSR-3000M generator, which is at

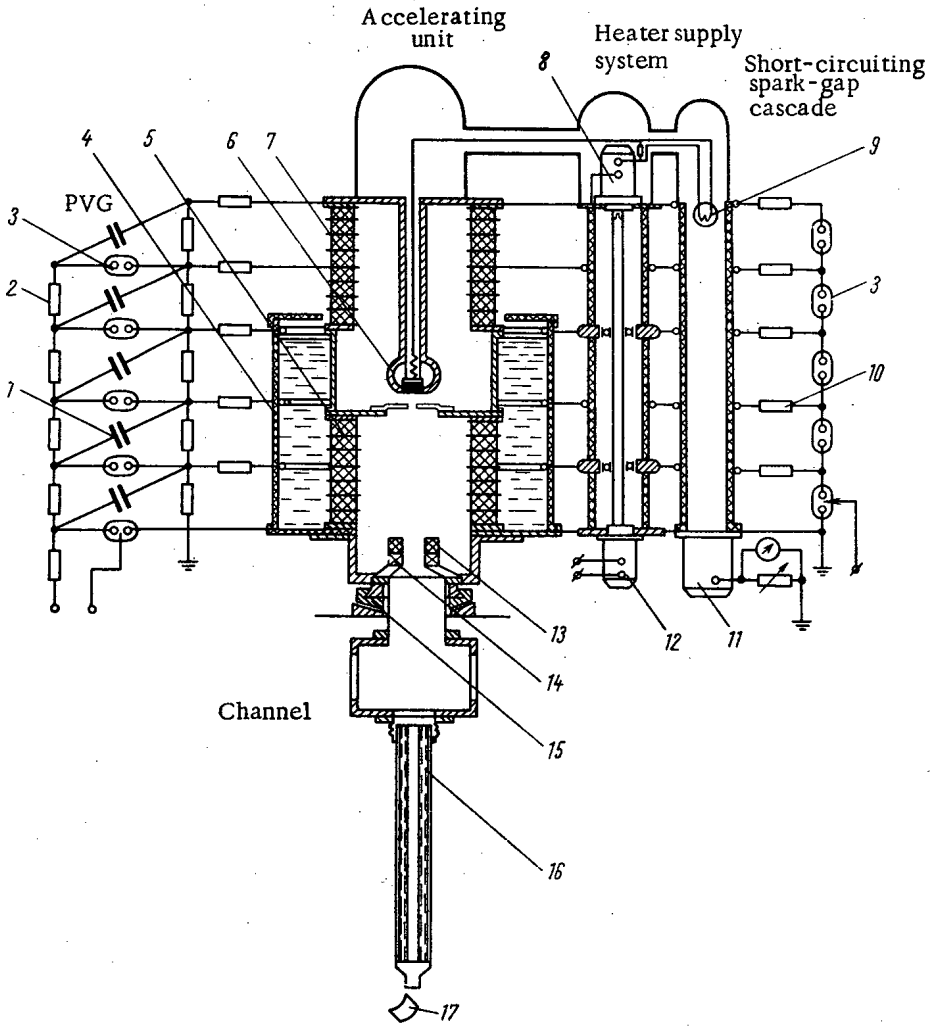

Fig. 1. Diagram of the injector: 1) IMY-100/0.1 condenser; 2) 200 kΩ resistance; 3) spark gap; 4) tank of transformer oil; 5) accelerator tube; 6) cathode assembly; 7) insulator; 8) cathode heater supply generator; 9) monitoring lamp; 10) 1.5 kΩ resistance; 11) photomultiplier; 12) motor; 13) Rogovskii coil; 14) lens; 15) aligning mechanism; 16) solenoid; 17) bending magnet.

Translated from Atomnaya Énergiya, Vol. 21, No. 1, pp. 43-44, July, 1966. Original article received February 18, 1966.

cathode potential and is driven by an insulated shaft. Heater current is controlled by a photomultiplier through the brightness of an incandescent lamp included in the heater circuit.

An electron-optical channel, consisting of magnetic lens, shielding solenoid, and bending magnet, serves to carry the beam through the betatron magnet yoke and to inject it into the chamber.

One can calculate the behavior of the beam in the channel by matching the solution for the variation in the dimensions of an intense beam y(z) in free space [2]:

$$y(z)=y_{\text{in}}+\left(\frac{dy}{dz}\right)_{\text{in}} z+\frac{A^2z^2}{y_{\text{in}}},$$

where

$$A^2=\frac{eI}{mc^3}\left(\frac{mc}{p}\right)^{3/2},$$

in the thin lens and solenoid. The behavior of the beam in the solenoid is described by the equation

$$\frac{d^2y}{dz^2}+\omega^2y-\frac{2A^2}{y}=0,\quad \omega=\frac{eH}{2pc},$$

whose solution is a periodic function. For $\omega^2 y_{\text{ent}} \sim 2A^2/y_{\text{ent}}$ and small $(dy/dz)_{\text{ent}}$ we have $y(z) \approx y_{\text{ent}}(1 + 1/2A\ (dy/dz)_{\text{ent}} \sin \sqrt{2}\,\omega z)$; in other cases, a solution can be obtained numerically. The parameters for the channel elements were selected on the basis of calculations of this type.

A current of ~ 2 A was obtained at the injector output. Beam dimension is 8 × 8 mm with ~ 2.5° angle of divergence.

LITERATURE CITED

1. G. I. Budker et al., Proceedings of the International Accelerator Conference, Dubna (1963) [in Russian], Moscow, Atomizdat (1964), p. 1065.
2. I. N. Meshkov and B. V. Chirikov, ZhTF, 35, 2202 (1965).

COMPOSITION AND SPATIAL DISTRIBUTION OF RADIATION AROUND A 10 GeV PROTON SYNCHROTRON BUILDING

V. N. Lebedev

UDC 577.391

A study of the relationships governing the propagation of mixed radiation from high-energy accelerators at large distances is of decisive importance in connection with the need for reliable prediction of radiation levels in planning new installations. In the case under consideration, the space profile of the radiation field around a proton synchrotron was determined along eight radial directions located at 45° to one another. In these directions, existing equipment made it possible to differentiate the following components: thermal neutrons; slow and intermediate neutrons (0.4 eV-0.1 MeV); fast neutrons (0.1-20 MeV); very fast nucleons (> 20 MeV) and pions (> 50 MeV); charged particles (electrons, muons) and γ rays of various energies.

The paper shows that fast neutrons (< 20 MeV) were distributed symmetrically at large distances from the target with respect to the center of the building. The effective energy of the fast neutrons was in the range 0.7-4 MeV. In the case of shield geometry, neutrons of such energies are the greatest hazard. The dose distribution for the radiation components mentioned are shown in the figure. The direction with maximum flux density of high-energy nucleons was taken as the basis for the determination of the dose from such particles. In this situation, the doses from fast neutrons and from high-energy nucleons were approximately equal.

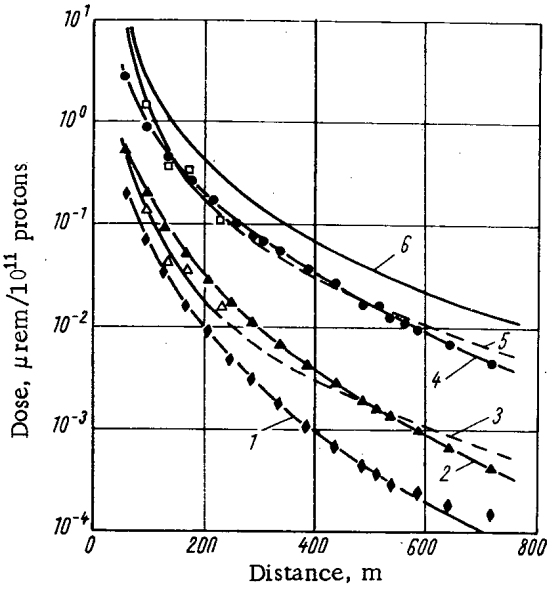

Dose as a function of distance from the geometric center of the accelerator building; 1) thermal neutrons; 2) slow and intermediate neutrons; 3) muons, electrons, and γ rays (tentative); 4) fast neutrons; 5) nucleons and pions; 6) total dose.

An empirical formula is presented in the paper for calculating the fast neutron flux at any distance from the accelerator. The results of measurements made at the proton synchrotron are compared with data obtained by other authors.

The experimentally determined function for the spatial dose distribution of 0.4 eV-20 MeV neutrons has the form

$$D(r)=\frac{IAk_1k_{\text{geom}}k_d}{4\pi r^2}e^{-\frac{r}{\lambda_{\text{eff}}}}\quad \mu\text{rem}/10^{11}\text{ protons.}$$

Here, I is the intensity (proton/sec) of the internal proton beam at an energy E_p, GeV; A is a factor taking into account target thickness and material, shielding thickness and configuration, and also the effective solid angle for the yield of radiation in the upper hemisphere; the factor A can be interpreted as the effective neutron yield in the upper hemisphere per unit flux of protons with energy E_p = 10 GeV ($A = 7.84 \cdot 10^{-2}$ n/p); k_1 is a factor taking into account the value of the final energy of the protons:

$$k_1=\left(\frac{E_p}{E_0}\right)^{0.7}$$

(where E_0 = 10 GeV); k_{geom} is a geometry factor:

$$k_{\text{geom}}\approx[1+2\cdot10^{-4}(r-100)^2e^{-\frac{r-100}{53}}]F(\theta)$$

Translated from Atomnaya Énergiya, Vol. 21, No. 1, pp. 44-45, July, 1966. Original article submitted February 18, 1966; abstract submitted April 9, 1966.

(where $F(\theta) = 0.5\text{-}1$, depending on the chosen radial direction); r is the distance from the axis of the vacuum chamber of the proton synchrotron to the point under consideration; λ_{eff} is the effective mean free path of the neutrons in air ($\lambda_{eff} = 391$ m); k_d is a dose conversion factor (for neutrons of the given spectrum, $k_d = 1.15 \cdot 10^{-2}$ μrem/n/cm^2).

FAST NEUTRON RADIATIVE CAPTURE IN Cu^{63}

V. A. Tolstikov, V. P. Koroleva,
V. E. Kolesov, and A. G. Dovbenko

UDC 539.17.012:539.172.4

This paper gives the results of measurements and of calculations of the fast neutron radiative capture cross section in Cu^{63}.

The relative activation method of measurement, which has been described in detail [1], was used. The U^{235} fission cross section for fast [2] and thermal [3] neutrons and the thermal neutron radiative capture cross section in Cu^{63} [4] were used as reference cross sections. The measured results are compared with data of other authors in the figure. Cross section calculations were made on the basis of the statistical theory of nuclear reactions using the optical model of the nucleus. The method of calculation has been described [5]. The potential in the calculation of nuclear surface penetrability contained a spin-orbit term. The parameters for the levels in the target nucleus, the values of $\overline{D}$, $\overline{\Gamma}_\gamma$, and of the parameter a were taken from [12, 4, 13], respectively. The sharp bend in the radiative capture cross section curve for neutrons with an energy of ~ 1 MeV is explained by competition from inelastic scattering.

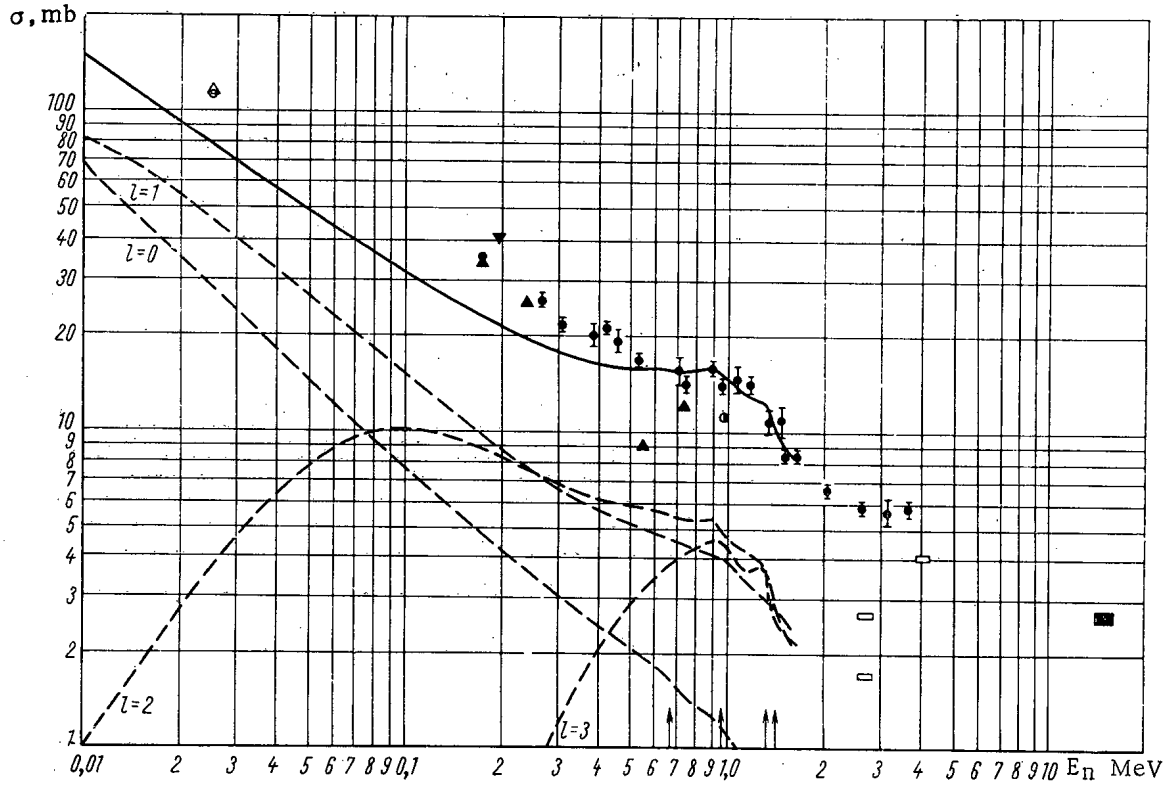

Results of neutron radiative capture cross section measurements for Cu^{63}: Data from: ●) this work; ▲)[3]; ○) [6]; △) [7]; ◑) [8]; ■) [9]; □) [10]; ▽) [11]. Arrows indicate the position of excited levels; ——) total capture cross section; – – – –) capture cross section for neutrons with different angular momenta.

Translated from Atomnaya Énergiya, Vol. 21, No. 1, pp. 45-46, July, 1966. Original article submitted February 18, 1966; abstract submitted April 9, 1966.

LITERATURE CITED

1. Yu. Ya. Stavisskii and V. A. Tolstikov, Nuclear Reactions at Low and Medium Energies [in Russian], Moscow, Izd-vo AN SSSR (1962), p. 562.
2. K. Parker, AWREO-82/63 (December, 1963).
3. Neutron Cross Sections, BNL-325, Second Edition, Supplement No. 2, Vol. III, Z-68 to 98 (February, 1965).
4. I. V. Gordeev, D. A. Kardashev, and A. V. Malyshev, Nuclear Physics Constants [in Russian], Moscow, Gosatomizdat (1963).
5. V. A. Tolstikov et al., Atomnaya Énergiya, 17, 505 (1964).
6. R. Booth, W. Ball, and M. MacGregor, Phys. Rev., 112, 226 (1958).
7. R. Macklin, N. Lazar, and W. Lyon, Phys. Rev., 107, 504 (1957).
8. D. Hughes, R. Garth, and J. Levin, Phys. Rev., 91, 1423 (1953).
9. J. Perkin, L. O'Connor, and R. Coleman, Proc. Phys. Soc., 72, Pt. 4, 505 (1958).
10. V. Dementi and D. Timoshuk, Compt. rend., Acad. Sci. URSS, 27, 929 (1940); M. Mescheryakov, Compt. rend., Acad. Sci. URSS, 48, 555 (1945).
11. W. Lyon and R. Macklin, Phys. Rev., 114, 1619 (1959).
12. R. Ricci, R. Girgis, and R. Lieshout, Nuovo Cimento, XI, 156 (1959).
13. A. V. Malyshev, ZhÉTF, 45, 311 (1963).

All abbreviations of periodicals in the above bibliography are letter-by-letter transliterations of the abbreviations as given in the original Russian journal. *Some or all of this periodical literature may well be available in English translation.* A complete list of the cover-to-cover English translations appears at the back of the first issue of this year.

THE HOMOGENIZATION OF A HETEROGENEOUS PERIODIC SYSTEM

V. M. Novikov

UDC 621.039.512.2:621.039.51.13

Homogenization of a heterogeneous periodic system consists in the replacement of this system by an equivalent homogeneous medium such that the neutron flux and current in that medium coincides with the corresponding quantities for the heterogeneous medium on the average in each elementary cell. Neutron diffusion in the equivalent homogeneous medium is described by the diffusion coefficient tensor D_{ik}, which obviously has a diagonal form in a coordinate system coinciding with the symmetry axes of the elementary cell. There are two known methods for calculating the tensor D_{ik} for a heterogeneous periodic system.

The method of mean-square ranges was first used by Behrens [1] for calculating neutron diffusion in a medium with hollow channels. The basic theorem of this method is the equality

$$L_i^2 = n\,\overline{(\mathbf{li})^2}, \tag{1}$$

where L_i is the diffusion length along the axis i; n is the average number of neutron mean free paths; $\overline{(\mathbf{li})^2}$ is the average value of the square of the neutron mean free path projected on the axis i; $\mathbf{i}$ is a unit vector.

The second method is based on the use of an integral neutron transport equation. This method was developed by Laletin [2] for weakly-absorbing media. The essence of the method is that the exact neutron flux is broken down into two terms: one of them- $\psi(r)$-takes into account the overall drop in flux over the entire system; the second, which is proportional to the gradient of ψ, takes into account the variation of neutron flux within an elementary cell of the medium. The second term, the so-called microflux, is zero for longitudinal diffusion in a medium with cylindrical channels.

However, the microflux is different from zero and makes a corresponding contribution to the magnitude of the diffusion tensor for the case of transverse diffusion. In [2], on the basis of a comparison of the results of that paper with Behrens' formula [1], it was asserted that the mean-square range method was not applicable to the calculation of neutron diffusion in a direction perpendicular to a channel axis.

The present paper shows that with correct consideration of the angular correlations between individual neutron mean free paths, both methods mentioned are completely equivalent to one another. To do this, Eq. (1) should be replaced by the more general expression

$$L_i^2 = \frac{1}{2}\,\overline{(\mathbf{Ri})^2}, \tag{2}$$

where R is the vector for total displacement of the neutron from an arbitrary point in the elementary cell. Writing R in the form of a sum of all separate neutron mean free paths, one can represent expression (2) in the form

$$L_i^2 = \frac{1}{2}\sum_{n=1}^{\infty} P_S(\mathbf{l}_1)\,P_S(\mathbf{l}_2)\ldots P_S(\mathbf{l}_{n-1})\,P_a(\mathbf{l}_n)\left[\sum_{k=1}^{n}(\mathbf{l}_k\mathbf{i})^2 + \sum_{k\neq k'=1}^{n}(\mathbf{l}_k\mathbf{i})(\mathbf{l}_{k'}\mathbf{i})\right], \tag{3}$$

where $P_S(\mathbf{l})$, $P_\alpha(\mathbf{l})$ are the probabilities that the range $\mathbf{l}$ is ended by neutron scattering and absorption, respectively. The first term in expression (3) reduces to equality (1) after appropriate transformations. The second term takes into account the contribution to the diffusion tensor from angular correlations between individual neutron mean free paths. It is shown in the paper that angular correlations exist in a homogeneous medium even for spherically symmetric scattering in all components of the medium. In a medium with cylindrical channels, these correlations of neutron mean free paths, which are specific for heterogeneous media, make a contribution to L_i^2 only for transverse diffusion, the sign of the quantity depending on the ratio between the scattering cross sections of the various components. An analysis of the equation which determines the microflux makes it possible to assert that the microflux in a heterogeneous medium is uniquely determined by the angular correlations of the neutron mean free paths.

Translated from Atomnaya Énergiya, Vol. 21, No. 1, pp. 46, July, 1966. Original article submitted January 21, 1966; abstract submitted April 18, 1966.

LITERATURE CITED

1. D. Behrens, Proc. Phys. Soc., A62, 607 (1949).
2. N. I. Laletin, Proceedings of the Second International Conference on the Peaceful Use of Atomic Energy (Geneva, 1958) [in Russian], Dokl. sovetskikh uchenykh, Vol. 2, Moscow, Atomizdat (1959), p. 634.

EQUILIBRIUM OF PLASMA IN A STELLARATOR WITH A CIRCULAR MAGNETIC AXIS

V. D. Shafranov

UDC 533.9

When plasma is introduced into a toroidal magnetic trap (for example, the stellarator [1]), a magnetic field perpendicular to the plane of the torus is developed, leading to a displacement of the plasma pinch from the center of curvature and distortion of the shape of the magnetic surfaces. In this paper we calculate the displacement of the plasma pinch for the case in which the cross sections of the magnetic surfaces are nearly circular. The solution is obtained by the perturbation method in the linear approximation with respect to the dimensionless parameter $\beta\mu^2 R/b$, where β is the ratio of the plasma pressure to the pressure of the magnetic field, μ is the torsional angle of the magnetic lines of force divided by 2π, R is the radius of the torus, and b is the transverse size of the system.

Our main approximation to the problem (which, in contrast to analogous papers [2, 3], enables us to obtain a solution in simple analytic form) is that the vacuum magnetic fields and surfaces are presented as expansions in powers of the distance from the magnetic axis.

Zero Approximation. Neglecting the curvature of the system, the magnetic field $B_0 = \nabla\Phi$ of an m-turn stellarator is described by the scalar potential

$$\Phi = B_0\left(s + \varepsilon\frac{u'}{m\varrho_0^{m-2}}\varrho^m \sin mu\right), \tag{1}$$

and the magnetic surfaces $\psi(r) = \text{const}$ by the function

$$\psi_0 = \varrho^2 + \varepsilon\frac{2}{m\varrho_0^{m-2}}\varrho^m \cos mu, \tag{2}$$

satisfying the equation $B_0\nabla\psi_0 = 0$. Here B_0 is the longitudinal magnetic field, s the longitudinal coordinate, ρ the distance from the axis (polar radius), ε and ρ_0 parameters characterizing the amplitude of the helical field and the form of the magnetic surfaces:

$$u = \omega + \frac{ns}{mR}, \quad u' = \frac{n}{mR}, \tag{3}$$

where ω is the azimuthal angle, and n is the number of periods of the field in the length of the torus. The amplitude of the azimuthal component of the helical field equals $B_0\varepsilon u'\rho_0(\rho/\rho_0)^{m-1}$. For m = 2 the parameter ρ_0 falls out and the configuration is characterized by a single dimensionless parameter $\varepsilon < 1$. For $m \geq 3$ the parameter ε may be taken as unity. In this case ρ_0 constitutes the distance from the axis to the edge of the separatrix [4]. Subsequently we shall consider that the second term in the expression for ψ_0 is small in comparison with the first, so that the sections s = const of the magnetic surfaces are nearly circular. Hence, in the calculations we may formally take $\varepsilon \ll 1$.

The derivative of the transverse magnetic flux with respect to the longitudinal, μ, related to the torsional angle i of the lines of force by the relation $i = 2\pi\mu$, is easily calculated by the method described in [5]; near the axis it equals

$$\mu(\varrho) = \frac{(m-1)n}{m^2}\varepsilon^2\left(\frac{\varrho^2}{\varrho_0^2}\right)^{m-2}. \tag{4}$$

The formulas given are valid for $\rho \lesssim R/n$.

Currents in the Plasma. The curvature of the system produces a certain distortion in the shape of the magnetic surfaces in vacuum. Let us neglect this effect and consider only the curvature of the magnetic surfaces associated with the presence of plasma. The density of the current arising on introducing plasma into the trap may be written in the form [6]

Translated from Atomnaya Énergiya, Vol. 21, No. 1, pp. 47-49, July, 1966. Original article submitted February 8, 1966.

$$\mathbf{j}=c\frac{[\mathbf{B}\nabla p]}{B^2}+h\mathbf{B}=cp'(\psi^{m-1})\left\{\frac{[\mathbf{B}\nabla\psi^{m-1}]}{B^2}+h_1\mathbf{B}\right\}, \tag{5}$$

where p is the plasma pressure, constituting a surface quantity [6], i. e., a function of ψ. From the solubility condition for the equation div j = 0, which corresponds to the requirement that the solution be finite at $\rho = 0$, it follows that the pressure must be an analytic function of $\mu\psi = \text{const}\ \psi^{m-1}$. Hence the function ψ^{m-1} is taken as argument of p. We note that, for finite plasma conductivity, the solubility condition for the electric-field scalar-potential equation $\mathbf{E} = -\nabla\varphi$

$$\mathbf{B}\nabla\varphi=-hB^2/\sigma_{\parallel} \tag{6}$$

($\sigma_{\parallel}$ being the longitudinal electrical conductivity of the plasma) requires that p should be an analytic function $\mu^2\psi = \text{const}\ \psi^{2m-3}$. The simplest distribution of plasma pressure in the zero approximation (neglecting curvature) which satisfies this condition has the form

$$p=p_0[1-(\varrho^2/a^2)^{2m-3}]. \tag{7}$$

The current continuity equation div $\mathbf{j} = 0$ leads to an equation for h_1 of the form

$$\mathbf{B}\nabla h_1=\frac{[\mathbf{B}\nabla\psi^{m-1}]\nabla B^2}{B^4}. \tag{8}$$

The main contribution to ∇B^2 is associated with the toroidal longitudinal magnetic field $B_S = B_0/[1-\rho/R(\cos\omega)]$. In the remaining terms of Eq. (8), $\mathbf{B}$ and ψ may be taken in the zero approximation described by Eqs. (1) and (2). In the lowest order of expansion with respect to ρ the equation for h_1 takes the form

$$\frac{\partial h_1}{\partial s}+\varepsilon\frac{u'\varrho^{m-1}}{\varrho_0^{m-2}}\left[\sin mu\frac{\partial h_1}{\partial\varrho}+\cos mu\frac{\partial h_1}{\varrho\partial\omega}\right]=q\varrho^{m-3}\sin\omega,\quad \text{where } q=\frac{4(m-1)}{R}. \tag{9}$$

It is easy to see that the solution of this equation takes the form

$$h_1=\frac{m\varrho_0^{2m-3}}{(m-1)\varepsilon^2u'}\left\{\frac{\varrho}{\varrho_0}\cos\omega+\frac{\varepsilon}{m}\left(\frac{\varrho}{\varrho_0}\right)^{m-1}\cos(mu-\omega)\right\}q. \tag{10}$$

Thus for $\varepsilon \ll 1$ the density of the longitudinal current $j_s = cp'(\psi^{m-1})h_1B_0$ is determined from the simple expression

$$j_s=-\frac{4cm^2}{B_0\varepsilon^2n}\varrho_0^{2(m-2)}p'(\psi^{m-1})\varrho\cos\omega=-\frac{2cm^2}{B_0\varepsilon^2n(m-1)}\left(\frac{\varrho_0}{\varrho}\right)^{2(m-2)}\frac{dp}{d\varrho}\cos\omega. \tag{11}$$

For comparison we write the transverse component of current density

$$j_{\perp\omega}=\frac{2(m-1)cp'(\psi^{m-1})\varrho^{2m-3}}{B_0}. \tag{12}$$

We note that the ratio of the mean squares of the longitudinal and transverse current density, $\xi = \langle j_s^2\rangle/\langle j_\perp^2\rangle$, determining the effective diffusion coefficient $D_{eff} = D_\perp(1+\xi\sigma_\perp/\sigma_{\parallel})$ and thermal conductivity $\varkappa_{eff} = \varkappa_\perp(1+0.8\xi)$ of the plasma, allowing for the effects of curvature, equals $\xi = 2/\mu^2(\rho)$, which corresponds to the results of [7, 8].

Magnetic Field of Plasma Currents. The transverse components B_ρ, B_ω of the magnetic field are determined by means of the s component of the equations rot $\mathbf{B} = 4\pi\mathbf{j}/c$ and div $\mathbf{B} = 0$, which have the following form in the approximation considered:

$$\frac{1}{\varrho}\cdot\frac{\partial(\varrho B_\omega)}{\partial\varrho}-\frac{\partial B_\rho}{\varrho\partial\omega}=\frac{4\pi}{c}j_s,\quad \frac{1}{\varrho}\cdot\frac{\partial(\varrho B_\rho)}{\partial\varrho}+\frac{\partial B_\omega}{\varrho d\omega}=0. \tag{13}$$

Taking account of the relationship $j_S \sim \cos\omega$, solution of these equations may be expressed in terms of a single function $B_1(\rho)$

$$B_\rho=B_1\sin\omega,\quad B_\omega=\frac{d(\varrho B_1)}{d\varrho}\cos\omega. \tag{14}$$

For B_1 we obtain a differential equation of the second order which can be integrated once. Thus we obtain

$$\frac{dB_1}{d\varrho}=-\frac{8\pi m^2\varrho_0^{2(m-2)}}{\varepsilon^2n(m-1)}\cdot\frac{1}{\varrho^3}\int_0^\varrho\varrho^{6-2m}\frac{dp}{d\varrho}d\varrho. \tag{15}$$

Let us assume that the radius of the plasma pinch, a, is smaller than the radius of the chamber. Then outside the plasma pinch

$$B_1(\varrho)=B_0\left[C-\frac{m\beta}{\varepsilon^2 n}\left(\frac{\varrho_0}{a}\right)^{2(m-2)}\frac{a^2}{\varrho^2}\right], \tag{16}$$

where C is a constant of integration and β denotes the integral

$$\beta=-\frac{4\pi m}{(m-1)B_0^2}\int_0^a\left(\frac{\varrho}{a}\right)^{6-2m}\frac{dp}{d\varrho}d\varrho. \tag{17}$$

For a two-turn stellarator (m = 2) we obtain $\beta = 8\pi\ p\ /B_0^2$, where p is the plasma pressure averaged over the cross section; for a three-turn stellarator $\beta = 6\pi p(0)/B_0^2$. The factor in front of the integral is chosen so that the pressure distribution of formula (7) corresponds to $\beta = 8\pi\ p\ /B_0^2$ for any value of m.

Distorted Magnetic Surfaces. The new magnetic surfaces in the presence of plasma, $\psi = \psi_0 + \psi_1$, may be found from the linearized equation $B\nabla\psi = 0$:

$$B_0\nabla\Psi_1=-B_1\nabla\Psi_0\approx-B_1(\varrho)\frac{d\Psi_0}{d\varrho}\sin\omega. \tag{18}$$

We put

$$\Psi_0=\psi_0^m, \tag{19}$$

$$\Psi_1=\psi_0 g_0+g, \tag{20}$$

Then for $\varepsilon \ll 1$ (remembering that $B_0\nabla\psi_0 = 0$) we obtain instead of (18):

$$\psi_0(\mathbf{B}_0\nabla g_0)+\mathbf{B}_0\nabla g_1=-2mB_0\left[C\psi_0-\frac{m\beta}{\varepsilon^2 n}\left(\frac{\varrho_0}{a}\right)^{2(m-2)}a^2\right]\varrho^{2m-3}\sin\omega. \tag{21}$$

This equation decomposes into two (for g_0 and g_1) identical with Eq. (9). The solution is easily found by analogy with expression (10). For $\varepsilon \ll 1$,

$$\Psi=\varrho^{2m}+\frac{2(m-1)Ra^{2(m-1)}}{\mu^2(a)}\beta\left(\varrho-\frac{\varrho^3}{b^2}\right)\cos\omega. \tag{22}$$

The constant C is chosen from the condition that the magnetic surface $\rho \approx b$ is fixed (for example, as a result of the existence of an ideally-conducting sheath). We now write the equation for the surface of the displaced plasma pinch (radius a) in the form $\rho = a - \Delta\cos\omega$. From the condition ψ on this surface, we obtain the displacement of the plasma pinch in the direction away from the center of curvature of the torus:

$$\Delta=\frac{(m-1)R\beta}{m\mu^2(a)}\left(1-\frac{a^2}{b^2}\right). \tag{23}$$

The condition that the displacement should be small, $\Delta < b$, leads to a limitation on the equilibrium value of parameter β:

$$\beta<\beta_0=\frac{m}{m-1}\cdot\frac{\mu^2(a)\,b}{R}. \tag{24}$$

The expression for the displacement with m = 2 coincides with that due to plasma pressure in the "Tokamak" [9].

The method described in this paper provides an easy solution for the distribution of equilibrium quantities, allowing for the curvature of the system and the intra-plasma pinch.

LITERATURE CITED

1. L. Spitzer, Phys. Fluids, 1, 253 (1958).
2. J. Green and J. Johnson, Phys. Fluids, 5, 510 (1962).
3. J. Green and J. Johnson, Nuclear Fusion, 2, 16 (1962).
4. A. I. Morozov and L. S. Solov'ev, In the book: Questions of Plasma Theory [in Russian], 2nd. Ed., Moscow, Gosatomizdat (1963), p. 3.
5. L. S. Solov'ev and V. D. Shafranov. Paper No. 133 presented by the USSR to the International Conference on Plasma Physics and Controlled Nuclear Fusion (Culham) [in Russian] (1965).
6. M. Krushkal and R. Kulsrud, Phys. Fluids, 1, 265 (1958).
7. G. Knorr, Phys. Fluids, 8, 1334 (1965).

8. B. B. Kadomtsev and V. D. Shafranov, Dokl. AN SSSR, 167, 65 (1966).
9. V. D. Shafranov, Atomnaya Énergiya, 13, 521 (1962).

All abbreviations of periodicals in the above bibliography are letter-by-letter transliterations of the abbreviations as given in the original Russian journal. *Some or all of this periodical literature may well be available in English translation.* A complete list of the cover-to-cover English translations appears at the back of the first issue of this year.

IONIZATION CHAMBER WITH SILVER ELECTRODES FOR MEASURING THERMAL-NEUTRON FLUXES WITH HIGH LEVELS OF ACCOMPANYING GAMMA RADIATION

A. I. Kukarin and A. I. Khovanovich

UDC 539.107.48

Thermal-neutron fluxes and pulses are usually measured by means of various indicators and electronic counting systems involving gas-discharge counters [1]. Although this method ensures the required accuracy and reliability of the measurements, it is very time-consuming and demands complex and cumbersome apparatus. In some cases special gas-discharge and scintillation counters [2] are used as thermal-neutron detectors. In view of their low resolving power and sensitivity to accompanying gamma radiation, however, these are not very useful for measuring thermal-neutron fluxes of high intensity.

The simplest detector for intense thermal-neutron fluxes, especially when accompanied by gamma radiation, is an ionization chamber with silver electrodes (Fig. 1). The body 1 of the chamber is made of organic glass 5 mm thick. The high-voltage and collecting electrodes 2 and 3 are made of silver foil consisting of a natural mixture of isotopes Ag^{107} (51.9%) and Ag^{109} (49.1%). The high-voltage source and the system for measuring the chamber current are attached to leads 4 and 5.

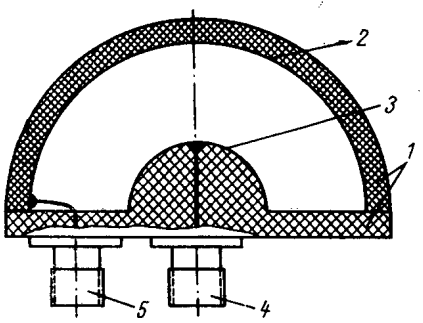

Fig. 1. Arrangement of ionization chamber with silver electrodes.

The thermal neutrons falling on the chamber are absorbed in the silver of the electrodes, the Ag^{107} and Ag^{109} being converted into the β active isotopes Ag^{108} and Ag^{110} with half-lives of 2.3 min and 24.5 sec respectively. The ionization current I_K in the chamber (after irradiation with thermal neutrons) varies in accordance with the decay laws of the isotopes in question and in general may be expressed in the form

$$I_K = C\Pi\left[\eta_1\sigma_1\left(1-e^{-\lambda_1 t_0}\right)e^{-\lambda_1 t}+\eta_2\sigma_2\left(1-e^{-\lambda_2 t_0}\right)e^{-\lambda_2 t}\right],$$

where C is the proportionality factor between the chamber current and the β activity of the electrode silver in A · sec/disintegration; $\eta_1, \sigma_1, \lambda_1$ are respectively the percentage content, capture cross section (cm^2), and decay constant (sec^{-1}) of the Ag^{108} isotope; $\eta_2, \sigma_2, \lambda_2$ are the same for the Ag^{110} isotope; t_0 is the irradiation period (sec), and Π is the neutron flux (neutrons/cm^2 · sec) falling on the chamber; C is found experimentally during calibration.

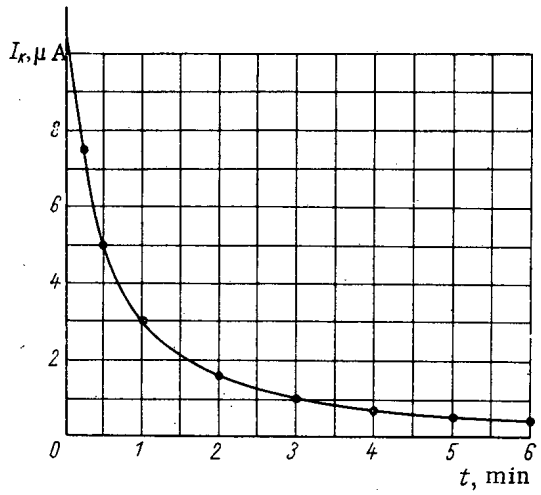

Fig. 2. Ionization-chamber current as a function of time after irradiating with a thermal-neutron flux of 3.10^{11} neutrons /cm^2 · sec for 5 min.

For constant chamber-irradiation time, the neutron flux Π being measured can be obtained from the relation

$$\Pi = \frac{I_K}{I_{K0}}\Pi_0,$$

where I_{K0} is the chamber current at an instant t after irradiation by a known neutron flux Π_0, and I_K is the chamber current at the same time t after irradiation by

Translated from Atomnaya Énergiya, Vol. 21, No. 1, pp. 49-50, July, 1966. Original article submitted December 23, 1963; revised January 20, 1966.

the unknown neutron flux Φ. Since the neutron flux is found by measuring the chamber current after irradiation, the accompanying gamma radiation will have no effect on the results.

The ionization chamber shown in Fig. 1 has a working ionization volume of $V = 80$ cm^3 and a silver-electrode weight of $P = 7.7$ g. The time variation of the ionization current in the chamber after irradiation by a thermal-neutron flux of $\Phi = 3 \cdot 10^{11}$ neutrons/cm$^2 \cdot$ sec for 5 min is shown in Fig. 2. On irradiating the chamber with any other flux, only the scale of the graph along the y axis is altered.

By measuring the current of the ionization chamber, for example, with a multirange microammeter of the M-95 type, we can directly determine values of thermal-neutron flux between 10^8 and 10^{13} neutrons/cm$^2 \cdot$ sec. By reducing the chamber-irradiation time or increasing the current range, thermal-neutron fluxes of much greater intensity can be measured.

In order to ensure saturation conditions in the chamber for the thermal-neutron fluxes in question, a supply source yielding up to 3 kV and 300 μA is required.

The proposed method and measuring apparatus may also be used for measuring total thermal-neutron fluxes from pulse sources. The load impedance for the chamber may conveniently consist of condensers of various capacity, the charge on which is proportional to the measured thermal-neutron fluxes or pulses.

The error in measuring neutron fluxes or pulses is determined by that of calibrating and measuring the chamber current or charge on the load condenser. On calibrating the chamber in a nuclear reactor with sodium indicators and measuring the current with an M-95 ammeter, the error in measuring thermal-neutron fluxes is no greater than ± 10%.

LITERATURE CITED

1. N. A. Vlasov. Neutrons [in Russian], Moscow, Fizmatgiz (1958).
2. K. K. Aglintsev et al. Applied Dosimetry [in Russian], Moscow, Gosatomizdat (1962).

SIMULTANEOUS STUDY OF CONCURRENT NUCLEAR REACTIONS BY MEANS OF A SCINTILLATION SPECTROMETER

D. L. Chuprunov, V. S. Zazulin, and T. N. Mikhaleva

UDC 539.107.5

When studying nuclear reactions taking place in a target under the influence of a beam of charged particles, it is convenient to examine the various concurrent reactions simultaneously, so as to have identical experimental conditions in each case and also to reduce the operating time of the accelerator. In this note we shall describe the arrangement of a spectrometer enabling (p, p') and (p, α) reactions to be recorded simultaneously in two multichannel analyzers of the AI-100 type, to the complete exclusion of gamma background.

In contrast to the spectrometer described by T. N. Mikhaleva et al.,† some new units were introduced into the slightly-improved circuit of the device (Fig. 1);these were: a time-gate-signal expansion circuit, a Schmitt circuit, coincidence and anticoincidence circuits, and a second gate for the photoelectron-multiplier collector signal. Pulses from the forming stage (multivibrator) pass to the coincidence and anticoincidence circuits.

The system operates as follows. After passing through the time gate, the pulses are shaped into rectangular form by the expansion circuit and are conveyed to the Schmitt circuit, the operating threshold of which is adjusted for a pulse amplitude corresponding to the recording of α particles. From the output of the Schmitt circuit the signal passes to the coincidence and anticoincidence circuits together with pulses from the multivibrator. If an α-particle passes into the detector, the coincidence circuit operates and gives a control pulse to gate I; an α-particle is recorded in analyzer I. If a proton arrives in the detector, the anticoincidence circuit operates, giving a control pulse to gate II, and the proton is recorded in analyzer II.

The dead time of the system does not exceed that of the AI-100 analyzer.

Proton and alpha spectra from the reactions Al^{27} (p, α) Mg^{24} and Al^{27} (p,p') Al^{27*} recorded simultaneously on two analyzers are shown in Fig. 2, and similar spectra for reactions Na^{23} (p, α) Ne^{20} and Na^{23} (p,p') Na^{23*} are shown in Fig. 3.

The energy of the incident protons is about 6.3 MeV. The aluminum target was made from foil and the sodium target by evaporating metallic sodium on to an organic substrate and subsequently depositing gold.

†T. N. Mikhaleva et al., Izv. AN SSSR, Ser. fiz., 30, 343 (1966).

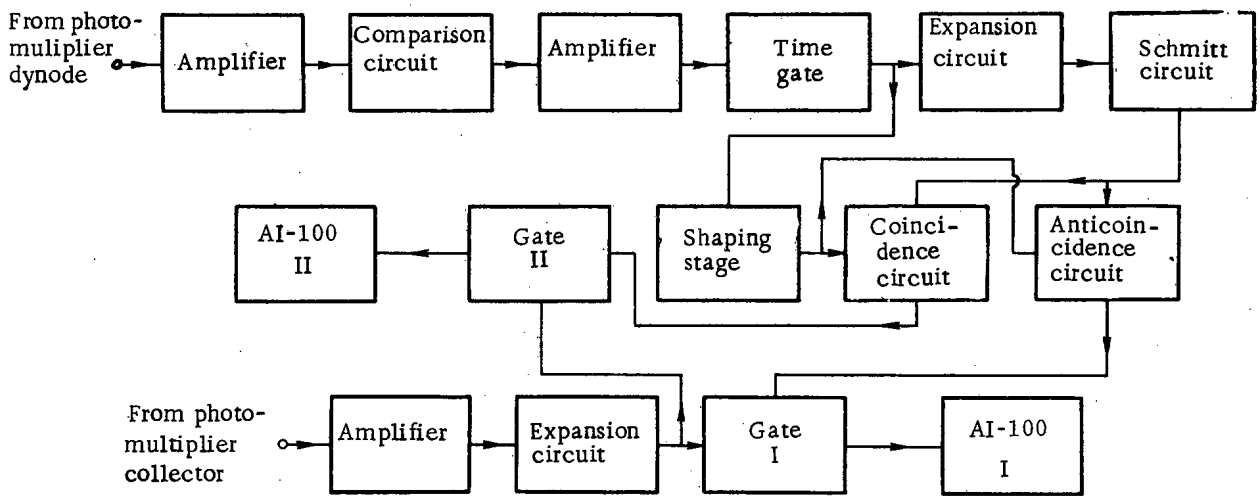

Fig. 1. Arrangement of the spectrometer.

Translated from Atomnaya Énergiya, Vol. 21, No. 1, pp. 50-51, July, 1966. Original article submitted October 6, 1965.

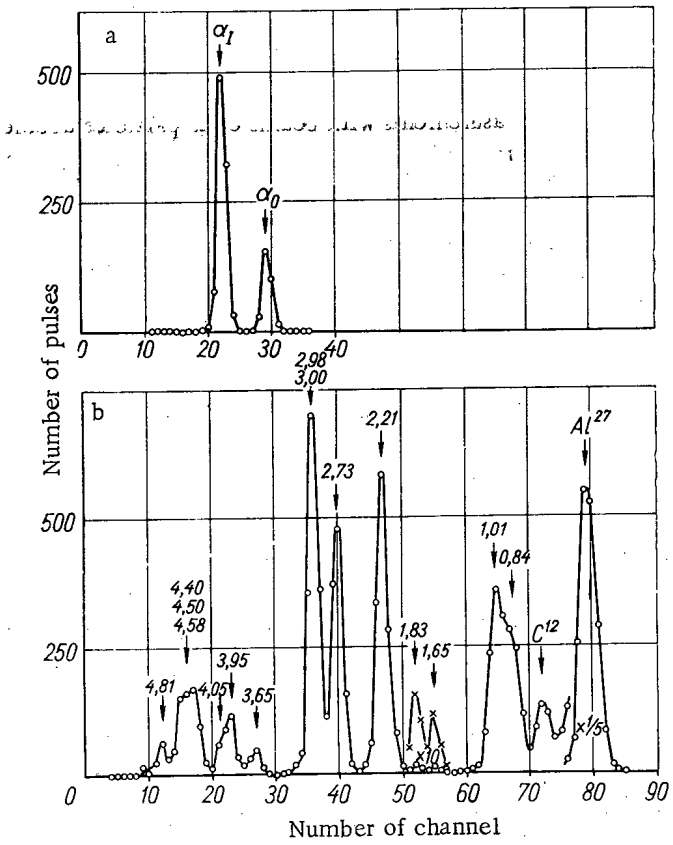

Fig. 2. a) Alpha-particle spectrum from reaction Al^{27} (p, α) Mg^{24} (α_0 and α_1 are maxima corresponding to α particles leaving the Mg^{24} nucleus in the ground and first excited states; E_p = 6.36 MeV, θ = 90°); b) proton spectrum from reaction Al^{27} (p, p') Al^{27*}. The symbols of the elements indicate maxima corresponding to elastic scattering; figures on the maxima indicate the excitation energy of the Al^{27} nucleus.

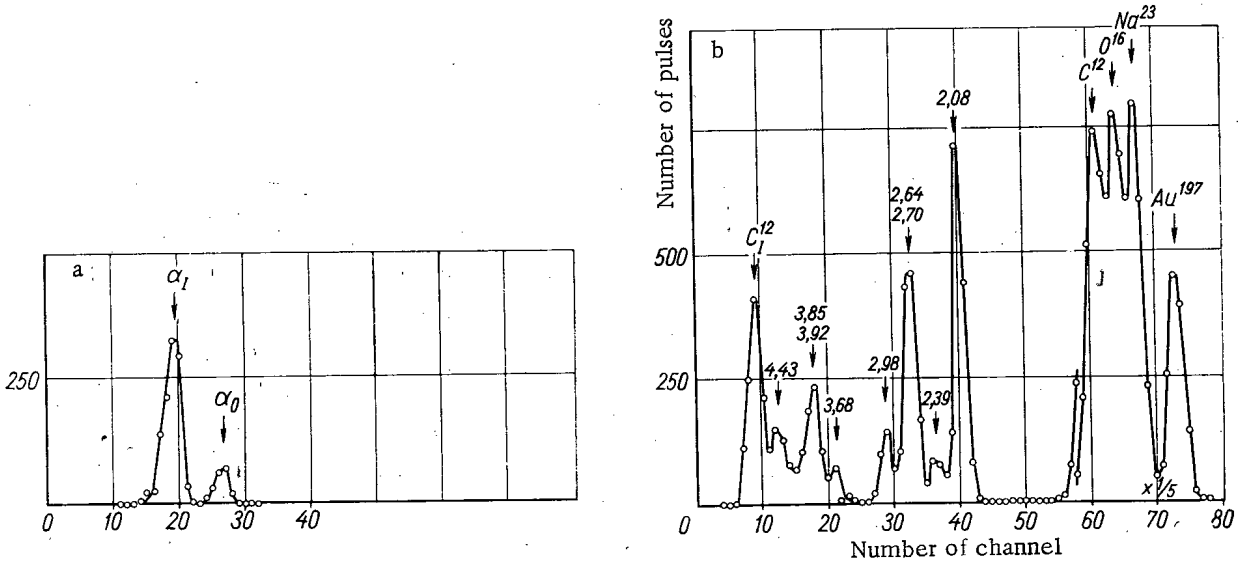

Fig. 3. a) Alpha-particle spectrum from reaction Na^{23} (p, α) Ne^{20} (α_0 and α_I are maxima corresponding to α particles leaving the Ne^{20} nucleus in the ground and first excited states; E_p = 6.26 MeV, θ = 90°); b) proton spectrum from reaction Na^{23} (p, p') Na^{23*}. The symbols of the elements indicate maxima corresponding to elastic scattering; figures on the maxima indicate the excitation energy of the Na^{23} nucleus.

The apparatus described was used to measure the angular distribution of protons and α particles arising on interaction between protons and aluminum nuclei over the range θ = 30 to 165°, for incident-proton energy 6.24 to 6.74 MeV. Elastically- and inelastically-scattered protons were recorded over the range 1.0 to 6.7 MeV and α-particles over the range 5.4 to 8.9 MeV. Measurements with beams of α-particles accelerated in the cyclotron showed that, with this arrangement of the circuit, the energy range of α-particles recorded simultaneously with protons was 3 to 15 MeV.

The authors express their thanks to S. F. Niyakii for help in the work.

YIELDS OF NUCLEAR REACTIONS USED FOR PREPARING Mn^{54} IN A CYCLOTRON

N. N. Krasnov and P. P. Dmitriev

UDC 621.039.554

The isotope Mn^{54} (half-life 290 days) decays by electron capture and is a monochromatic emitter with E_γ = 840 keV. It is extensively used in research work.

The literature data on yields of Mn^{54} from thick targets are scanty [1-10]; no description has been given of the formation of Mn^{54} in reactions with alpha particles.

In the present article we examine six methods of obtaining Mn^{54} (see table), including all the high-yield preparation methods. The work was done with the 1.5-meter cyclotron of the Physico-Energetics Institute [11].

We measured the Mn^{54} yield for various particle energies by irradiating metal specimens of chromium, vanadium, manganese and iron in the form of 10 mm diameter disks. Irradiation was by a deflected beam. The target thickness was greater than the free path of the bombarding particles. The energies of the protons, deuterons and alpha particles were varied by absorption in foils which were placed in front of the specimens. The particle free paths were determined by the method described in [12].

Methods of Preparing Mn^{54}

Method of preparation	Formation reaction	Energy threshold of reaction, MeV	Content of initial isotope, %	Published data on yields: Particle energy, MeV	Yield, $\mu Ci/\mu A \cdot h$	Source
Cr + p	$Cr^{54}(p, n)$	2,2	2,38	22	0,45	*
				20	0,5	[3]
				22	0,5	[6]
Mn + p	$Mn^{55}(p, pn)$	10,4	100	22	21	*
				22	20	[6]
Cr + d	$Cr^{53}(d, n)$	—	9,55	21	1,95	*
	$Cr^{54}(d, 2n)$	4,6	2,38	10	0,65	[10]
				14	1,15	[7]
				20	2	[9]
Fe + d	$Fe^{56}(d, \alpha)$	—	91,7	21	2,8	*
				13,5	0,57	[8]
				14	0,1	[1]
	$Fe^{54}(d, 2p)$	2,2	5,8	15	1,4	[3]
				19	0,29	[4]
	$Fe^{57}(d, \alpha n)$	2,1	2,2	20	3,3	[9]
				25	3,2	[5]
				30	5	[2]
V + α	$V^{51}(\alpha, n)$	4,6	100	42	1,7	*
Cr + α	$Cr^{52}(\alpha, pn)$	13,8	83,76	42	5,8	*
	$Cr^{53}(\alpha, p2n)$	22,3	9,55			

*Present author's data.

Translated from Atomnaya Énergiya, Vol. 21, No. 1, pp. 52-53, July, 1966. Original article submitted January 21, 1966; revised February 18, 1966.

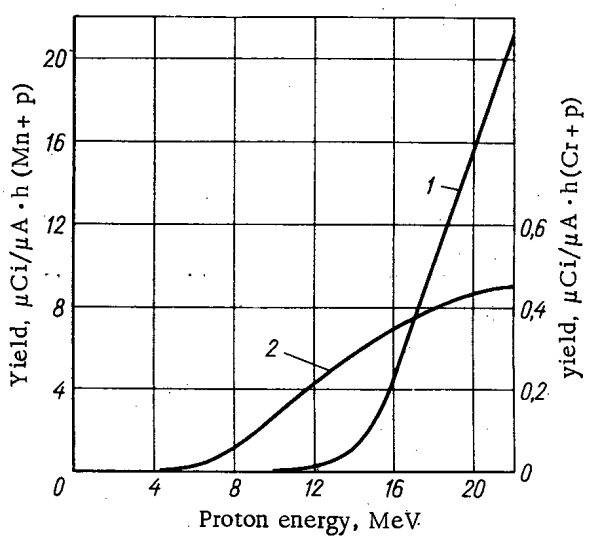

Fig. 1. Yield of Mn^{54} versus proton energy, for thick targets of manganese and chromium. (1) Mn + p; (2) Cr + p.

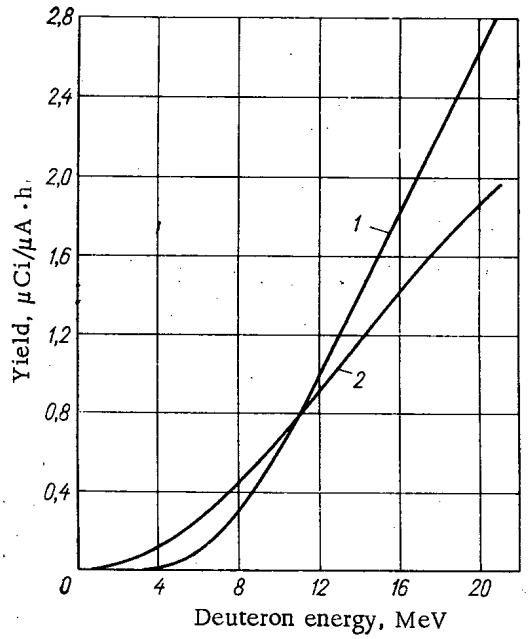

Fig. 2. Mn^{54} yield versus deuteron energy, for thick targets of iron and chromium. (1) Fe + d; (2) Cr + d.

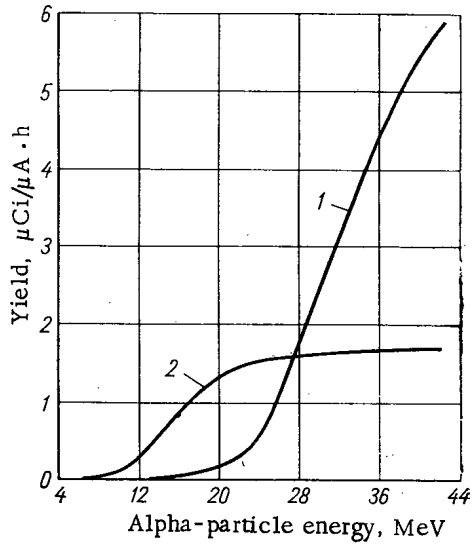

Fig. 3. Mn^{54} yield versus alpha particle energy, for thick targets of chromium and vanadium. (1) Cr + α; (2) V + α.

The integral irradiation currents were measured by means of the induced activity of Zn^{65} with the aid of copper monitor foils. Calibration data on the Zn^{65} activity induced in the foils were previously found experimentally, using a precision current integrator.

The Mn^{54} activity was measured with a 100-channel scintillation gamma spectrometer with NaI(Tl) crystal of size 40 × 40 mm, with gamma-line photo-peak area 840 keV. The photo-efficiency of the gamma spectrometer was determined by means of the activity of aliquot parts of Mn^{54} solution measured in an ionization chamber. The chamber was calibrated with standard Co^{60} sources.

The present authors measured the Mn^{54} yield versus particle energy for thick targets: the results are given in Figs. 1, 2, and 3. The errors in the Mn^{54} yields are due to errors in the measurements of Mn^{54} activity, integral beam current and particle energy, and amount to ± 15%.

The greatest Mn^{54} yield was observed on irradiation of manganese by protons, but the product is obtained in a carrier. In addition, it is difficult to prepare heat-resistant manganese targets. The remaining five methods give Mn^{54} without a carrier: the highest yield from these is from irradiation of chromium with alpha-particles. Since a method has been perfected for preparing heat-resistant targets by galvanic coating of a copper substrate with chromium, this latter method must be preferred.

The authors would like to thank Z. P. Dmitrieva and G. A. Molin for help with the work, and Yu. G. Sevast'yanov for the radiochemical separation of the Mn^{54}.

LITERATURE CITED

1. W. Garrison and J. Hamilton. Chem. Rev., 49, 237 (1951).
2. A. Aten. Phillips Techn. Rev., 16, No. 1 (1954).
3. J. Gruverman and P. Kruger. Internat. J. Appl. Rad. and Isotopes, 5, 21 (1959).
4. K. Chackett et al. Nucl. Instrum. and Methods, 14, 215 (1961).

5. H. Moeken. Productions of Radioisotopes with Charged Particles, Amsterdam (1957).
6. J. Martin et al. Nucleonics, 13, No. 3, 28 (1955).
7. P. Kafalas and J. Irvine. Phys. Rev., 104, 703 (1956).
8. K. Wagner. Kernenergie, 5, 853 (1962).
9. M. Z. Maksimov. Proceedings of Conference on Preparation and Use of Isotopes (Moscow, 1957), Moscow, Izd. AN SSSR (1957), p. 31.
10. P. P. Dmitriev et al. Ibid, p. 28.
11. N. N. Krasnov et al. Pribory i tekhnika éksperimenta, 4, 22 (1965).
12. M. Z. Maksimov. ZhÉTF, 38, 127 (1959).

All abbreviations of periodicals in the above bibliography are letter-by-letter transliterations of the abbreviations as given in the original Russian journal. *Some or all of this periodical literature may well be available in English translation.* A complete list of the cover-to-cover English translations appears at the back of the first issue of this year.

CALCULATION OF THE DÖPPLER TEMPERATURE COEFFICIENT OF REACTIVITY FOR ISOLATED RESONANCES IN A HOMOGENEOUS MEDIUM

P. E. Bulavin and G. I. Toshinskii

UDC 621.039.512.26

The calculation of the Döppler temperature coefficient of the reactivity in a nuclear reactor is linked with calculation of the temperature derivative of the self-screening factor at the resonances. Reference [1] gives calculated results for the temperature derivative of the self-screening factor for isolated resonances in a non-homogeneous plane medium (curves of G. Roe). These results can clearly also be used for a homogeneous medium if we go to the limit of zero thickness of the absorber and moderator plates. However, [1] does not give the method of calculation, and therefore we cannot assess the accuracy of the results. We have therefore calculated the temperature derivative of the self-screening factor for isolated resonances in a homogeneous medium. Below we give the method of calculation and the results.

The expression for the self-screening factor at an isolated resonance in a homogeneous medium can be written in the following form (see, e. g., [2, 3]):

$$f(\xi, h)=\frac{1}{\pi}\int_{-\infty}^{\infty}\frac{\Psi(x, \xi)}{1+h\Psi(x, \xi)}dx, \tag{1}$$

where

$$\Psi(x, \xi)=\frac{\xi}{2\sqrt{\pi}}\int_{-\infty}^{\infty}\frac{e^{-\frac{\xi^2}{4}(x-y)^2}}{1+y^2}dy \tag{2}$$

is the approximate form of the resonance, allowing for the Doppler effect for the gas model of an absorber; $\xi = \Gamma/\Delta$ is the Breit-Wigner ratio and the Döppler resonance width; $\Delta = 2\sqrt{E_r kT/A}$ is the Döppler width;* $h = \rho\sigma_0/\Sigma_s$ (in the case of the narrow-resonance approximation)†; ρ is the nuclear concentration of the resonance absorber; σ_0 is the total cross section at the resonance maximum; and Σ_s is the total cross section of potential scattering.

Expression (1) is valid on the assumption that we can neglect the effect of interference between resonance and potential scattering. This assumption is satisfied for purely absorptive resonance ($\Gamma_n \ll \Gamma$) or for a dilute medium ($\rho\sigma_{pa} \ll \Sigma_s$ where σ_{pa} is the cross section of potential scattering of the resonance absorber).

When $h \ll 1$ the integrand in (1) can be expanded in a series in h and is limited by terms of order h. Then, using the relation $\int_{-\infty}^{\infty}\Psi^2(x, \xi)\,dx = \frac{1}{2}\pi\Psi(0, \xi\sqrt{2})$ [4], we get

$$f(\xi, h)=1-\frac{h}{2}\Psi(0, \xi\sqrt{2}). \tag{3}$$

Differentiating (3) with respect to T, we get, for $h \ll 1$,

$$T\frac{\partial f}{\partial T}=\frac{h}{4}[(1+\xi^2)\Psi(0, \xi\sqrt{2})-\xi^2]. \tag{4}$$

*For a crystalline substance T is the temperature of the substance, provided that $\theta_D \ll T$ (θ_D = Debye temperature). If $\theta_D \gtrsim T$, we must replace T by the effective temperature T_{eff} [5].

†In the case of the wide-resonance approximation [6], $h = \rho\sigma_{0a}/\Sigma_{sm}$, where σ_{0a} is the capture cross section at the resonance maximum, and Σ_{sm} is the cross section for potential scattering by all the nuclei except the resonance absorber.

Translated from Atomnaya Énergiya, Vol. 21, No. 1, pp. 54-56, July, 1966. Original article submitted January 21, 1966.

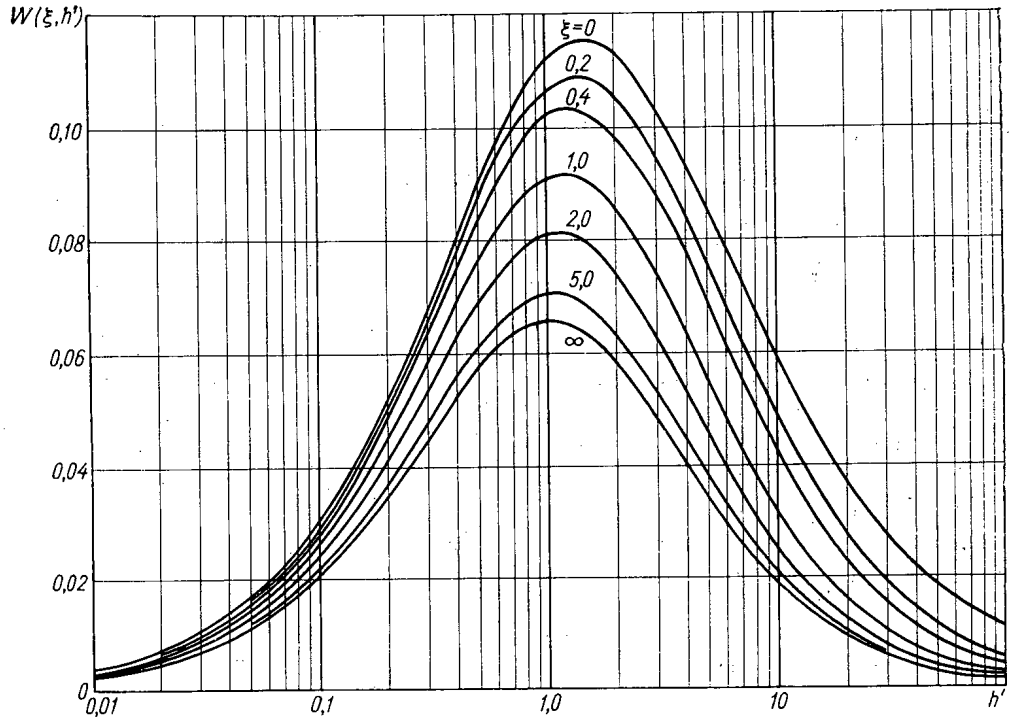

Curves for calculating Doppler temperature coefficient

$W(\xi, h')=\frac{T\partial f/\partial T}{1-\Psi(0, \xi)}$,

where

$\Psi(0, \xi)=\frac{\sqrt{\pi}}{2}\xi e^{-\xi^2/4}$

$\times[1-\mathrm{erf}\,(\xi/2)]$.

Using (1) and (2) we obtain an expression for $T(\partial f/\partial T)$ for any h,

$$T\frac{\partial f}{\partial T}=\frac{1}{\pi}\int_0^\infty \frac{\left[\frac{\xi^2}{2}(x^2-1)-1\right]\Psi(x, \xi)+\frac{\xi^2}{2}-x\xi^2\Phi(x, \xi)}{[1+h\Psi(x, \xi)]^2}dx, \tag{5}$$

where

$$\Phi(x, \xi)=\frac{\xi}{2\sqrt{\pi}}\int_{-\infty}^{\infty}\frac{ye^{-\frac{\xi^2}{4}(x-y)^2}}{1+y^2}dy. \tag{6}$$

The functions $\psi(x, \xi)$ and $\Phi(x, \xi)$ bear the following relations to the real and imaginary parts, $u(x, y)$ and $v(x, y)$ of the complex probability integral:

$$\Psi(x, \xi)=\frac{\xi}{2}\sqrt{\pi}\,u\left(\frac{\xi}{2}x, \frac{\xi}{2}\right); \tag{7}$$

$$\Phi(x, \xi)=\frac{\xi}{2}\sqrt{\pi}\,v\left(\frac{\xi}{2}x, \frac{\xi}{2}\right). \tag{8}$$

Tables of the functions $u(x, y)$ and $v(x, y)$ are given in [7].

The function $T(\partial f/\partial T)$, for which an expression is given by (5), has maxima in ξ and h. For convenience, let us introduce a new function [1],

$$W(\xi, h')=\frac{T\frac{\partial f}{\partial T}}{1-\Psi(0, \xi)}, \tag{9}$$

which has no maximum in ξ, and, when $\xi\to 0$ or $\xi\to\infty$, has nonzero limits which differ from one another very little. From (5) we get an expression for the function $W(\xi, h')$:

$$W(\xi, h')=\frac{1}{\pi[1-\Psi(0, \xi)]}\int_0^\infty \frac{\left[\frac{\xi^2}{2}(x^2-1)-1\right]\Psi(x, \xi)+\frac{\xi^2}{2}-x\xi^2\Phi(x, \xi)}{\left[1+h'\frac{\Psi(x, \xi)}{\Psi(0, \xi)}\right]^2}dx, \tag{10}$$

where $h' = \frac{\varrho\sigma_0\Psi(0, \xi)}{\Sigma_s}$ is the ratio of the macroscopic cross section at the resonance maximum (allowing for the Döppler effect) to the total cross section of potential scattering.

For resonance close to the Breit-Wigner type (with $\xi \gg 1$), using an asymptotic expansion of ψ and Φ[7] and integrating (10), we get

$$W(\infty, h) = \frac{4+3h}{2h\sqrt{(1+h)^3}} + \frac{4}{h^2\sqrt{1+h}} - \frac{4}{h^2}. \tag{11}$$

For resonance close to the Döppler type, using the expansion of ψ and Φ[7], we get, for $\xi \ll 1$,

$$W(0, h') = \frac{1}{\sqrt{\pi}} \int_0^\infty \frac{(2v^2-1)\,e^{-v^2}}{[1+h'e^{-v^2}]^2}\,dv. \tag{12}$$

When $h' < 1$, the integrands in (10) and (12) can be expanded in series in h'. We then get the following formulae:

$$W(\xi, h') = \sum_{n=0}^{\infty} (-1)^n \beta_n(\xi)\, h'^{n+1}, \tag{13}$$

$$\beta_n(\xi) = -\frac{n+2}{[1-\Psi(0, \xi)]} \cdot \frac{1}{\pi} \int_0^\infty \left\{ \left[\frac{\xi^2}{2}(x^2-1) - 1 \right] \Psi(x, \xi) + \frac{\xi^2}{2} - x\xi^2\Phi(x, \xi) \right\} \left[\frac{\Psi(x, \xi)}{\Psi(0, \xi)} \right]^{n+1} dx;$$

$$W(\infty, h) = \frac{1}{2} \sum_{n=0}^{\infty} (-1)^n \frac{(2n+3)!!}{(2n+2)!!} \cdot \frac{n+1}{n+3} h^{n+1}; \tag{14}$$

$$W(0, h') = \frac{1}{2} \sum_{n=0}^{\infty} (-1)^n \frac{n+1}{\sqrt{n+2}}\, h'^{n+1}. \tag{15}$$

From (10)-(15) we can calculate the function $W(\xi, h')$ in the ranges $0.01 \leq h' \leq 100$ and $0 \leq \xi \leq \infty$. The results are shown in the figure.

$W(\xi, h')$ varies little with ξ, and can therefore easily be interpolated for any value of ξ (when $\xi > 1$ it is more convenient to interpolate with respect to $1/\xi$). The results of our calculation of $W(\xi, h')$ differ appreciably from those of [1], where the case of a homogeneous medium is obtained by taking the limit when $\mu\tau N(\theta)$ tends to $h'/2$. This discrepancy is found even when $\xi \to \infty$ ($\theta = 1/\xi^2 \to 0$), when there is an analytic expression for $W(\xi, h')$ (11).

LITERATURE CITED

1. Nuclear Reactors. Publications of A.E.C. of USA [Russian translation]. Moscow, IL (1956), p. 246.
2. G. Goertzel. Estimation of Döppler Effect in Intermediate and Fast Neutron Reactors, A/conf, 8/P/613, USA (1955).
3. I. V. Gordeev et al. Atomnaya Énergiya, 3, 252 (1957).
4. H. Bethe and G. Placzek. Phys. Rev., 51, 450 (1937).
5. W. Lamb. Phys. Rev., 55, 190 (1939).
6. L. Dresner. Resonance Absorption in Nuclear Reactors. Moscow, Gosatomizdat (1962).
7. V. I. Faddeeva and N. M. Terent'ev. Tables of Functions of the Probability Integral of a Complex Argument. Moscow, Gostekhizdat (1954).

MODERATION OF A HIGH-ENERGY NEUTRON FLUX BY HETEROGENEOUS SHIELDING

L. N. Zaitsev, M. M. Komochkov,
V. V. Mal'kov, B. S. Sychev,
and E. P. Cherevatenko

UDC 621.039.512.45

This letter gives experimental data on the distributions of fluxes of neutrons of various energy groups in layered shielding.

The experiments were carried out with the OIYaI* synchrocyclotron. The neutron fluxes were obtained by bombarding a beryllium target with 660 MeV protons. The experimental geometry was described in [1]. The neutrons were detected by threshold detectors of In^{115}, P^{31}, and C^{12}, of which the brief characteristics are given in [2]. Also used were x-ray plates for individual gamma ray dosimetry.

The shielding was composed of the following materials: iron-water, iron-heavy concrete†, water-iron-water. The neutron attenuation curves are given in figures 1-3. Figure 3 also gives the distribution of gamma-ray dose rate in the shielding.

*United Institute of Nuclear Research [translator's note].

† The composition of the concrete was given in [3].

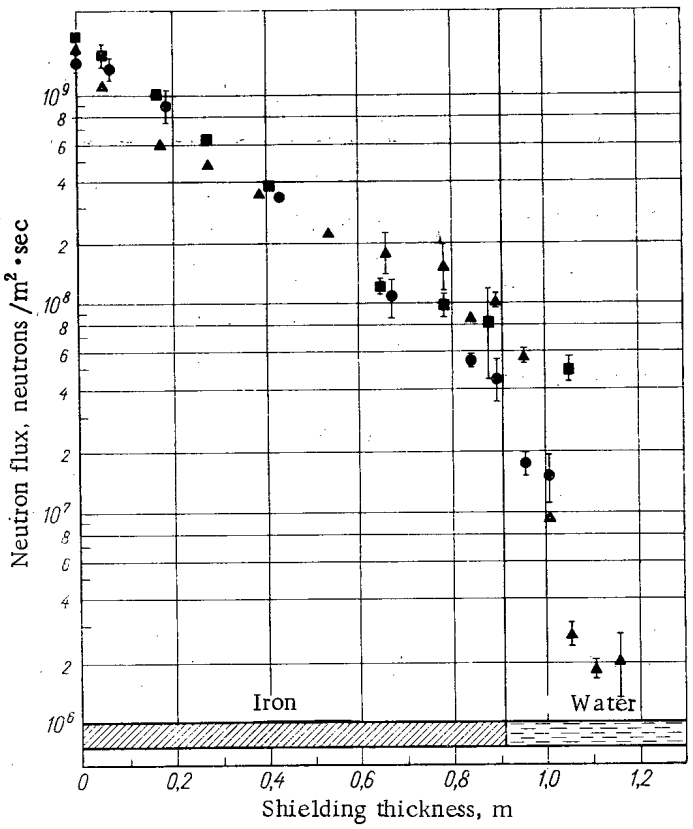

Fig. 1. Distribution of neutron fluxes in iron-water shielding. ■) Distribution of high-energy neutrons (E > 20 MeV); ●) fast neutrons (1.5 < E < 20 MeV); ▲) resonance neutrons (E ≈ 1.44 MeV).

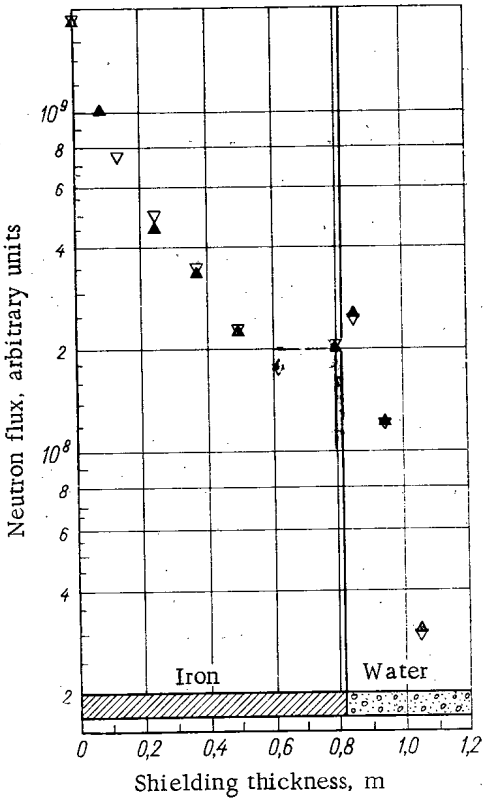

Fig. 2. Distribution of neutron fluxes in shielding of iron-heavy concrete. ▽, ▲) Distribution of fluxes of resonance neutrons, according to data from two experiments.

Translated from Atomnaya Énergiya, Vol. 21, No. 1, pp. 56-57, July, 1966. Original article submitted February 22, 1966.

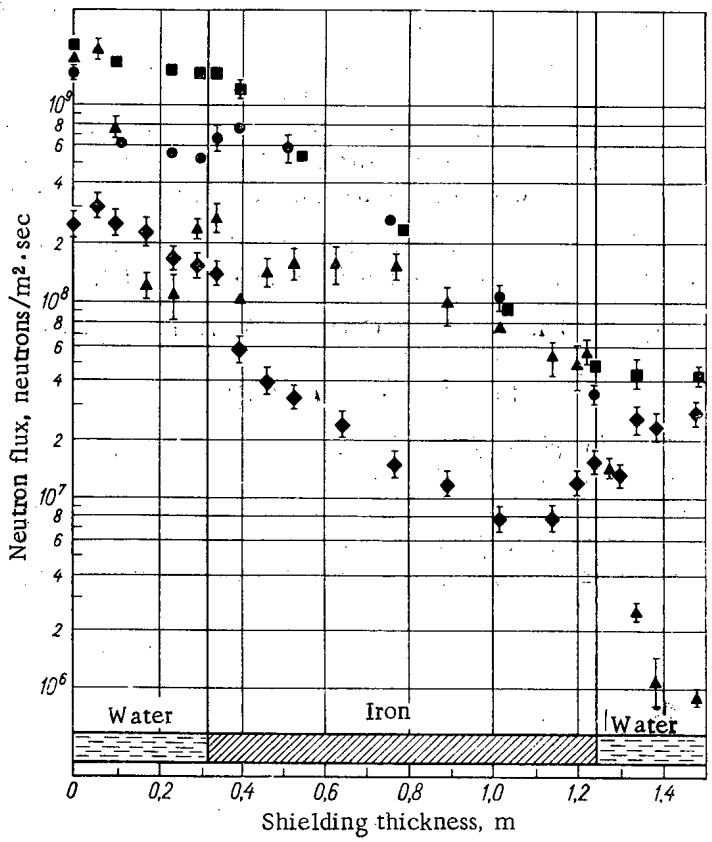

Fig. 3. Distribution of neutron fluxes in water-iron-water shielding. ■) Distribution of high-energy neutrons; ●)fast neutrons; ▲)resonance neutrons. ◆) Distribution of gamma-ray dose rate, 10^{-5} μr/sec.

On analysing the experimental results shown in Figs. 1-3, we conclude that, within the experimental error, the presence of a preceding layer has no effect on the attenuation of fluxes of high-energy neutrons in the following layer.

Statistical data for many shielding materials [4] indicate that there is a linear relation between the inelastic-interaction cross section Σ_{in} of high-energy neutrons (E > 100 MeV) and the density ρ (in g/cm^3), to within about 5%:

$$\Sigma_{in} = 0.59\,(1.5+\varrho)\ \text{м}^{-1}. \tag{1}$$

The extraction cross section Σ_{rem} of high-energy neutrons is proportional to Σ_{in} [2, 3, 5]:

$$\Sigma_{rem} \approx \frac{\Sigma_{in}}{\alpha}, \tag{2}$$

where the parameter α varies from 0.9 to 1.4, according to the neutron spectrum, and varies little with the material of the shielding. In homogeneous shielding of sufficient thickness [2, 5] the following relation holds good:

$$\frac{\Phi_f}{\Phi_h} \approx \bar{n}\,\frac{\Sigma_{in}}{\Sigma^f_{rem}}, \tag{3}$$

where Φ_f and Φ_h are the fluxes of fast and high-energy neutrons, respectively, $\bar{n}$ is the mean number of evaporative neutrons emerging from the excited nuclei, and Σ^f_{rem} is the extraction cross section for fast neutrons.

The value of $\bar{n}\,\Sigma_{in}/\Sigma^f_{rem}$ increases with the atomic weight of the shielding material. It was estimated to vary from ~ 0.1 for water to 1 for iron. The varying values of this quantity for each layer satisfactorily explain the behavior of a flux of fast neutrons.

Surges in the fluxes of resonance neutrons at the boundary between two materials are due to the difference in these materials's moderating properties and also to deformation of the intermediate-neutron spectrum with increasing distance from the boundary.

Attenuation of the resonance-neutron flux in the material behind the iron can be regarded as exponential, after short transitional sections. The transitional sections are approximately equal to the relaxation lengths, and are $\lambda_1 \approx 3$ cm in water and $\lambda_2 \approx 9$ cm in heavy concrete. For these materials, the ages of the intermediate neutrons up to 1.44 eV ($E_0 = 1.5$ MeV) are approximately $\tau_1 \approx 30$ cm^2 and $\tau_2 \approx 120$ cm^2 [5]. From these values of τ and λ, we can infer that, to a certain approximation, $\sqrt{\tau}$ characterizes the attenuation of a flux of intermediate neutrons in the second layer. The increased indications of the x-ray film in the layer of water following a layer of iron (cf. Fig. 3) are due to the hard component of the scattered capture gamma radiation.

Owing to the appreciable accumulation of intermediate neutrons in the heavy materials, especially in steel, it is desirable to make a subsequent layer of shielding of water-containing material.

The authors would like to thank Z. Tsisek and A. P. Cherevatenko for help in the experimental work.

LITERATURE CITED

1. L. N. Zaitsev et al. Atomnaya Énergiya, 12, 525 (1962).
2. B. S. Sychev et al. Atomnaya Énergiya, 20, 323 (1966).
3. B. S. Sychev et al. Atomnaya Énergiya, 20, 355 (1966).
4. L. N. Zaitsev et al. Atomnaya Énergiya, 19, 303 (1965).
5. D. L. Broder et al. Concrete in Shields for Nuclear Plant. Moscow, Atomizdat (1966).

HEAT EMISSION FROM POTASSIUM BOILING IN A TUBE IN THE REGION OF MODERATE VAPOR CONTENT

V. M. Borishanskii, A. A. Andreevskii, K. A. Zhokhov, G. S. Bykov, and L. S. Svetlova

UDC 621.039.517.5

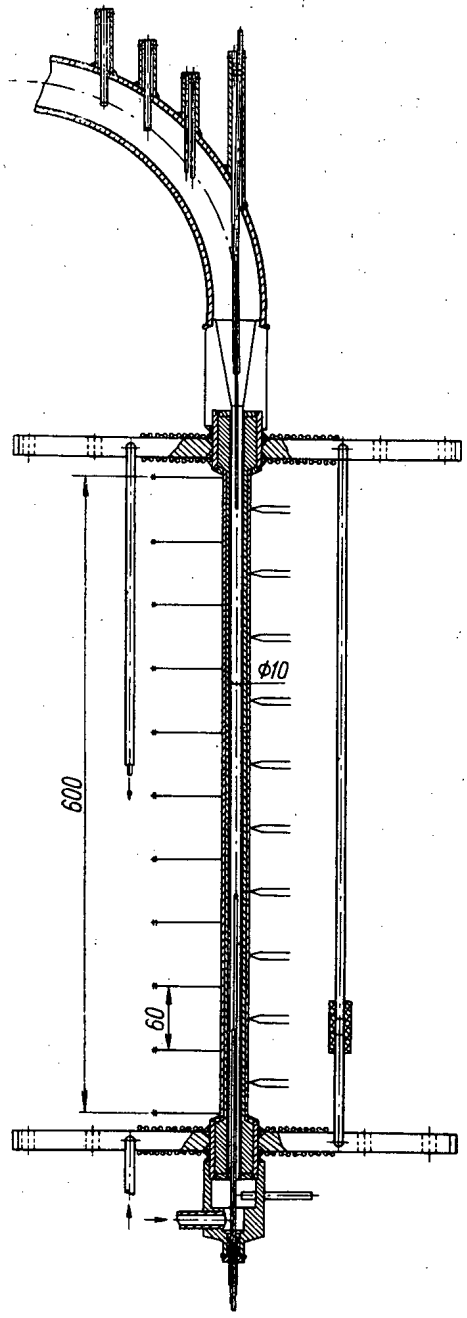

Fig. 1. Working section of apparatus.

Until recently, heat exchange during the boiling of alkali metals has been studied mainly for the case of free convection of the liquid in a large vessel [1-4]. In [1] it was shown that, for sodium or potassium boiling with bubble formation in a large vessel, the heat-transfer coefficient is proportional to the 0.7th power of the specific thermal load, i. e., the relation between α and q is the same as for the boiling of nonmetallic liquids. A similar relation was found by the authors of [2, 3]. This problem was analyzed theoretically in [5, 6]. However, less work has been done on the boiling of alkali metals in tubes.

In this letter we give some results on heat transfer during the boiling of potassium in circular tubes of diameter 10 mm and length 600 and 800 mm.

The apparatus used for this work consists of a closed circulation loop made of steel 1Kh18N9T. The main unit is the working section (calorimeter), which is directly heated by an electric current, and consists of two tubes (Fig. 1). To reduce the electrical resistance, the gap between the tubes was filled with copper. It was calculated that, for the given thickness of the copper layer (δ = 4 mm), the heat emission in the liquid metal (in absence of vapor formation) was less than 10% of the total heat emission in the working section. During boiling practically all the heat was emitted in the walls. The wall temperature was measured at ten positions along the working section, in each of which was installed a chromel-alumel thermocouple. The temperature of the potassium was measured at the inlet to the working section, and also inside it at 30, 90 and 210 mm from the inlet and 30 mm from the outlet.

The experiments took place at saturation pressures in the range $p_s \approx 0.42$-3.38 atm ($t_s \approx 678$-910°C) with thermal loads of up to

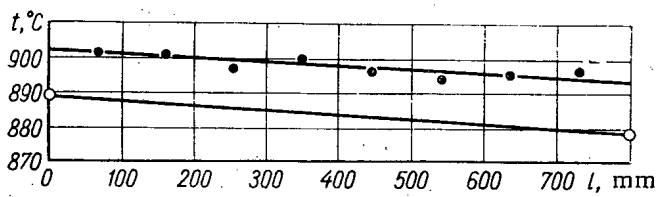

Fig. 2. Temperature distribution along working section. Operating conditions: q= 263,000 kcal/m^2 · h; G = 131.5 kg/h; p = 3.2 atm; x_{out} = 10.8%.

Translated from Atomnaya Énergiya Vol. 21, No. 1, pp. 58-59, July, 1966. Original article submitted February 18, 1966.

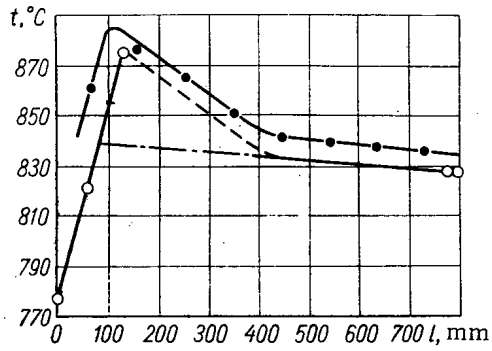

Fig. 3. Temperature distribution along working section. Operating conditions: q = 460,000 kcal/m^2 · h; G = 84 kg/h; p = 1.78 atm; x_{out} = 25.6%.

530,000 kcal/m · h. The vapor content at the inlet was ~15% by weight. The apparatus was constructed so that potassium could be fed to the working section both after heating to the saturation temperature and with a content of the vapor phase.

Figure 2 gives the temperature distribution curve along the working section with the vapor content at the inlet slightly above zero. It will be seen that the temperature head, and hence also the coefficient of heat transfer, are approximately constant along the tube.

During the experiment the potassium was observed to become superheated above the saturation temperature. This phenomenon took place when the working section was fed with liquid metal not heated to the saturation temperature, so that further heating took place in the working section. However, after the potassium reached saturation temperature, it became further heated during the course of its motion. The extent of the superheating was 30-50° C above the saturation temperature. After this the temperature of the potassium rapidly fell to near the saturation value. This process was accompanied by strong temperature pulsations of the wall and vapor-liquid mixture throughout the length of the working section. The maximum amplitude of these temperature pulsations was observed to occur in the superheating zone and amounted to ± 20° C.

Figure 3 plots the temperature distribution along the working section when the latter was fed with potassium not heated to saturation temperature.

Our experimental results on heat transfer are plotted in Fig. 4; this diagram also gives results from [1] on potassium boiling in a large vessel, and from [7] on potassium boiling in tubes of diameters 8.3 and 22 mm. Satisfactory agreement is observed between the data for the large vessel and the tubes, in the region of moderate vapor content. The experimental points are grouped near the line which represents the equation given in [1] for boiling with free circulation in a large vessel:

$$\alpha = 3q^{0.7}p^{0.15}, \qquad (1)$$

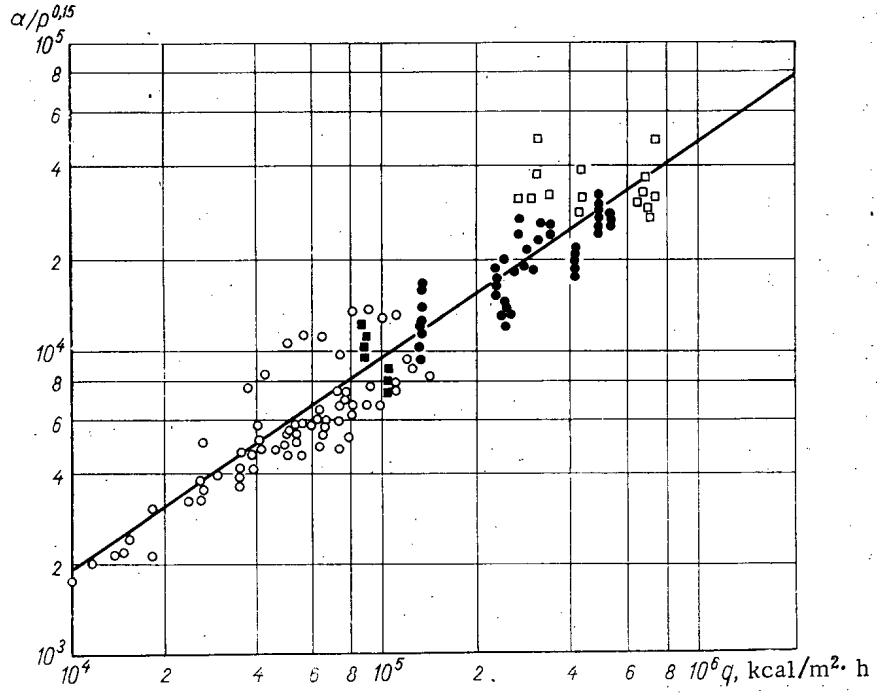

Fig. 4. Heat emission for potassium boiling in a large vessel and in tubes of various diameters. ○) Large vessel (data of present work); ●) d = 10 mm (data of present work); □) d = 8.3 mm [7]; ■) d = 22 mm [7].

where α is the coefficient of heat transfer in kcal/m^2 · h · °C, q is the thermal load in kcal/m^2 · h, and p is the pressure in atm. Thus, Eq. (1) can be used to calculate the heat transfer from potassium boiling in a tube, in the absence of effects due to the vapor content.

LITERATURE CITED

1. V. M. Borishanskii et al. Atomnaya Énergiya, 19, 191 (1965).
2. R. Lyon, A. Faust, and A. Katz. Chem. Engng Progr. Sympos. Series, 51, No. 7 (1955).
3. R. Noyes. Trans. ASME (Series C), 5, No. 2 (1963).
4. N. Madsen and C. Bonilla, Chem. Engng Progr. Sympos. Series, 56, No. 30 (1960).
5. V. M. Borishanskii and K. A. Zhokhov. Atomnaya Énergiya, 18, 294 (1965).
6. V. I. Deev and A. N. Solov'ev. Inzh.-fiz. zh., No. 6, 8 (1964).
7. A. Fraaz. Atomnaya Tekhnika za Rubezhom, No. 6, 12 (1964).

All abbreviations of periodicals in the above bibliography are letter-by-letter transliterations of the abbreviations as given in the original Russian journal. *Some or all of this periodical literature may well be available in English translation.* A complete list of the cover-to-cover English translations appears at the back of the first issue of this year.

CHANGES IN THE MECHANICAL PROPERTIES OF AN AGING ALUMINUM ALLOY AFTER USE IN A NUCLEAR REACTOR

A. P. Kuznetsova and B. V. Sharov

UDC 621.039.56:669.715

This investigation deals with the alloy "Avial' Mark SAV-1", which consists of aluminum plus 0.6-1.2% silicon and 0.45-0.9% magnesium.

The phase diagram of the system Al-Mg-Si contains a quasibinary eutectic between an aluminum-based solid solution and the intermetallic compound Mg_2Si. The solubility of Mg_2Si in aluminum decreases from 1.85% at the eutectic temperature to ~0.1% at room temperature [1]. Thus, after quenching of the alloy, age hardening takes place, owing to the appearance in the aluminum matrix of zones enriched with the alloy components and the formation of particles of Mg_2Si during the later stages of aging.

TABLE 1. Mechanical Properties of Specimens

Section of tube	f, neutrons/cm³·sec	ft, neutrons/cm²	σ_B, kg/mm²	$\sigma_{0.2}$, kg/mm²	δ, %	No. of specimen
1	$\sim 10^{19}$	$\sim 10^{16}$	30,5±0,6	22,8±1,6	11,5±0,8	10
2	—	—	30,2±0,7	23,5±1,4	11,6±0,9	8
3	$2 \cdot 10^{12}$	$6 \cdot 10^{19}$	30,1±0,4	23,2±0,6	10,4±0,5	5
4	$2 \cdot 10^{13}$	$6 \cdot 10^{20}$	30,3±0,6	24,8±0,9	10,3±1,1	11
Before irradiation		—	27,5±0,6	21,1±0,9	12,5±0,2	13

SAV-1 is used as a structural material for reactor cores, because it contains no substances with a large absorption cross section for thermal neutrons.* It is also resistant to corrosion in water, carbon dioxide and other media.

We have studied the properties of the material of an "Avial'" tube which has been acting as a process channel in the reactor of the Institute of Theoretical and Experimental Physics (Fig. 1). The "Avial' "

*References [2, 3] give some data on the effect of irradiation on the properties of annealed SAV-1 and the similar American alloy 6061(61S).

TABLE 2. Results of Tests on Control Specimens and on Specimens Irradiated by 6.10^{20} neutrons/cm²

Conditions of creep test			Specimen	Residual deformation after creep, %*	Results of rapid testing to destruction after creep tests			
T, °C	σ, kg/mm²	t, h			σ_B, kg/mm²	$\sigma_{0,2}$, kg/mm²	σ, %	No. of tests performed
154±4	7	230	Control	2,3±1	19,2±1,6	16,6±2,1	10±1,7	3
			Irradiated	1,8±1	19,1±1,8	16,1±1,5	10±1,7	3
154±4	5	350	Control	2,5±1	18,0±1,2	16,0±0,6	7,9±0,1	3
			Irradiated	1,4±1	14,7±1,1	12,3±1,3	10,9±0,7	4
100±5	5	2200	Control	<0,5	25,7±1,8	22,7±1,2	8,5±1,4	7
			Irradiated	<0,5	24,5±1,8	21,7±1,2	7,8±0,5	7

*Mean of seven specimens.

Translated from Atomnaya Énergiya, Vol. 21, No. 1, pp. 60-62, July, 1966. Original article submitted January 22, 1966.

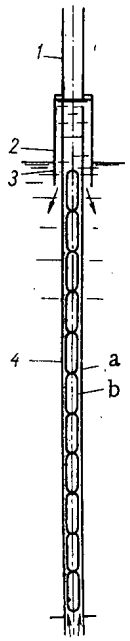

Fig. 1. Diagram of process channel of reactor. (a) "Avial' " tube; (b) uranium heat-emitting element; (1, 2, 3, 4) parts of tube under investigation.

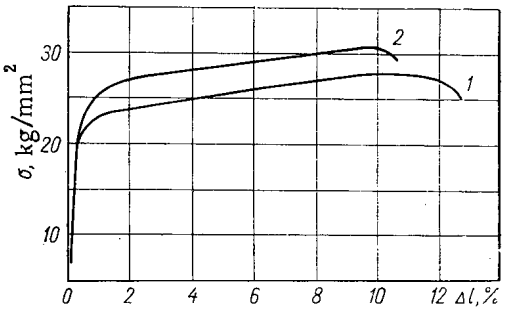

Fig. 2. Tension-elongation diagrams of avial' specimens. (1) Before irradiation; (2) after irradiation by 6.10^{20} fast neutrons per cm^2.

was in contact with heavy water on the inside and outside at a temperature below 80° C. The part above the water was situated in an atmosphere of helium which was also at a temperature below 80° C. The temperature of the tube wall was practically equal to that of the media in which it was placed. The tube was installed in the reactor after it had been aged and hardened*. Specimens were cut from the walls of the "Avial'" tube, of thickness 1 mm, by means of a punch. Their effective length was 20 mm, and their cross-sectional area 3 mm^2. The mechanical properties of the specimens were the same whether they were cut along or across the tube axis.

Rapid Tests to Destruction. Table 1 gives the mechanical properties of specimens corresponding to the tube before operation in the reactor, and also the properties of the material after use in the reactor for two years, together with the intensities and total fluxes of fast neutrons. Figure 2 gives tension diagrams of the "Avial' " specimens.

These data show that during use in the reactor the tempered "Avial' " becomes harder and less plastic. The changes in mechanical properties were observed both in those parts of the tubes which were subjected to intense neutron irradiation and in those parts which were outside the reactor core and were thus irradiated by small fluxes. Similar changes in mechanical properties were also observed after keeping non-irradiated control specimens, warmed to the same temperature, outside the reactor for the same period.

Creep Tests. Creep tests were carried out under tensile stress. The residual deformation was measured. After the creep tests the specimens were tested rapidly to destruction. The test results are given in Table 2.

*According to our observations, there was no change in the mechanical properties of "Avial' ", not tempered or cold-worked, after irradiation at ~ 100° C by a flux of 10^{20} fast neutrons per cm^2.

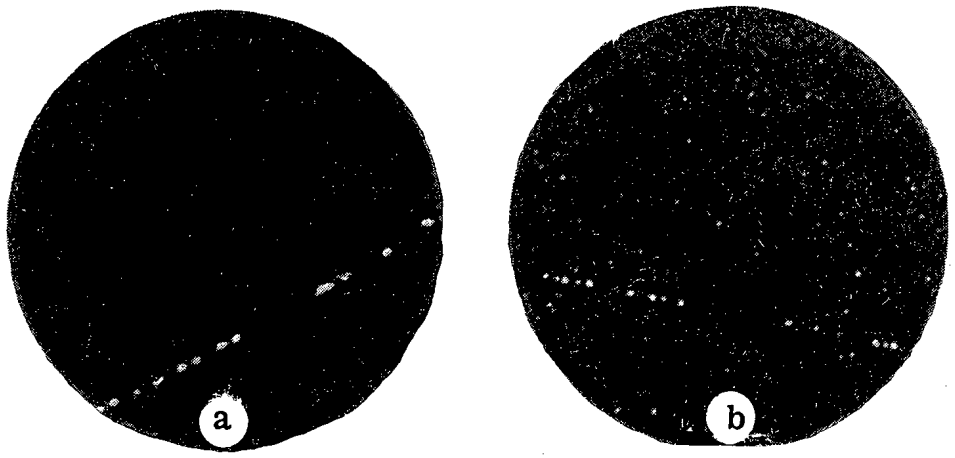

Fig. 3. Microstructure of "Avial'" (× 11,400). (a) Before irradiation; (b) after irradiation by 6.10^{20} neutrons/cm^2.

From the table it is seen that the residual deformations of the irradiated specimens scarcely differ from those of the non-irradiated specimens. Aging of the specimens during the creep tests altered their mechanical properties under rapid testing to destruction. The irradiated material, before the creep tests, was in fact subjected to artificial aging by operation in the reactor.

Measurement of Normal Modulus of Elasticity. The modulus of normal elasticity, measured at room temperature, was found to be 7080 ± 200 kg/mm^2 both for the control specimens of "Avial' " and for those irradiated by 6.10^{20} neutrons/cm^2.

Microstructure of Specimens. Examination under the optical microscope did not reveal any structural changes in the "Avial'."

Examination under the electron microscope revealed finely-dispersed segregations (Fig. 3) formed in the "Avial'" after two years' irradiation. Similar segregations occur on annealing outside the reactor in identical conditions.

Measurements of the irradiated "Avial'" with an x-ray diffractometer did not reveal the presence of an Mg_2Si phase.

We thus find that when tubes, made of tempered, aged SAV-1 alloy, are used in the core of a reactor, at a temperature below 80° C, with integral flux of 6.10^{20} fast neutrons/cm^2, they become hardened. The reserve of plasticity is quite high, and the material can be used as a structural material.

The experiments showed that the main cause of the changes in the properties of the tempered "Avial' " was simply the prolonged warmth (artificial aging), and not the irradiation by neutrons. The present authors' data agree numerically with results on tempered, aged 6061(61S) alloy, which has a similar chemical composition to SAV-1 [3].

In conclusion the authors would like to thank S. A. Gavrilov for help with the work.

LITERATURE CITED

1. V. G. Kuznetsov and E. S. Makarov. Izv. AN SSSR, Sektor fiziko-khimicheskogo analiza, 13, 177 (1939).
2. P. A. Petrov et al. Action of Nuclear Radiation on Materials. Symposium, Moscow, Izd. AN SSSR (1962), p. 100.
3. R. Steele and W. Wallace. Metal Progr., 68, 114 (1955).

A MERCURY MASS-DIFFUSION COLUMN FOR ISOTOPE SEPARATION

B. I. Nikolaev, Yu. P. Neshchimenko,
G. A. Sulaberidze, and V. M. Lalayan

UDC 541.182.3.543.52

The efficiency of separation in a mass diffusion column depends largely on the properties of the working liquid. The choice of mainly organic liquids as vapor-formers in all previous works [1-3] was determined by efforts to obtain an optimum ratio between the molecular weight of the vapor and the molecular weights of the components of the gas mixture being separated, corresponding to the greatest possible difference between the diffusion coefficients. Calculations show that, if we neglect parasitic effects in the column (in particular, solubility of the gas mixture in the film of condensate), the degree of separation in the column can be very great with organic liquids (the theoretical separation coefficient can be of order ten to a hundred). In addition, organic liquids always permit the choice of a substance with suitable boiling point and adequately low saturated vapor pressure. However, the rather high solubility of the separated gases in the condensate markedly reduces the separation effect. The organic liquids hitherto used as vapor formers in mass diffusion columns, e. g., xylene, nitrobenzene, tetrachloroethane, etc. [1-3], are good solvents; moreover, they decompose on prolonged boiling. The use of water vapor is very limited owing to its low molecular weight.

We have used metallic mercury as the working liquid: it has a fairly high molecular weight and a suitable saturated vapor pressure. Gases are almost insoluble in it. We shall here give a short description of the mass diffusion column used, together with the results of preliminary experiments on the separation of neon isotopes in mercury vapor, in arbitrary conditions. The column is shown diagramatically in the figure. The diameter of the vapor feed tube is 28 mm, that of the diaphragm 38 mm, and the internal diameter of the external cylinder is 45 mm. The working section of the column is 1 m long. Vapor is fed via holes in the vapor feed tube arranged at intervals along its length (25 rows of 1 mm diameter holes with 12 holes in each row). To stimulate circulation an additional row of holes is drilled in the lower part of the vapor feed tube. Inside the vapor feed tube there is an additional heater to ensure uniform heating of the vapor along its height and to eliminate condensation of mercury on the diaphragm and vapor feed tube. All the components of the column are made of materials which do not form amalgams. The porous diaphragm is a stainless steel gauze with 10,400 holes per square centimeter; the cell size is 4.10^{-3} mm^2 (wire diameters 64 and 32 microns). After special treatment the gauze was folded into two layers. As a result of preliminary experiments on separation of the neon isotopes on the above column, we obtained a maximum column separation factor of 17 with a two-layer diaphragm, a working pressure of 20 mm Hg of the mixture, and arbitrary conditions. Research is continuing on the separation process.

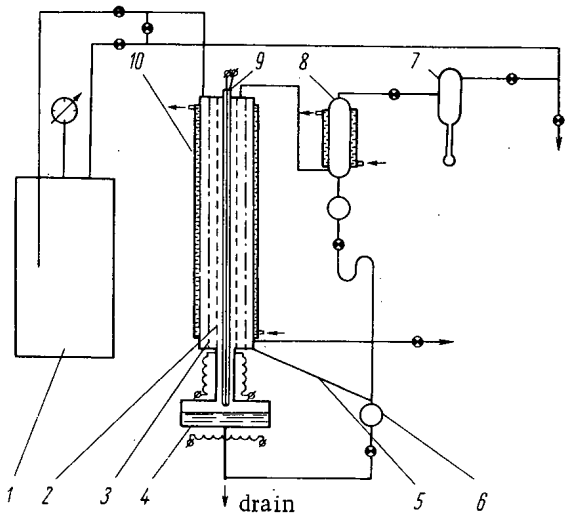

Diagram of mass diffusion column. 1) Ballast space; 2) vapor feed tube; 3) porous diaphragm; 4) vaporizer; 5) condensate drain; 6) calibrated volume; 7) capillary flowmeter; 8) external condenser; 9) extra heater; 10) internal condenser.

The authors would like to thank I. G. Gverdtsiteli for suggesting the problem and for valuable advice and information, Yu. V. Nikolaev for technical help in constructing the equipment, A. A. Sazykin and R. Ya. Kucherov for looking at the results and giving useful advice, and Z. N. Sabirov for performing the mass-spectrometric analyses.

Translated from Atomnaya Énergiya, Vol. 21, No. 1, p. 62, July, 1966. Original article submitted April 12, 1966.

LITERATURE CITED

1. I. G. Gverdtsiteli et al. Proceedings of Second International Conference on the Peaceful Uses of Atomic Energy, Geneva (1958). Reports of Soviet Scientists, Vol. 6, Moscow, Atomizdat (1959), p. 69
2. W. de Web and J. Los. Z. Naturforsch., 19a, 747 (1964).
3. M. Benedict and A. Boas. Chem. Eng. Progr., 47, 51 (1951).

USE OF AN AMPOULE WITH HYDRAULIC SHUTTER IN POWERFUL GAMMA-RAY RADIATION-CHEMISTRY PLANTS

A. V. Bykhovskii, V. E. Drozdov, and G. N. Lisov

UDC 621.039.55

An important problem in the development of radiation chemistry is the development of radiation-chemical apparatus with powerful radiation sources for research and industrial purposes. As experience has been gained in the use of preparations with high specific activity, the necessity has arisen to develop additional measures to secure the required thermal conditions for the radiation sources [1] and to prevent radioactive contamination of the operative parts of the equipment [2-4].

In the use of present types of radiation sources, it is important to construct radiation equipment which will prevent access of radioactive contamination into industrial plants.

It is well known that both types of gamma source—with water or dry shielding—have their advantages and drawbacks [5]. As presently used preparations have high specific activity, to secure normal thermal conditions [1] it is necessary to construct a special cooling system in equipments of the dry type. Great promise for radiochemical applications is offered by equipments of the mixed type, in which the shielding for the radiation sources during storage is of water, while actual irradiation is performed in a dry chamber.

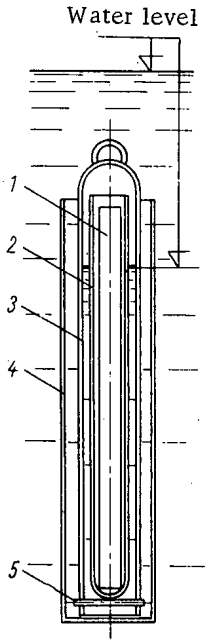

Fig. 1.

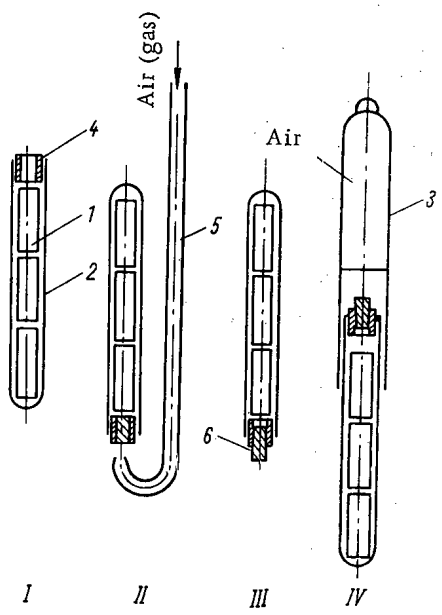

Fig. 2.

Fig. 1. Sealed ampoule with hydraulic shutter for storage of radioactive sources (first type). 1) Radioactive source; 2, 3, 4,) cylindrical vessels; 5) shutter.

Fig. 2. Sealed ampoule with hydraulic shutter for storage of radioactive sources (second type). 1) Radioactive source; 2, 3) cylindrical vessels; 4, 6) auxiliary stoppers; 5) tube for gas feed.

On one gamma-ray plant of this type, the construction of the radiation source unit includes the principle of the hydraulic shutter [6]. Provision is made for the use of two types of ampoule with hydraulic shutters. Ampoules of the first type are used if the operating chamber contains a manipulator and an optical system for loading the ampoule with the radioactive preparations. In plants where the radioactive preparations are kept continually in water, the ampoule with hydraulic shutter consists of two cylindrical vessels 2 and 3 (Fig. 1), one inside the other. The radioactive preparation is placed in vessel 2 by means of the manipulator. In plants where the preparations are periodically removed from the water, the ampoule consists of three vessels (2-4). The third vessel 4 is necessary to protect the hydraulic shutter, preventing contact between the water round the source with the working space of the chamber and ensuring the best possible heat removal from the preparations. Vessel 2 is retained in vessel 3 by means of the shutter device 5. When the ampoule is submerged in water to the depth of the biological shielding (4-5 m), the air in vessels 2 and 3 is compressed; the level in the space between the vessels goes up, but does not reach the upper edge of vessel 2, thanks to the choice of appropriate shape and size for the vessels.

Translated from Atomnaya Énergiya, Vol. 21, No. 1, pp. 63-64, July, 1966. Original article submitted October 30, 1965.

The ampoules may be of various lengths, depending on the number of sources. In our case, each ampoule contains up to 13 standard preparations of Co^{60} (diameter 11 mm, length 81 mm).

An ampoule of the second type (Fig. 2) is used when there is no manipulator in the operating chamber. In this case, all the operations required to load the preparation into the ampoules are carried out in the tank under the shielding water. During charging, the water is displaced from the ampoule by air (gas) supplied under the inverted ampoule. Since the ampoule can be charged under the water quite rapidly, there is no appreciable contamination of the water in the tank. Figure 2 shows the sequence of operations for charging the ampoule under the water. After the preparations 1 have been placed in vessel 2 (position I), stopper 4 is inserted, with a hole of diameter smaller than that of the preparation; this stopper retains the preparations in the vessel during the subsequent movements. To displace water, the ampoule is turned upside down, and then either it is removed from the tank, or an air (gas) tube is inserted a little way below the hole in the stopper. The air bubbles go through the hole in the stopper and displace the water (position II). To prevent the air from escaping from the ampoule, the hole in stopper 4 is closed with another stopper 6 (position III). Vessel 2, closed by the stoppers, is inverted again, and vessel 3 slipped over it; the air in 3, as the latter descends over 2, drives the water out of the space between the vessels (position IV). After installation of the supports, the source is ready for work. During use, stoppers 4 and 6 do not take part in sealing the vessels.

When preparations with high specific activity are used while the ampoule is outside the water tank, the ampoule must be cooled, e. g., by a water spray. When the ampoule with sources is in the storage position, cooling is by heat transfer to the storage water.

Ampoules with hydraulic shutters are used in the KSV-500 plant mounted in the UK-1 installation [7].

When radiation-chemistry processes are in operation, a cylindrical irradiator of diameter 100 cm is situated in the operating chamber, which has biological shielding; during storage, it is in the shielding water in the tank.

On account of our long successful experience of the KSV-500 equipment, we can recommend ampoules with hydraulic shutters for use in various gamma-ray plants with water or mixed shielding.

LITERATURE CITED

1. S. S. Gurvits et al. Health Rules for Construction and Use of Powerful Isotope Gamma-Ray Plants, No. 482-64. Moscow, Izd. Ministerstva zdravookhraneniya SSSR (1964).
2. A. V. Bykhovskii et al. Topics in Radiation Safety for Charging and Use of Powerful Gamma Sources for Radiation Chemistry (scientific proceedings of Institutes of Labor Protection VTsSPS). Moscow, Profizdat, No. 3 (35) (1965), p. 52.
3. A. V. Sedov and O. I. Yurasova. In the book: Problems of Health in Connection with the Development of Heavy Chemistry. Moscow, Izd. Pervogo Moskovskogo Meditsinskogo Instituta (1964), p. 137.
4. R. Cloutier and M. Brucer. Health Phys., 6, 32 (1961).
5. Proceedings of All-Union Scientific Conference on the Use of Radioactive and Stable Isotopes and Radiation in the National Economy and Science. Moscow, Izd. AN SSSR (1957).
6. G. N. Lisov, V. E. Drozdov, and A. V. Bykhovskii. Russian Patent Avt. Svid. No. 177998. Byulleten' izobretenii No. 2, January (1966).
7. V. L. Karpov et al. Atomnaya Énergiya, 15, 302 (1963).

SCALED-UP RADIATION CROSSLINKING OF POLYETHYLENE INSULATION FOR ELECTRICAL CABLEWARE

S. M. Berlyant, V. E. Drozdov, E. E. Finkel', P. A. Orlenko, L. M. Suroegin, A. Kh. Breger, V. L. Karpov, and V. A. Zorin

UDC 621.039.55:541.15

Modification of polyolefins in order to improve their thermal resistance and certain other parameters of the materials is one of the more promising radiation-chemical processes. But the allowable period of time during which the irradiated polyethylene can be exposed to air at elevated temperatures is limited by a precipitous loss of elasticity and increased brittleness due to a rapid oxidative process occurring under those conditions. This has led to attempts [1-4] to develop a method for thermally stabilizing irradiated polyethylene in order to lengthen its service life at elevated temperatures appreciably and at the same time to capitalize to the fullest on the potentials of this polymer as a thermostable material.

Figure 1 shows how the relative elongation of specimens of cableware polyethylene and compositions of this material with ordinary and combined additives, irradiated in helium with a dose of 100 Mrad, are affected by length of time exposed to air at temperatures of 150° and 200° C. The service life of this type of radiation-modified polyethylene exposed to air at 150° C lasts ~5000 to 6000 h, but only 100 to 150 h when exposed to air at 200° C (the material has a useful life extending several thousand hours in oxygen-free atmospheres).

Irradiated thermostabilized polyethylene is in essence a new electrically insulating material which has been used in the design of cableware for a variety of applications. Investigations of these cable products have revealed [5] that they are far superior in performance to their counterparts using insulation of unirradiated polyethylene. In addition to the improved quality manifested in the broader range of service temperatures, advantages from irradiation include higher reliability, a particularly crucial point considering the exacting conditions under which cable products have to function.

The development of techniques for thermostabilization of irradiated polyethylene and proper conditions for laboratory irradiation processes have entailed a need to build large-scale facilities and equipment for scaled-up irradiation of cableware and similar products.

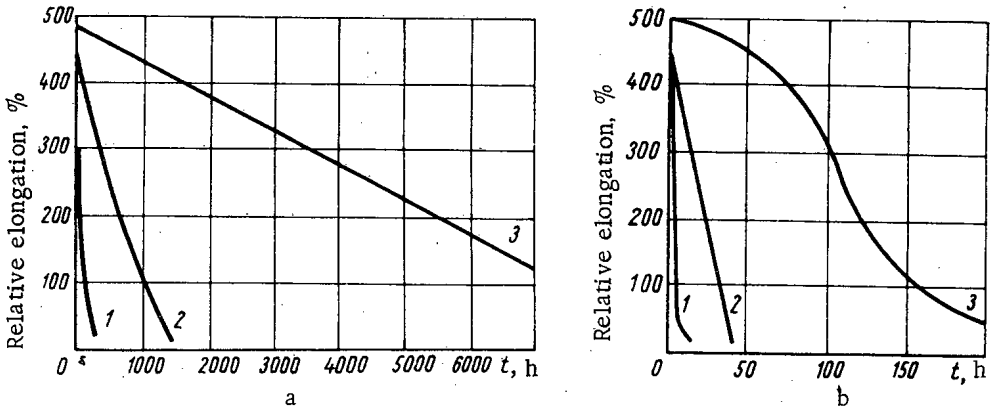

Fig. 1. How relative elongation of irradiated polyethylene specimens is affected by length of time exposed to air at 150° (a) or at 200° C (b): 1) Pure polyethylene; 2) composition of polyethylene plus ordinary additive; 3) composition of polyethylene plus combined additive.

Translated from Atomnaya Énergiya, Vol. 21, No. 1, pp. 64-66, July, 1966. Original article submitted October 16, 1965.

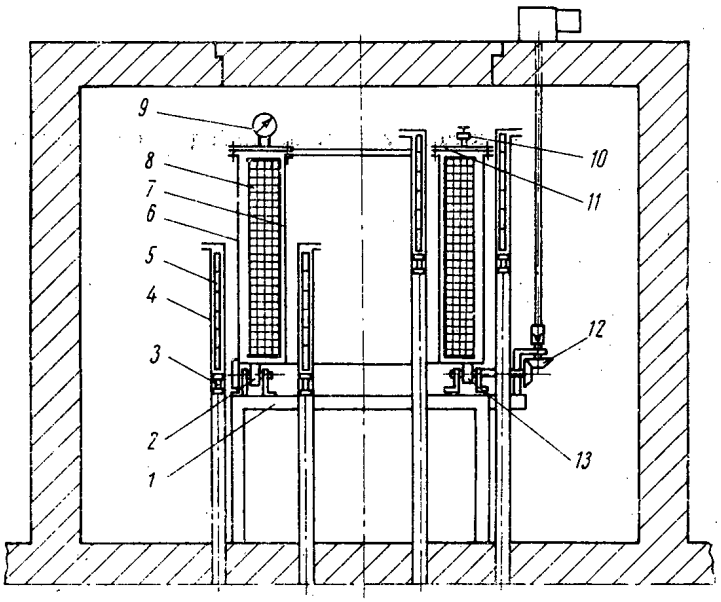

Fig. 2. Diagram of facility designed for radiation crosslinking of polyethylene insulation for cableware: 1) Worktable; 2, 13) bearings; 3) rod (pusher); 4) irradiator channel; 5) radiation sources; 6) radiation-chemical processor; 7) coil bobbin; 8) cable; 9) pressure and vacuum meter; 10) pipe outlet; 11) processor cover; 12) power drive.

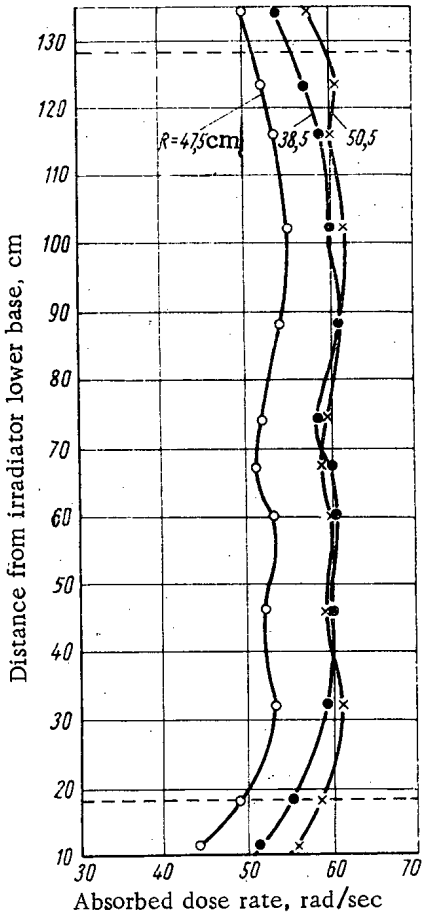

Fig. 3. Experimental dose rates throughout volume of annular processor filled with cable material, with lead filters placed across irradiator (height of irradiator: 150 cm): R) Distance from irradiator axis; – – – –) height of wound cable.

The facility described below was designed as a multipurpose facility, but one of the concrete directions in the work was irradiation of the insulated polyethylene cable core in a geophysical cable 6.5 mm in outer diameter intended for drilling at unusually great depths. Specific features of this cable include: length ≈ 9 km, weight ≈ 380 kg, volume ≈ 400 liters. The cable is intended for service in drilling fluid or in water at temperatures to 200°C and at pressures above 300 atm.

The design of the irradiator and radiation-chemical equipment of the size required presented certain difficulties in carrying out this and other scaled-up processes on isotope gamma-ray facilities. Nonuniformity of the dose field throughout the volume of the irradiated specimen (the cable) was specified not to exceed ± 10%. According to tentative calculations (taking into account allowable nonuniformity in dose rate), the thickness to which the cable is wound should not be greater than 13 cm. The height of the cable winding was set at 110 cm in order to accommodate a cable 9 km long with a coil inner diameter of 70 cm (Fig. 2). The radiation-chemical process equipment consisted of a pressuretight annular cylinder housing the inner and outer irradiator units. The equipment was designed to receive the coil bobbin with the cable wound on it. The size of the radiation-chemical plant was: height 130 cm, O. D. 105 cm, I. D. 65 cm.

The cable must be irradiated in an inert atmosphere, say argon, in order to forestall oxidation. Before commencing the irradiation, the processor together with the cable loaded into it is to be "washed" with argon by successively evacuating and refilling the space three times. After this operation the radiation-chemical processor is filled with argon to an overpressure of 0.3 atm, and the cable is then irradiated in the argon environment. A large amount of hydrogen (as much as 160 liters daily) is given off during the irradiation process, and for that reason the argon-hydrogen mixture is pumped out every 12 hours the plant is in operation, after which the plant is refilled with argon to an overpressure of 0.3 atm.

The KP-200 radiation-chemical plant [6] using a Co^{60} gamma-ray source with a total activity of 180,000 gram-equivalents of radium proved well suited to the purpose. The irradiator in this unit consists of 20 individual channels placed, in this application, on two concentric circles. The inner irradiator consists of six operating channels, with a diameter of 55 cm, while the outer irradiator consists of 14 channels and is 113 cm in diameter. The activity distribution between the inner and outer irradiators was decided upon in such a way as to provide the required uniformity of dose field in the horizontal cross section. There were seven Co^{60} preparations in each channel, forming line sources 74 cm in height. The radiation sources were transferred from the storage pond to the irradiator channels under compressed air at 0.4 atm.

Calculations of the dose-rate field distribution in the horizontal cross section of the radiation-chemical processor were checked experimentally with the aid of ferrocuprosulfate dosimeters placed in a processor filled with water or cable material. The choice of water as simulator is dictated by the close agreement between the values of the bulk density of the cable material and the specific weight of water (respectively 0.95 and 1 g/cm^3).

Discrepancies between calculations based on data reported in [7] and the experiment kept to within 2%. The processor was rotated on its axis at a speed of 2 rpm in order to obtain the required uniformity of dose-rate field over the cylindrical surfaces concentric about the surface of the irradiators. The height of the irradiator had to be increased to 150 cm in order to obtain a uniform field of dose rates up the entire height of the cable-filled radiation-chemical processor. Pneumatic conveying of the radiation sources made it possible to cope with this problem with ease (i. e., doubling the irradiator height) by positioning the sources in two tiers.

Experimental checking revealed a need to smooth out the dose-rate field along the height of the radiation-chemical processor. The existence of a clearance of 3 cm between the top and bottom tiers of sources in the irradiator, plus partial shielding of the middle of the irradiators by lead filters 20 cm high and 2 mm thick, brought about the required field uniformity of absorbed dose throughout the volume of the cable-filled processor. The experimental dose-rate field values throughout the volume of the processor loaded with cable, with lead filters in place, are shown in Fig. 3.

The dose required for different types of cables was chosen on the basis of product specifications and service conditions. When an insulated core in the geophysical cable was irradiated, a dose of 140 Mrad ± 10% was arrived at on the basis of preliminary experiments. The productivity of the facility was 0.7 kg of cable per hour at a dose rate of 63 r/sec and exposure time of 610 h. This means a gamma-radiation efficiency of ~ 13% for the plant.

Crosslinking of polyethylene insulation for the insulated core of geophysical cable 9 km in length was brought about on a KP-200 isotope facility. The practical realization of this process demonstrated how feasible it is to use isotope facilities for radiation-chemical processes in the treatment of large-size stock.

The authors are indebted to G. N. Lisov for his part in the design of the facility, and to M. E. Eroshov, M. D. Larionov, L. K. Topil'skii, Yu. D. Kozlov, and the late N. A. Kuznetsov for their kind assistance in the experimental phase of the work.

LITERATURE CITED

1. E. E. Finkel' et al. In the book: Proceedings of the Cable Industry Research Institute [NIIKP] [in Russian], No. VI, Moscow, Gosénergoizdat (1962), p. 151.
2. N. P. Gashinova et al. Ibid., No. VII, Moscow, Gosénergoizdat (1963), p. 109.
3. E. E. Finkel'. Coll: Applications for Plastics in the Cable Industry [in Russian], Moscow, All-Union Research Institute for Electromechanics (1964), p. 25.
4. V. L. Karpov et al. Proceedings of the II All-Union Conference on Radiation Chemistry, Moscow, Izd. AN SSSR (1962), p. 547.
5. G. I. Gladkov et al. In the book: Proceedings of the Cable Industry Research Institute [in Russian], No. IX, Moscow, Gosénergoizdat (1963), p. 131.
6. N. G. Gusev et al. Shielding Against Emission by Extended Sources [in Russian], Moscow, (Gosatomizdat) (1961).
7. V. I. Volgin et al. Atomnaya énergiya, 18, 546 (1965).

THE PEACEFUL ATOM AT THE POLYTECHNICAL MUSEUM

An exhibition hall devoted to the peaceful use of atomic energy in the USSR has found great popularity among visitors to the Polytechnical Museum. A central position in the exhibition hall is assigned to a section showing the role of nuclear power in the USSR. Numerous models, posters, and exhibits illustrate recent advances in nuclear power in the USSR. Among the most interesting of them is a working model of an atomic power station which will soon be put into operation at Shevchenko with the BN-350, the first commercial, fast-breeder power reactor in the USSR. Energy generated in the reactor will be used both for the production of electrical power and for a desalinization plant with a capacity of 100,000 m^3/day.

A prominent place in the exhibition is occupied by low level nuclear power, which is represented by models of a 1500 kW portable atomic power station with a boiling-water, water-cooled reactor and of a 750 kW organic-cooled reactor (ARBUS-2).

At the center of the hall, there are working models of the largest Soviet atomic power stations complete with buildings and equipment—the Kurchatov station at Beloyarsk and the one at Novo-Voronezh.

At the Beloyarsk atomic power station, uranium-graphite reactors have been installed which have nuclear superheating of steam to ~ 500° C making it possible to use series turbines. The efficiency of the station is 35-38%. The reactor of one section of the Novo-Voronezh atomic power station has six circulating coolant loops, each pair of loops producing steam for one 70,000 kW turbogenerator. A single reactor forms a unit with three turbogenerators. This reactor is enclosed in a vessel in the form of a steel cylinder 3.8 m in diameter and 12 m high. The reactor core contains 312 operating fuel assemblies each of which contains 91 uranium dioxide fuel elements enriched to 1.5%. The efficiency of the station is 26.6%.

Attracting the attention of visitors is a model of the First Atomic Power Station reactor and operating engineering loops which demonstrate clearly, and in detail, the operating principles of an atomic power station and of a reactor core.

Of great interest is an exhibit of a model of the Romashka device, an outstanding direct converter of thermal energy to electricity. The device was shown at the Third International Conference on the Peaceful Use of Atomic Energy. The energy source in the device is a fast reactor with fuel in the form of 49 kg of 90% enriched uranium carbide. Energy is converted by means of semiconductor thermal converters. Temperature at the reflector surface is 1000° C, and power of the device is 0.5-0.8 kW.

Tables presented in the exhibits reveal the prospects for the development of nuclear power in the USSR and the economic efficiency of an atomic power station in comparison with an ordinary coal-fired station. They indicate how the competitiveness of an atomic power station with respect to a coal-fired station increases in proportion to increase in the power of the atomic power station.

In addition to nuclear power, the exhibition hall includes other fields in the peaceful use of atomic energy.

Models of thermonuclear devices, toroidal chambers, and of the Ogrenok device give an idea of the work on mastering thermonuclear power. Of them, the most interesting is a model of the Ogrenok magnetic trap for thermonuclear research which is a cylindrical vacuum chamber with longitudinal magnetic field and magnetic mirrors. To produce a high-temperature plasma, deuterium ions, previously accelerated by a powerful accelerator, are injected into the chamber. Charged particles in the plasma are captured by the magnetic field.

Also shown in the hall are instruments and equipment which demonstrate modern capabilities for the detection and measurement of radioactive radiations. Of particular interest is a model and diagram of a scintillation counter intended for measuring intense radiation fluxes and also for counting individual particles. The radiation detection efficiency is extremely high (it is about 100% for α and β radiation, and as much as 50% for γ radiation). A model and diagram is also shown for a gas-discharge counter intended for detecting individual radioactive particles (the detection efficiency for α and β particles is close to 100%).

Several instruments illustrate the use of radiation counters in various pieces of apparatus. For example, type SCh-3 equipment for counting neutrons is intended for the measurement of neutron fluxes by recording the electrical

Translated from Atomnaya Énergiya, Vol. 21, No. 1, pp. 74-76, July, 1966.

impulses produced by neutrons in a SKM-5A boron counter, the latter acting as a sensor. The equipment is used for monitoring reactor operation and for research. The resolving time of the equipment is less than 50 μsec. Also on exhibit is a type B-2 counting equipment which consists of a VSP (1) scaler with electromechanical pulse counter and scintillation attachment for measuring the intensity of radiation with a scintillation counter, the apparatus being intended for detection and pulse counting in the measurement of α, β, and γ radiation. The count rate of the apparatus goes to 6400 cts/sec separated by more than 50 μsec. In a number of exhibits, there are PS-100 scalers with special decatron tubes in which counting rates of 20,000 cts/sec are achieved. The use of counters in biology is demonstrated by IMA-1 tracer atom ratemeters which are intended for qualitative and quantitative differential determination of soft and hard β and γ radiation in working with tracer atoms. The instrument makes it possible to follow the path and the point of accumulation of tracer atoms in plants and animals. Indications of radiation intensity are given by measuring instruments, sound, and light signals. The pulse sensor is an SBT-7 end-window halogen counter in a hermetically sealed case.

A special section is devoted to the use of radioactive isotopes and to equipment, and the operation of equipment, using radioactive isotopes for flaw detection and measurement. Among the interesting exhibits in this section is a CUP-Co-0.5-1 flaw-detector for industrial x-ray work and a portable GUP-Ti-0.5-3 which makes it possible to manage without expensive x-ray equipment. Also exhibited is working demonstration equipment—a Sliva radioactive soil-meter which makes it possible to measure the percent content (from 0 to 40%) of soil in the silt passing through the silt pipes of a dredge; this enables one to regulate the optimal mode of dredge operation. Operation of the instrument is based on the measurement, with an ionization chamber and tube circuit, of the radioactive radiation passing through the soil pipe from a radioactive source. Any change in the consistency of the silt produces some kind of attenuation in radiation intensity and a corresponding change in the reading of the instrument.

Of interest is a UR-4 radioactive level gauge which is intended for continuous, contact-free measurement of the height of the interface between two media by illuminating the object with γ rays from a Co^{60} source. The instrument consists of two columns and an electronic unit. The columns contain movable carriages, one of which carries a container with the radioactive source, and the other, two STS-8 counters.

Dosimetric equipment is also exhibited in the hall. Included is the Tiss type universal radiometer which is intended for measurement and warning when a given level of radioactive contamination by α- and β-active materials is exceeded on the surface of equipment, or on the clothing and hands of operating personnel. Instruments on exhibit enable one to measure radiation dose—the Kaktus microroentgenometer (a fixed line-fed instrument for measuring γ-ray dose rate) and the KND-1 individual dosimeter (for measuring total doses of 0.02-2 R from γ rays with energies from 115 keV to 2 MeV).

Numerous posters and illustrations acquaint one with a brief chronicle of the most important events in the field of the peaceful use of atomic energy and also show the structure of the atom and the nucleus simply and clearly; they tell about radioactivity, nuclear reactions, the principle of chain reaction, and the operation of fast and thermal nuclear reactors.

— V. B.

SESSION OF THE JINR SCIENTIFIC COUNCIL

In Dubna, the jubilee session of the Scientific Council of the Joint Institute for Nuclear Research has completed its work. It was decided to confer the name of Academician Igor Vasil'evich Kurchatov on the new, one-hundred-fourth element in the periodic table in memory of his outstanding service in the development of Soviet and world-wide physics.

Research carried out at Dubna on the synthesis of elements one hundred two, one hundred three, and one hundred four indicated that the most promising method of synthesis was connected with the irradiation of heavy elements by accelerated, complex nuclei. This is particularly apparent in the work on element one hundred four. The first data on the properties of the new element were obtained in 1964 in the JINR Nuclear Reactions Laboratory by G. N. Flerov, Yu. Ts. Oganesyan, Yu. V. Lobanov, V. I. Kuznetsov, V. A. Druin, V. P. Perelygin, K. A. Gavrilov, S. P. Tret'yakov and V. M. Plotko. One hundred and fifty spontaneous fission events in the new element were recorded as the result of extremely complex and lengthy experiments. Its lifetime turned out to be about thirty seconds. After completion of the physical experiments, a group of Soviet and Czechoslovak staff members—I. Zvara Yu. T. Chuburkov, R. Tsaletka, T. S. Zvarova, M. R. Shalaevskii, B. V. Shilov—began a study of the chemical properties of element 104.* This problem was proposed by G. N. Flerov, and the development of techniques had already started in 1960. The investigations used original, rapid methods for continuous separation of the products of nuclear interactions.

The method developed by the chemists made it possible to study the chemical properties of an element in fractions of a second while having only individual atoms at their disposal. The idea of chemical identification was based on an assumed sharp difference in the properties of the higher chlorides of element 104. In the chemical experiments, atoms of element 104 were separated from all actinides. It was shown that the new element was an analog of hafnium. Thus the cycle of research on the identification of element 104 was completed.

Now a new element, bearing the name of an outstanding Soviet scientist, must take its place in the periodic table.

*The paper of I. Zvara et al., Chemical properties of element 104, will be published in the August issue of Atomnaya Énergiya.

Translated from Atomnaya Énergiya, Vol. 21, No. 1, p. 76, July, 1966.

BIBLIOGRAPHY

NEW BOOKS

M. A. Heald and C. B. Wharton, Plasma Diagnostics with Microwaves. New York–London–Sydney, John Wiley and Sons (1965), 452 pages.

Microwave diagnostics of plasma is a widely used technique, not only in thermonuclear fusion experiments, but also in space research, ionosphere studies, the development of spacecraft engines, MHD energy converters, microwave instruments, and other applications. The great advances in microwave diagnostic techniques have rendered it a standard technique in plasma investigation in many laboratories throughout the world. In this connection the book by M. A. Heald and C. B. Wharton, pioneers in this field, is of enormous interest. These authors set themselves the goal of writing a book which would serve as reference text and handbook for the experimental physicist first approaching the study of plasmas by microwave techniques. The book contains an exhaustive presentation of the theoretical fundamentals, plus a very detailed and what appears to be a unique, to date, description of the experimental technique. One special merit of this book, written by experimental physicists for experimental physicists, is the large number of photographic plates, oscillograms, graphs, and diagrams, which will be valuable tools to anyone working in the field.

The presentation of the material begins at the elementary level and gradually rises to the frontier of research in this field. In the first chapter, the authors acquaint the reader with the now familiar theory of wave propagation through a cold plasma. In the second chapter, discussion centers on the role of collisions, especially electron–ion coulomb collisions. The third chapter applies kinetic theory to wave propagation in a hot plasma, when the random thermal velocities of the electrons are commensurate with the phase velocity of the wave. This chapter concludes with a brief discussion of Landau damping. The fourth and fifth chapters deal with the theory of wave propagation in a confined plasma. They take up microwave probing of plasma and the theory of plasma-filled waveguides and resonators. The sixth chapter presents a detailed discussion of all possible practical schemes of active microwave diagnostics of plasma (measurement of transmission, attenuation, and reflection of waves, microwave interferometers, measurements of Faraday rotation, wave scattering experiments, and so forth). The next two chapters take up the theory of microwave emission by the plasma itself as a result of both thermal and nonthermal processes, and discusses techniques of passive radiometric diagnostics. The ninth chapter cites a very detailed description of microwave equipment and microwave plumbing for use in plasma diagnostics. The tenth and concluding chapter of the book gives a brief description of other plasma diagnostics techniques. Here we find laser measurements, Langmuir and magnetic probes, optical spectroscopy, and similar topics, plus a discussion of how to use the various techniques to check the other diagnostic techniques. The book ends with a generous bibliography (mentioning over 500 titles) and an alphabetically ordered subject index.

J. H. Sanders. The Fundamental Atomic Constants. Oxford Univ. Press, Oxford (1965), 98 pages.

This is the second edition of a monograph devoted to the fundamental atomic constants. It includes: the charge on an electron (e), the mass of the electron (m), the mass of the proton (M), the speed of propagation of electromagnetic radiation in vacuum (c), Planck's constant (h), Avogadro's number (N), Boltzmann's constant (K), and the gravitational constant (G).

Modern atomic physics requires a knowledge of the exact values of these constants. The experimental (direct and indirect) and theoretical determination of these values is the subject of a large number of papers which serve as the basis for this book (the list of pertinent literature extends over 213 titles). The content of the monograph can be divided into four basic sections: earlier measurements of the constants, modern exact measurements and measurements of the speed of light, and deviations in values of the constants.

The appendices give the commonly used designations for the constants, standardization of measurements, and a table of values of the constants with precision indicated.

The monograph will be of interest to both theoretical and experimental physicists as a reference containing the most exact values available for the atomic quantities in question.

Translated from Atomnaya Énergiya Vol. 21, No. 1, pp. 77-80, July, 1966.

Seventh Report on the Activities of the [European Nuclear Energy] Agency. Paris, ENEA (1965), 125 pages.

The European Nuclear Energy Agency, in which 18 European nations enjoy membership, issued its seventh report on its activities in 1965. The report starts off with a description of the work carried on in joint efforts at the Halden and Dragon reactors and at the Eurochemic spent-fuel reprocessing plant. The reactors are presently in operation, and the reprocessing plant will be on stream before the end of 1966.

A description of the collaborative efforts of the ENEA in the field of nuclear constants, reactor physics, reactor safety programs, computer programming, neutron constants, irradiation of foodstuffs, power production with radioactive isotopes, and similar topics, takes up a lot of space in the report.

Close attention is given to international rules and regulations on reactor safety, radiation shielding, disposal of radioactive wastes, transportation of radioactive materials, etc. The outlook for the development of nuclear power in member nations of the ENEA and is dealt with in brief, and the fuel-power balance of those countries is also described.

The book has several appendices: the organizational structure of the agency, the work of the committee on reactor safety terminology, irradiation programs, a list of power reactors, research reactors, and critical assemblies in the ENEA member-nations.

The report is mainly of an informative and descriptive character and may prove useful to those readers who are primarily interested in the activities, organization, and administration of international atomic agencies.

Use of Plutonium for Power Production. Vienna, IAEA (1965), 162 pages.

This publication comprises a collection of papers submitted to an IAEA-sponsored conference on the use of plutonium in power production. The increase in production of plutonium in power reactors of different countries places added emphasis on plutonium recycle operations and on more efficient utilization of plutonium supplies. For example, ~3000 kg of plutonium will be produced annually in Great Britain's reactors during the Seventies; the annual production of plutonium in the USA is expected to reach 15,000–20,000 kg by 1980.

The collection of papers is divided into two parts. The first section presents papers from different countries (twelve papers in all); the second section presents brief reviews summarizing the discussion at the conference (7 reviews).

The research program on the use of plutonium in Belgium's reactors is discussed in a paper by E. Bemben. The brunt of this paper is the description of trends in research and the organization of research work. There are some brief remarks on irradiation experiments in the BR-3 reactor using plutonium fuel elements.

A costs analysis of a plutonium recycle fuel cycle in thermal reactors appears in a report by O. Reynolds (Canada). The author concludes that the use of plutonium produced in CANDU type reactors in water-cooled water-moderated reactors will bring down the fuel component of power costs to 0.05 cent per kWh. The physics of plutonium utilization as nuclear fuel is discussed in a paper by J. Vandres et al. (France). Costs are discussed in general outline. Similar topics are discussed by S. Paranipe (India), but here attention is centered on fuel cycles utilizing thorium fuel in systems with thermal and fast reactors.

L. Sani (Italy) centered his attention on the isotope compositions of fuel discharged from the reactor at different burnup levels. The next two papers are from Japan. The first (S. Omachi) deals with the status of research work on plutonium utilization in Japan, and the second (M. Takahashi) deals with the outlook for plutonium utilization in electric power generation.

Great Britain submitted a fundamental paper on plutonium utilization (H. Kronberger). Physics in thermal reactors and fast reactors, fuel element fabrication, costs, burnup in thermal reactor, and fast reactors are discussed. F. Albauch (USA) cited a large amount of experimental data on plutonium fuel technology for thermal reactors. This report was complemented with one by S. Lawrowski (USA) on the USA fast reactor plutonium utilization program. The technology and fabrication techniques of plutonium fuel elements, plutonium fuel material, and their utilization were stressed in this report.

The last two reports were presented by Euratom. These were a paper by W. Rajewski on plutonium utilization research and one by H. Mikhaelis on plutonium utilization costs. The reports gave most of their space to the outlook for plutonium production and plutonium utilization (extrapolated to 1980).

International Symposium on Working Methods in High Activity Hot Laboratory. Volumes I, II. Paris, European Nuclear Energy Agency (1965), 1030 pages.

A symposium, whose proceedings appear in a separate publication, was organized by the Commission of Economic Cooperation and Development of ENEA in collaboration with Euratom, and held at Grenoble in June 1965 at the atomic research center of the Commissariat de l'Energie Atomique of France.

Representatives of sixteen nations and five international bodies participated in the symposium. The two-volume publication includes 53 papers and material on 12 discussions following presentation of the papers. All the papers are grouped by according to the six sessions, each of which was devoted to a particular topic.

X-radiographic and similar radiographic inspection of irradiated fuel elements were discussed at the first two sessions, as well as several nondestructive techniques for inspecting fuel elements and experimental capsules (gamma-ray spectroscopy, ultrasonic inspection, eddy current techniques, fluoroscopy, metrologic determinations of dimensional changes and warpage, remote photography and remote inspection techniques). The reports cite diagrams of remote control facilities designed for these studies.

A. Fudge, R. Coser (Great Britain), H. Engelman (France), et al. discussed topics pertaining to the study of fission product distribution and migration in the interior of fuel elements by gamma-ray scanning techniques. Results were cited.

Reports by F. Browne (USA) and G. Vinebliss (Great Britain) et al. discussed various methods for nondestructive inspection of fuel elements, and cited some diagrams of remote control accessories and facilities for sampling gaseous fission products to determine their composition and quantity.

The third session was devoted to various techniques and equipment for disassembly and mechanical treatment of spent fuel elements and experimental capsules in hot caves for the fabrication of inspection samples.

The fourth session discussed several techniques and methods for the transportation of spent fuel elements and experimental capsules following in-pile irradiation. Close attention is given to shielding techniques designed to eliminate contamination of rooms, equipment, and the surrounding atmosphere at fuel reloading sites (paper submitted by F. Larsen, Denmark). The problem is handled by correct organization of the ventilation system (inflow–discharge), by bringing about a proper rarefaction in rooms occupied by personel, in hot caves in α-, β-, and γ-shielded glove boxes. Reports by P. Pesenti (Euratom), M. Heeren (West Germany), et al. cited diagrams and sequencing of reloading operations, with all manner of polyethylene and polyvinyl chloride films 0.3 to 0.4 mm thick in jacket and sleeve configurations employed for protecting the environmental atmosphere from α-, β-, and γ-contamination.

P. Graf (Switzerland), G. Schult (USA), A. Ritchie (Great Britain), P. Gotlob (West Germany), and others discussed various types and designs of transporting and reloading devices employed in hot laboratories in their respective countries.

Reports submitted at the fifth session discussed deactivation of rooms, hot caves, α-, β-, and γ-shielded boxes, manipulators, and various approaches and techniques in the conveyance of contaminated materials from radiation-hazard zones to deactivation and maintenance rooms. Reports by C. Watson (USA), H. Wells (Great Britain), et al. cited a number of physical deactivation techniques (ultrasonic cleaning, pneumatic chisel treatment of contaminated surfaces, treatment of contaminated surfaces with metal brushes, abrasive grinding wheels, vacuum suction dust collectors and moisture collectors, etc.) and chemical deactivation techniques (acids, alkalis, organic solvents, water), and the equipment and materials utilized in this work. Recommendations are given for the deactivation of floors, walls, ceilings, and the structural materials employed in building hot caves and glove boxes. Reports by H. Brinkmann (West Germany), C. Cesarino (Italy), L. Hayette (France), and others cited examples of organization and planning of rooms for deactivation of contaminated equipment (manipulators, α- and β-shielded glove boxes for work in hot cells, instruments, facilities, devices). All the authors are of the view that deactivation operations should always be carried out in a specially isolated room which is properly planned and equipped (air locks) and designed to prevent the propagation of radioactive contaminants through clean rooms in a hot laboratory. Examples of correct organization and outfitting of rooms for deactivation are cited.

The last session heard reports on planning of hot laboratories (USA, Great Britain, etc.) and shops for reprocessing and inspecting spent fuel elements; organization of ventilation systems, transportation of irradiated materials, equipment for inspection of fuel elements in hot caves with heavy shielding against gamma rays, glove boxes shielded for α- and β-emissions, and organization of inspection, measures to prevent radioactive contamination of laboratory rooms, shops, and surrounding premises or of the equipment used in those facilities.

Sections appended to those symposium papers list hot laboratories in the participant nations represented at the symposium, their locations, brief data on them, and some indication of the work pursued there. A list of contributing authors is also given.

The symposium materials are accompanied by a large number of illustrations and diagrams, with references to the literature.

The appearance in print of this collection of symposium papers will enable many specialists working with highly radioactive materials to familiarize themselves with techniques in use, and to broaden their horizon on topics pertaining to the proper organization of conveying radioactive materials in hot laboratories and deactivation of different types of contaminated equipment. These materials will also be of great value to designers of hot caves, glove boxes, and hot laboratories.

M. S. Orlov

Exchange Reactions. Vienna, International Atomic Energy Agency (1965), 417 pages.

"Exchange reactions" is the title of the proceedings of a symposium on exchange reactions organized by IAEA and held in May-June 1965 at Brookhaven National Laboratory (USA). The collection contains 29 papers, with abstracts in English, French, Russian, and Italian. Each paper is followed by a brief account of the ensuing discussion.

Some of the papers deal with the theory of reactions involving electron transfer and their significance in structural effect, with the effect of the stability of complex compounds on electron exchange reactions, with electron transfer and proton transfer by the Grothus mechanism in aqueous solutions and in biological systems, and with techniques used in the study of exchange reactions (mass spectroscopy of exchange regions of isotopes and investigation of exchange reactions of alkyl groups in aluminoalkyl compounds by proton magnetic resonance). The bulk of the reports submitted concern research on concrete systems. The mechanism and kinetics of electron transfer reactions in systems of elements of differing valency (tetravalent and hexavalent uranium, divalent and trivalent iron, trivalent and pentavalent antimony) occurring in aqueous and organic media. One of the papers reported the effect of the nature of the solvent, of salts present, and of temperature on exchange reactions in systems containing neptunium and uranium. Many of the papers dealt with exchange reactions in complex compounds (hexachlorides and pentachlorides of trivalent radium; complexes involving divalent platinum; halide complexes of elements of the platinum group with coordination number six) and in organic systems (electron exchange reactions of aromatic molecules, electron transfer in vinyl aromatic polymers, etc.). Finally, some of the papers reported results on exchange reactions occurring on the surface of ionic crystals.

Nondestructive Testing in Nuclear Technology. Vienna, IAEA (1965), 393 pages (Volume I) + 446 pages (Volume II).

This is a collection of 46 papers presented by leading specialists from 20 countries and two international organizations at a Budapest May 1965 international symposium, as well as accounts of the discussion at the symposium sessions. The collection reflects the advances registered in recent years in the use of nondestructive testing methods for quality control of structural materials and finished products employed in nuclear technology. Included are methods for detecting cracks and latent defects, gaging of dimensions of tubes and fuel elements, and mapping uranium and plutonium distributions in fabricated fuel elements. Much attention is given to both already established and recently proposed techniques of nondestructive testing to secure detailed data on physical properties and the state of materials, and on the effect of processing technology on those properties.

The papers presented are buttressed by a generously detailed bibliography (over 380 titles), and will be greeted with interest by specialists and production experts in nuclear power industry.

Atomic Handbook. Vol. I—Europe. Edited by Y. W. Shortall. London, Morgan Brothers Ltd. (1965), 868 pages.

This first volume of a reference handbook set encompasses Europe, with socialist countries included, and consists of 6 sections. The first section presents a brief review of the current status of atomic industry and of the development of scientific research in 29 countries in Europe. According to incomplete data, capital investments in all sectors of atomic industry are estimated at four billion dollars, and Europe's 1965 "atomic budget" is placed at around one billion dollars, the minimum estimate of the number of personnel employed in atomic industry and scientific institutions is 230,000, the total power output of electric power generating stations now on the line is 326 million kW, with nuclear-fueled power stations accounting for 3.3 million kW out of that total. The number

of nuclear power generating stations is: 26 now in operation, 23 under construction, 17 in the planning stage. Reactors and critical assemblies number 160, and there are 92 atomic research centers.

The second section contains information on international organizations (IAEA, Euratom, CERN, COMECON, and others) based on European countries. The third, and principal, section contains reference material on European countries: atomic research and development programs, membership in international organizations, agreements with individual countries, jurisprudence in atomic power, utilization of radioactive isotopes, atomic budget, number of persons employed in atomic industry, development of electric power on the whole, and development of nuclear power in particular, reactors, research centers, governmental organizations, private films, universities, and miscellaneous organizations concerned with atomic energy.

The fourth section lists periodicals and newspapers (with specialists and pertinent journalists indicated) which regularly publish material on atomic energy, the fifth section lists leading personnel in the principal firms and atomic agencies, and the sixth section lists yearbooks and reference handbooks on atomic energy published in European countries.

Crystallization Processes

Edited by N. N. Sirota, F. K. Gorskii and V. M. Varikash

Institute of Solid State Physics and Semiconductors Academy of Sciences of the Belorussian SSR, Minsk.

Translated from Russian by Geoffrey D. Archard

Corrected by the editors for the American edition.

Devoted to a consideration of the mechanism and kinetics of crystallization and the production of single-crystal semiconductor materials, their purification and the controlled distribution of impurities. Several articles in this important new volume cover theoretical and experimental aspects of the relief and the state of the surface of growing crystals and the surface energy at crystal-melt boundaries. Attention is given to the competing mechanism in crystallization processes, compared with experimental data on the temperature-dependence of crystallization parameters, the linear velocity of crystallization, and the rate of crystal growth. A number of papers consider the structural and kinetic laws of crystal dissolution and the role of the structure of liquids in crystallization processes.

Most of the articles in this collection were presented at the All-Union Conference on the Theory of Crystallization, Thermodynamics, and the Kinetics of Phase Transformations. Translated from a four-part Russian volume, *Mechanism and Kinetics of Crystallization*, the present work comprises two of the sections. The remaining two parts are being published simultaneously in a translation entitled *Solid State Transformations*. The Russian text from which the translation was prepared was thoroughly corrected by the editors.

169 pages

Crystallization Processes: $22.50

Solid State Transformations: $22.50

Set Price: $40.00

CONSULTANTS BUREAU 227 West 17th Street, New York, New York 10011

A DIVISION OF PLENUM PUBLISHING CORPORATION